ALPHA-PARTICLES FROM B^{12}; THE ASTROPHYSICAL SIGNIFICANCE

Thesis by

Charles W. Cook

In Partial Fulfillment of the Requirements

for the Degree of

Doctor of Philosophy

California Institute of Technology

Pasadena, California

1957

ACKNOWLEDGMENTS

The author wishes to express his gratitude to the faculty of the Kellogg Radiation Laboratory for the opportunity to conduct this research. Without the active participation of Professors T. Lauritsen, W. A. Fowler, and C. C. Lauritsen this work would not have been completed. Thanks are also due Professor R. F. Christy and Dr. R. W. Kavanagh for many helpful discussions.

ABSTRACT

Alpha-particle emission associated with the β-decay of B^{12} has been detected and the energy spectrum investigated. These studies show that 1.3 ± 0.4 percent of all decays of B^{12} lead to the second excited state of C^{12} and 0.13 ± 0.04 percent of the decays lead to what is most probably a broad state of higher excitation in C^{12}. The most probable spin and parity assignments for the second excited state appear to be $J = 0^+$, and analysis of the alpha-spectrum yields $Q(C^{12*} - Be^8 - He^4) = 278 \pm 4$ kev, corresponding to an excitation energy in C^{12} of 7.653 ± 0.008 Mev. A new determination of the disintegration energy of Be^8 yields $Q(Be^8 - 2He^4) = 93.7 \pm 0.9$ kev and hence $Q(C^{12*} - 3He^4) = 372 \pm 4$ kev. It is concluded, from the general principle of reversibility of nuclear reactions, that the second excited state of C^{12} as predicted by Hoyle is of a suitable character to act as a stellar thermal resonance in the Salpeter process, $2He^4 \rightleftharpoons Be^8$; $Be^8(\alpha,\gamma)C^{12}$ under conditions expected in red giant stars. The high-energy spectrum is consistent with a broad level peaking at an excitation energy 10.1 ± 0.2 Mev in C^{12} and having a width at half maximum of $\Gamma \approx 2.5$ Mev. The most probable spin and parity assignments for this level are $J = 0^+$ although $J = 2^+$ cannot definitely be excluded; for $J = 0^+$, the width is approximately the Wigner limit.

TABLE OF CONTENTS

I. INTRODUCTION*

It has been suggested (1, 2) that the fusion of three alpha-particles into a C^{12} nucleus and the subsequent formation of O^{16}, Ne^{20}, etc. by successive (α,γ) reactions play an important role in the energy generation and element synthesis in red giant stars. These processes are believed to occur at a late stage of the red giant evolution in which gravitational contraction (3) has raised the central temperature to $\sim 10^8$ deg. K., and the density to $\sim 10^5$ gm/cc. The rate of the fusion reaction into C^{12} is extremely sensitive to the presence of resonances in the energy regions where the interactions effectively occur, that is, of the order of thermal energies attained in the stellar interiors. The existence of a Be^8 ground state level, therefore, greatly enhances the reaction rate over that expected for ordinary three-body collisions in the absence of resonances (1). This conclusion followed from experimental measurements (4, 5, 6) which established the fact that the Be^8 was, in fact, unstable to disintegration into two alpha-particles but only by 95 kev with an uncertainty of about 5 kev. This small center of mass energy thus guarantees a long lifetime on a nuclear scale since the probability of barrier penetration is small.

---

*A prior summary of much of this work has been submitted for publication in the Physical Review: "B^{12}, C^{12}, and the Red Giants" by C. W. Cook, W. A. Fowler, C. C. Lauritsen, and T. Lauritsen. Some sections of the report are reproduced here with only slight modification.

These circumstances give rise to a small but important equilibrium (1) ratio of Be^8 to He^4 nuclei equal to $\sim 10^{-9}$ and the problem reduces to finding the rate of the $Be^8(\alpha,\gamma)C^{12}$ reaction. Detailed consideration of the reaction rates and of the resulting relative abundances of He^4, C^{12}, and O^{16} led Hoyle (7) to the prediction that this reaction, in which C^{12} is produced, must also exhibit resonance within its relevant energy region. The predicted value for the resonance energy was 0.33 Mev, corresponding to an excited state in C^{12} at 7.70 Mev (7).

Hoyle's prediction of resonance was made in the face of conflicting evidence in regard to the existence of an excited state in C^{12} in the vicinity of 7.7 Mev. Early investigators had reported such a state, but some later research had failed to confirm its existence. Holloway and Moore (8) and Guggenheimer et al. (9), in measurements of the range of alpha-particles from $N^{14}(d,\alpha)C^{12}$, had reported a level in C^{12} at 7.62 Mev and 7.3 Mev respectively. However, magnetic analysis of the alpha-particle groups from the same reaction by Malm and Buechner (10) gave no evidence of a transition to a level in this neighborhood.

Early studies (11, 9, 12) of the neutron spectrum from the deuteron bombardment of natural boron targets revealed a group with a Q-value of about 6 Mev, which could be ascribed either to the ground-state transition in $B^{10}(d,n)C^{11}$ or to a transition to an excited state at ~ 7.5 Mev in C^{12}, through the reaction $B^{11}(d,n)C^{12*}$. An investigation by Gibson (13), who used separated B^{10} and B^{11}

targets, showed that the main contribution to the group in question was in fact from $B^{10}(d,n)C^{11}$, but it was suggested that a residual peak observed with B^{11} targets was probably due to a genuine C^{12} level at $\sim$ 7.7 Mev. Still later work by Johnson (14) failed to reveal such a level, although a weak group could not be excluded.

In the reaction $Be^{9}(\alpha,n)C^{12}$, a neutron group corresponding to a 7.5-Mev level (15) has been observed. In addition, 7-Mev electron-positron pairs ($e^{\pm}$) attributed to a monopole transition ($0^{+} \rightarrow 0^{+}$) to the ground state (16), and 3.16-Mev cascade radiation (17) through the state at 4.43 Mev have been reported. Protons inelastically scattered from C^{12} also gave evidence for a level at 7.5 Mev (18).

With the realization of the possible astrophysical significance of such a level, the matter was reinvestigated by Hoyle et al. (19), using the reaction $N^{14}(d,\alpha)C^{12}$. With a high-resolution magnetic spectrometer they clearly identified the alpha-particle group leading to the excited state of C^{12} in question and obtained a level energy of 7.68 $\pm$ 0.03 Mev and a width of less than 25 kev. The low intensity of the group - some 6 percent of the next higher energy group - accounts for some of the earlier difficulties. Later work by Pauli (20) and Ahnlund (21) on the same reaction yielded excitation energies of 7.66 $\pm$ 0.02 and 7.658 $\pm$ 0.027 Mev respectively.

The reaction rate for the conversion of helium into carbon by the $2He^{4} \rightleftharpoons Be^{8}$; $Be^{8}(\alpha,\gamma)C^{12}$ process is calculated by

using the Breit-Wigner single-level formula for the reaction cross-sections and integrating the Maxwell energy distribution over each of the two relevant resonances. Salpeter (1) has shown the same result can be obtained more simply by applying the mass-action law of statistical mechanics. This follows from the fact that the concentration of the C^{12*} is also in equilibrium with the concentrations of Be^{8} and He^{4}, since, as will be discussed later, the partial width for the decay of the second excited state (C^{12*}) is small compared with the width for its breakup into $Be^{8} + He^{4}$. In either case the reaction rate is given by

$$p = -\frac{1}{x_\alpha}\frac{dx_\alpha}{dt} = 3^{5/2}\,8\pi^3\,\frac{\hbar^5}{M_\alpha^5(kT)^3}\,(\rho x_\alpha)^2\,\frac{\Gamma_\gamma\,\Gamma_\alpha}{\Gamma_\gamma+\Gamma_\alpha}\exp(-Q/kT)\quad \text{sec}^{-1}$$

where ρ is the density, T the temperature, x_α the concentration by weight of helium, M_α the alpha-particle mass, Γ_γ and Γ_α the partial widths of the C^{12*} for γ and α-decay, and Q is the energy equivalent of the mass difference ($C^{12*} - 3He^{4}$). For ρ in grams/cc, T_8 in 10^8 deg. K, Q in kev, Γ_γ in ev, and $\Gamma_\gamma \ll \Gamma_\alpha$ as discussed later, we have:

$$p = 2.34 \times 10^{-4}\,(\rho x_\alpha)^2\,\frac{\Gamma_\gamma}{T_8^3}\exp(-Q/8.62\,T_8)\qquad \text{sec}^{-1}$$

Since Q/kT appears in the argument of the Maxwell-Boltzmann exponential factor and since the range of values of T is limited by other considerations, the reaction rate depends critically on Q. This energy can be calculated somewhat indirectly from the results discussed above and from tabulated

mass values (22) as 385 ± 17 kev. One objective of the present experiments was a more direct determination of this energy.

It is, of course, crucial to the theory that the C^{12} level be of such a character that it can be formed by $Be^{8} + He^{4}$, i.e., that it have even spin and even parity or odd spin and odd parity, and a non-vanishing alpha-particle width. It must also have a reasonable probability for γ or $e^{\pm}$ -decay if C^{12} is to be formed. These questions could best be explored by bombarding Be^{8} with alpha-particles, but since Be^{8} is unstable, recourse must be had to a study of the two possible modes of decay of the excited state of C^{12}, namely $C^{12*} \rightarrow Be^{8} + He^{4}$ and $C^{12*} \rightarrow C^{12} + \gamma$ (in case γ-radiation is forbidden or weak, the emission of $e^{\pm}$ -pairs must be considered). By the principle of reversibility of nuclear reactions, it is evident that observation of α and γ-decay of the 7.7-Mev C^{12} state would guarantee the feasibility of the process in question; in fact, a measurement of the decay widths for these processes would make it possible to calculate the cross-section for $Be^{8}(\alpha,\gamma)C^{12}$ using the one-level Breit-Wigner formula.

Experimental evidence on the character of the 7.7-Mev C^{12} is not entirely clear. It seems well-established that the state does not radiate directly to the ground state but rather cascades via the 4.43-Mev state (17, 23). The absence of ground-state transitions suggests $J = 0$ or $J \geq 3$; the observation of 7-Mev electron-positron pairs would favor $J = 0$, since a one-photon

radiative transition for $0 \rightarrow 0$ states is strictly forbidden while $e^{\pm}$ -emission is allowed. As mentioned above, pairs have been reported (16, 24), although more recent investigations (25, 26, 27) place, at best, a much lower limit on their relative number. Inelastic scattering of alpha-particles by C^{12} yields a group of alpha-particles corresponding to this level, with no corresponding C^{12} recoils, indicating that the C^{12} state must break up mainly by alpha-emission (28). Analysis of the angular distribution of the inelastically scattered alpha-particles in this reaction is in good agreement (29) with $J = 0^+$. Gamma-gamma correlation experiments (30, 31) reported in $N^{14}(d,\alpha)C^{12}$ and $Be^{9}(\alpha,n)C^{12}$ are consistent with $J = 0$ but do not separately exclude $J \geq 3$ and $J = 2$ respectively*. The angular distribution of electrons inelastically scattered from C^{12} at 187 Mev (32) indicates $J = 0^+$. It would thus appear reasonably certain that $J = 0^+$ is the correct assignment. However, emission of alpha-particles has not heretofore been observed; estimates of the fraction of decays leading to alpha-particle emission vary from $<<$ 50 percent (23) to $>$ 97 percent (25, 33). The object of the present experiment was to observe the alpha-particles directly, if possible, and to make a precise determination of their energy to permit calculation of the Q-value referred to above.

---

*Steffen et al. use $\gamma(3.22)/\gamma(4.43) = 0.03$ in agreement with Beghian et al. (17).

Since the alpha-particles were expected to be of low energy and of relatively low intensity in any easily available reaction, it was decided to look for them first in the decay of B^{12}, where advantage could be taken of the radioactive delay to reduce the background due to particles from prompt reactions. The processes involved are:

$$B^{12} \rightarrow C^{12*} + \beta^- + \nu$$

$$C^{12*} \rightarrow Be^8 + He^4$$

$$C^{12*} \rightarrow C^{12} + \gamma$$

Boron 12, with a half-life of 20.6 ± 0.9 milliseconds (34), is copiously produced in the reaction $B^{11}(d,p)B^{12}$ and is known to decay to both the ground and 4.43-Mev states of C^{12}, the latter to the extent of 1.5 percent (35, 36). The beta spectrum suggests (37) additional decays to considerably higher states of C^{12}. The decay of N^{12} is known to yield alpha-particles (38) from the breakup of higher states of C^{12}, and it seemed thus not impossible that B^{12} could decay through the 7.7-Mev level and yield low energy alpha-particles. The energetics of B^{12} decay are shown in Fig. 1; only the low lying levels of C^{12} are shown.

II. EXPERIMENTAL ARRANGEMENT

The experiments to be described consisted of producing B^{12} by the deuteron bombardment of B^{11} nuclei, cutting off the beam from the target, and searching for delayed alpha-particles with a magnetic spectrometer. The experimental arrangement is shown schematically in Fig. 2. The deuteron beam from an electrostatic accelerator passed through a magnetic analyzer to bombard boron targets located at the focal point of a low-dispersion, strong-focusing magnetic spectrometer (39). Alpha-particles focused by the spectrometer were detected by a CsI crystal wafer which was glued to a glass plate and mounted on a Dumont 6291 photomultiplier tube. The crystal was milled as thin as possible and then water polished to a thickness of approximately 0.7 mil in order to reduce the background from stray neutrons and gamma-rays to a minimum.

The deuteron beam was periodically interrupted at a position remote from the target by a rotating shutter, driven synchronously with a similar shutter which closed off the spectrometer during bombardment of the target. The counting system was electronically gated to permit counting only when the deuteron beam was interrupted. The spectrometer shutter and the photoelectric tube, which controlled the electronic gate, are schematically shown in Fig. 3. During target bombardment, light passed through the gate shutter and illuminated the photoelectric tube, thus

activating the gate and thereby turning off the counting equipment. The synchronism of the two rotating shutters and the electronic gate was observed by the use of an oscilloscope, permitting accurate alignment and easy monitoring. An assembly drawing of the target holder, spectrometer shutter, and target chamber is shown in Fig. 4.

Various combinations of target thickness, target angle, and spectrometer resolution were used in the experiments. The data reported here were obtained with targets placed at 15° grazing incidence to the beam, thus presenting a large number of B^{11} nuclei to the incident deuterons and at the same time diminishing the energy loss to the emerging alpha-particles. With this target angle the beam position is extremely critical, the spectrometer (40) being very sensitive to source displacements along the beam direction. The beam was therefore aligned while viewing the beam spot on the quartz window of the target chamber with a low-power telescope. By this method the beam could be aligned to better than 1/64".

The spectrometer was used with a solid angle of 0.0063 steradians and a momentum (p) resolution of $\Delta p/p = 5$ percent. At each spectrometer setting a complete pulse height spectrum was recorded by means of a 10-channel discriminator. Interposition of a 2.2-mg/cm^2 Al foil in front of the spectrometer slit permitted separate determination of background due to stray neutrons or gamma-rays. Typical pulse height spectra are shown in Fig. 5. Pulse heights for calibration purposes were obtained from deuterons and protons of known energies, and alpha-particles from Po^{210}(5.3 Mev)

and the breakup of Be^8. In general, for a given Bρ setting, one expects two groups, corresponding to He^+-ions and He^{++}-ions, differing in energy and pulse height by a factor of four. Up to an energy of ~ 200 kev, the doubly charged group is practically negligible; on the other hand, correction for neutral atoms is significant below 500 kev (41). Above 1 Mev the ions are predominantly doubly charged. Fig. 6 shows the fraction of the total beam assumed by each charge component as a function of energy.

III. EXPERIMENTAL RESULTS AND DISCUSSION

A. LOW-ENERGY ALPHA-PARTICLES

The low energy alpha-particle data reported here were obtained with a 39 μgm/cm^2 B^{11} target (42). Fig. 7 exhibits the observed momentum spectrum, extending from E_α = 100 - 260 kev, plotted as actual counts recorded versus Bρ. In Fig. 8 the experimental points are replotted, after correction for charge exchange (41). The spectrum exhibits a broad distribution of alpha-particles, terminating at an energy of about 200 kev. That these alpha-particles were in fact associated with the B^{12} decay was confirmed by several blank experiments using Be, Cu and Ta as targets and by a lifetime measurement. The lifetime was measured by covering one open section of the spectrometer shutter and then alternately reversing the direction of rotation of the shutter, thus alternately changing the time between bombardment and observation from 2.9 to 18.3 milliseconds. The value found for the half-life was 16 milliseconds, in rough agreement with the β-decay half-life (20.6 milliseconds) of B^{12}.

The momentum spectrum shown in Figs. 7 and 8 contains alpha-particles (designated α_1) resulting from the disintegration $C^{12*} \rightarrow Be^8 + He^4 + Q_1$, and the subsequently emitted particles (α_2) from the decay of $Be^8 \rightarrow 2He^4 + Q_2$. Ignoring for the moment the recoil imparted to the C^{12*} nucleus by the β-decay, the α_1-particles will constitute a monochromatic group, with

$E(\alpha_1) = 2/3\ Q_1$, or momentum $p_o(\alpha_1) = \sqrt{4Q_1M_\alpha/3}$ (the zero subscript is appended to indicate neglect of the C^{12*} recoil from the B^{12} β-decay). The Be^8 nucleus so formed is in motion in the laboratory system, and its velocity will be added to the velocities resulting from the breakup into two alpha-particles. On the assumption that the breakup is isotropic, the number of α_2-particles produced with momentum $p(\alpha_2)$ per unit momentum interval is

$$\frac{dN(\alpha_2)}{dp(\alpha_2)} = \frac{2N(\alpha_1)}{(Q_2M_\alpha)^{1/2}} \frac{p(\alpha_2)}{p_o(\alpha_1)}$$

where $N(\alpha_1)$ is the total number of α_1-particles. The limits on $p(\alpha_2)$ are $\left|(Q_1M_\alpha/3)^{\frac{1}{2}} \pm (Q_2M_\alpha)^{\frac{1}{2}}\right|$. As will appear below, $Q_1 = 278$ kev and $Q_2 = 94$ kev, so the α_2-distribution has a triangular shape, extending from a minimum $p(\alpha_2) \simeq 0$ to a maximum $p(\alpha_2) \simeq p_o(\alpha_1)$. The predicted thin-source spectrum is shown schematically in Fig. 9a.

When the β-recoil is taken into account, it is found that the α_1-particles are distributed over a range $p_o(\alpha_1) \pm \frac{1}{3} p_{max}(\beta)$, where $p_{max}(\beta)$ is the maximum β-particle momentum. Because of the the relatively high energy available, 5.7 Mev, this effect is quite appreciable, amounting to a spread of $\pm$ 5.5 percent in $p(\alpha_1)$. With the assumption that the β-particles and associated neutrinos have a simple Fermi distribution and that the beta-neutrino correlation is characterized by the tensor coupling $(1 + 1/3 \cos \theta)$,

the α_1-distribution is found to be:

$$\frac{dN(\alpha_1)}{dp(\alpha_1)} = \frac{5}{16 p_{max}(\beta)} \frac{p(\alpha_1)}{p_o(\alpha_1)} (7 - 6x^2 - x^4) \qquad -1 \leqslant x \leqslant 1$$

where $x \equiv 3\left[p(\alpha_1) - p_o(\alpha_1)\right] / p_{max}(\beta)$. In consequence of this distribution, the α_2-particle spectrum is rounded off at the upper limit as indicated in Fig. 9b. Since there are two α_2-particles for each α_1-particle, the area of the broad distribution is twice that in the α_1-group. It has been tacitly assumed throughout that the C^{12*} and Be^8 decay before slowing down, as would be expected from their lifetimes.

Derivation of the thick-source spectrum requires a knowledge of the distribution of the B^{12} in the target. Although the B^{11} layer is itself only about 75 kev thick to outgoing 200-kev alpha-particles, a large fraction of the B^{12} nuclei are actually driven to a considerable depth in the target backing in the course of their formation, thus increasing the escape distance for the alpha-particles. In the reaction $B^{11}(d,p)B^{12}$, the bombarding 1.6-Mev deuterons impart a velocity of 1.9×10^8 cm/sec to the center of mass of the system, and the ejected protons impart a velocity of 1.8×10^8 cm/sec to the recoiling B^{12}. Combination of these velocities gives the B^{12} nuclei a maximum and minimum energy of 860 kev and 2 kev respectively in the forward direction. On the

assumption that the angular distribution is isotropic in the center of mass system and that the range is proportional to velocity, these recoil effects combine to produce an approximately uniform distribution of B^{12} nuclei in the target extending about 1 mg/cm^2 in Ta. Measured in the direction of the emerging alpha-particles (83° from the deuteron beam, 22° from the target normal), the depth amounts to about 0.7 mg/cm^2, nearly equal to the range of the maximum-energy α_1-particles. Thus, again under the assumption of a constant rate of momentum loss, a simple integration of the calculated $N(\alpha_1)$ and $N(\alpha_2)$ distribution functions yields the required thick-source spectrum, illustrated in Fig. 9c.

When the calculated integral spectrum is folded with the known resolution function of the spectrometer, a final curve is obtained which may be compared with the experimental points. Two such curves, calculated for $Q_1 = 276$ kev and $Q_1 = 286$ kev, with $Q_2 = 94$ kev, are shown in Fig. 8, where it will be seen that the general shape observed is well accounted for, at least in the top 25 percent of the spectrum. The deviations at lower momenta may result from uncertainty in the charge-exchange corrections or from straggling in energy-loss of alpha-particles emerging from deep layers in the source. Interpolation between the curves shown in Fig. 8, together with other observations not reproduced here, yields $Q_1 = 278 \pm 4$ kev, or $C^{12*} - C^{12} = 7.653 \pm 0.008$ Mev. The difference $(C^{12*} - 3He^4)$ is given more precisely by $Q_1 + Q_2 = 372 \pm 4$ kev.

In the analysis described above, it has been assumed that the alpha-particle emission actually proceeds in two stages, with Be^8 in its ground state as an intermediate product, and the width of the Be^8 state has been neglected. Direct evidence on the latter point is available in the observed small width of particle groups from various reactions leading to the ground state of Be^8; for example, observations made here on the spread of the deuteron group in $Be^9(p,d)Be^8$ permit an upper limit of about 1 kev to be placed on this width. Considerably smaller values, ≤ 3.5 ev (43) and 4.5 ± 3 ev (44) are obtained from analysis of scattering of alpha-particles in helium. These values correspond to a mean life of $\sim 2 \times 10^{-16}$ sec or more, which is long compared to characteristic nuclear times, a fact which is to be expected on the basis of the small barrier-penetrability factor for two alpha-particles with a center of mass energy of only 94 kev. It is concluded that Be^8 acts essentially like a stable nucleus in "prompt" nuclear transmutations. The front slope of the spectrum of Fig. 8 is consistent with zero width for both the Be^8 and C^{12*} states and places an upper limit of about 10 kev for either.

The possibility that the present results might be equally well explained by a direct 3-body disintegration of C^{12} has been considered. In view of the strong electrostatic repulsions, it would be expected that the most probable outcome of such a process would be approximate equipartition of the energy among

the three alpha-particles, leading to a spectrum peaked more or less sharply at one third of the energy difference corresponding to $(C^{12*} - 3He^{4})$. The observed spectrum in this case would exhibit an inflection at this energy, rising to a maximum at a somewhat lower energy, and eventually falling linearly to zero at zero energy. In Fig. 8 the point of inflection occurs at $E_{\alpha} = 180$ kev, leading to a Q-value of 540 kev, clearly inconsistent with previous determinations of the C^{12*} level energy. In addition, the fact that the curve remains approximately level indicates the contribution of just such a lower energy group as α_2 in Fig. 9. It is concluded that the present results indicate a two-stage reaction and are inconsistent with a direct 3-body process.

B. HIGH-ENERGY ALPHA-PARTICLES

As may be seen in Fig. 8., the alpha-particle spectrum does not vanish entirely above the "end-point" but continues for some distance beyond. In addition, there was observed an appreciable number of high-energy pulses, corresponding to He^{++}-ions whose intensity increased slowly with increasing $B\rho$. Investigation of these particles showed a considerable number of alpha-particles (henceforth called the high-energy alpha-particles) quite distinct from the low-energy group. The spectrum will be discussed in detail later.

The high-energy spectrum was studied in the same manner

as the low-energy spectrum with only slight modification. CsI crystals of slightly greater thickness (several mils) were employed in much of the work to guarantee complete stopping of the more energetic particles within the crystal. Targets in this case consisted of the same thin B^{11} target used for the low-energy work and a natural boron target containing 143-μgm/cm^2 of B^{11}. The latter target was obtained by evaporating natural boron onto a thick Be backing and its thickness was measured by comparing the beta-ray yield with that of the thin B^{11} target. The high-energy spectrum obtained with the natural boron target is shown in Fig. 10 where the actual number of counts recorded is plotted versus Bρ. In Fig. 11 the experimental points are replotted against momentum, ZBρ. Comparison of the two curves representing He^{+} and He^{++} with Fig. 6 makes it clear that the decrease of the former and the initial rise of the latter are simply the result of the gradual increase in the ratio He^{++}/He^{+} with energy. The actual alpha-particle spectrum is therefore given by the sum of the two curves, with a small correction at low momenta for the neutral component He^{o}. The experimental points to be added were obtained on consecutive runs thus permitting more reliable addition than could be obtained by taking the complete He^{+} and He^{++} spectra individually. The spectrum so obtained again reduced to counts per unit momentum interval, N(p), is shown in Fig. 12. No evidence of fine structure is observed with this momentum resolution

($\frac{\Delta P}{P}$ = 5 percent) of the spectrometer. A similar spectrum taken earlier with the B^{11} target but with much poorer statistics is shown in Fig. 13.

The shape of the spectrum suggests a broad distribution of α_1-particles at high momenta, the α_2-particles filling in the spectrum at lower momenta where α_1 and α_2 are defined as before, i.e.,

$$C^{12*} \rightarrow Be^{8} + \alpha_1 + Q_1$$
$$Be^{8} \rightarrow 2\alpha_2 + Q_2$$

The absence of fine structure in the spectrum rules out the combination of several narrow distributions corresponding to the known states of C^{12}. The experimental evidence for a broad level in this region is not clear. Jackson and Wanklyn (45) have reported a level at 9.7-Mev excitation with an observed width of 1.6 Mev in the reaction $C^{12}(n,n')3He^{4}$. Goward and Wilkins (46) in $O^{16}(\gamma,4\alpha)$ also reported a level at 9.7 Mev with an observed width of 1.5 Mev and a true width of approximately 1.3 Mev. Both authors associated their observations with the well-known level at 9.61 Mev. However, this level is now known to be quite narrow, and Douglas et al.(47) in the reaction $N^{14}(d,\alpha)C^{12*}$ have accurately measured its width to be 30 $\pm$ 8 kev. The published spectra of Livesey and Smith (48) in $C^{12}(n,n')3He^{4}$ and $O^{16}(\gamma,4\alpha)$ are consistent with a broad level in C^{12} overlapping a narrow level at 9.6 Mev. This situation could perhaps account for the discrepancies in the reported width of the 9.61 Mev level. A broad level of low intensity is not inconsistent with most, if not all, of the information available

in this energy region (13, 14, 18, 24, 27, etc.) and hence will be assumed here.

Assuming a broad level in C^{12}, a theoretical spectrum can be deduced and compared with the experimental results. A similar problem has arisen in the case of the first excited state of Be^8; the procedure adopted here being similar to that of Bonner et al. (49, 50) in the treatment of the alpha-particle spectrum from Li^8. The broad level in Be^8 has also been treated in other reactions by various authors (51, 52).

We assume the level to be of the form (53, 54, 52):

$$\frac{dn(E)}{dE} \propto \frac{\Gamma(E)}{(E_\lambda + \Delta_\lambda - E)^2 + \left[\frac{\Gamma(E)}{2}\right]^2}$$

where E is the energy above $E(Be^8 + He^4)$, E_λ is the true resonance energy (55), Δ_λ is the resonance level shift (55), $dn(E)/dE$ is the number of states per unit energy interval, and $\Gamma(E)$ is the total width at energy E. With this density of states in C^{12} the Fermi theory for allowed β-decay gives the following electron distribution (56, 57) from B^{12}:

$$\frac{dN(W)}{dW} \propto F(Z,W)\left[W^2 - 1\right]^{\frac{1}{2}} W \int_0^{Q'-W} \frac{dn(E')}{dE'}\left[Q' - E' - W\right]^2 dE'$$

where W, E', and Q' are the total electron energy, the energy above $E'(Be^8 + He^4)$, and the total energy available for the β-decay (atomic

mass difference $B^{12} - Be^{8} - He^{4}$, plus $m_o c^2$) respectively with all energies being expressed in units of $m_o c^2$ and F is the Coulomb factor. The β-decay thus leaves the state populated with the distribution:

$$\frac{dN(E')}{dE'} \propto \frac{dn(E')}{dE'} \int_{1}^{Q'-E'} F(Z,W) \left[Q' - E' - W\right]^2 (W^2 - 1)^{\frac{1}{2}} W \, dW = \frac{dn(E')}{dE'} \quad f(Z,Q' - E)$$

Under the usual approximations, Z = 0, F(Z,W) = 1 we have

$$\frac{dN(E')}{dE'} \propto \frac{dn(E')}{dE'} \left[\frac{(Q' - E')^5}{30} - \frac{(Q' - E')^3}{6} + \ldots\right] = \frac{dn(E')f}{dE'}$$

The distribution of center-of-mass energies for alpha-emission is then:

$$\frac{dN_\alpha(E)}{dE} = \frac{\Gamma_\alpha(E)}{\Gamma(E)} \frac{dN(E)}{dE} = \frac{\Gamma_\alpha(E) \quad f}{(E_\lambda + \Delta_\lambda - E)^2 + \left[\frac{\Gamma(E)}{2}\right]^2}$$

where we define

$$\Gamma_\alpha(E) = 2kR \left(\frac{3}{2} \frac{\hbar^2}{MR^2}\right) \theta_\alpha^2 P_\ell$$

in which k is the relative wave number of the emitted alpha-particle, θ_α^2 is the dimensionless reduced width, and P_ℓ is the penetration factor for relative angular momentum ℓ .

In fitting the theoretical expression to the experimental points the parameters E_λ, θ_α^2, R and ℓ were varied, the remaining quantities being fixed. The α_1-distribution was obtained by numerically

integrating $dN_{\alpha}(E)/dE$ over the target thickness, assuming as before that the B^{12} nuclei were uniformly distributed in the target, and taking into account in a crude manner, the energy variation of the energy loss in the target. The α_2-distribution was also obtained numerically, summing the distributions corresponding to the α_1-particles. In this case the spatial distribution of B^{12} nuclei in the target was assumed to be in the form of four equally spaced groups, the α_2-particles originating in each group suffering a common energy loss in escaping from the target. Two theoretical fits, A and B, obtained in this manner are shown in Fig. 14. Maximum energy loss for escaping 2-Mev alpha-particles in the natural boron target was about 500 kev; the recoil of the C^{12*} nuclei was negligible. Table I lists typical values used in the computations. The function $dN_{\alpha}(E)/dE$ has been plotted in Figs. 15, 16, and 17 for various combinations of the parameters thus enabling one to estimate the effects of changes in the parameters without effecting a complete fit.

A value of 5.21×10^{-13} cm was chosen for the radius of interaction of the Be^8 and He^4 from analysis of the Stanford work on electron scattering (59) at this laboratory. A radius somewhat larger might be expected in this case since the Be^8 and He^4 are apparently loosely bound. It appears, however, that small changes in the radius have little effect on the final spectrum, in fact as seen from Fig. 15, radii as large as 7.5×10^{-13} cm improve the fit of A only slightly. This is to be expected, however, since at these

TABLE I

Typical Values Used in the Calculations of $dN_\alpha(E)/dE$ Assuming $R = 5.21 \times 10^{-13}$ cm and $\theta_\alpha^2 = 1.5$.

E_{CM} (Mev)	$E(\alpha_1)$ (Mev)	Δ_λ (Mev)	f	P_o	$\Gamma_\alpha(\ell = 0)$ (Mev)
0.6	0.4	1.8	6652	0.0025	0.093
0.9	0.6	1.4	5109	0.038	0.17
1.2	0.8	1.1	3863	0.11	0.58
1.5	1.0	0.83	2853	0.21	1.2
1.8	1.2	0.64	2080	0.32	2.1
2.1	1.4	0.51	1493	0.41	2.9
2.4	1.6	0.41	1033	0.48	3.7
2.7	1.8	0.34	701	0.54	4.4
3.0	2.0	0.28	459	0.59	5.0
3.3	2.2	0.25	285	0.63	5.6
3.6	2.4	0.22	175	0.66	6.1
3.9	2.6	0.20	94	0.68	6.5

(P_o and Δ_λ were obtained from the Chalk River Graphs of Coulomb Functions (58))

energies the penetration factor is a slowly varying function of the radius as well as the energy. The upper limit of θ_α^2, according to Wigner, is one. It is expected, however, that for certain collective motions of nuclei, values greater than one can occur; values as large as 2 have appeared in the literature (52). Values less than one give α_1-spectra that are too narrow and hence large dips in the final spectrum; values greater than 1.5 require larger values of E_λ to fit the high-energy end. Values of $\ell > 0$ require large values of θ_α^2 and E_λ to obtain reasonable fits. For $\ell = 2$ a value of $\theta_\alpha^2 = 7.5$ gives a fair fit for $E_\lambda = 3.38$, further increase in both seems not to improve the fit. It would seem that a value of $\theta_\alpha^2 = 7.5$ would be rather unlikely.

It appears that curve B probably gives the best overall fit, that is with $E_\lambda = 3.00$ Mev, $\theta_\alpha^2 = 1.5$, $R = 5.21 \times 10^{-13}$ cm and $\ell = 0$. This corresponds to a asymmetric state in C^{12} (after the β-ray energy dependence has been removed) peaking at 10.1 ± 0.2 Mev and falling to half-maximum at ~ 9.2 Mev and ~ 11.7 Mev.

It has again been assumed throughout this analysis that the alpha-particle emission proceeds in two stages, with Be^8 in its ground state as an intermediate product. At higher excitations in C^{12} it is thought that some breakups occur through the 2.9-Mev state of Be^8. This appears not to be the case here.

In order for the 2.9-Mev state to participate to a reasonable extent in the reaction, the α_1-particles would have to arise from an excitation in C^{12} greater than about 7.37 + 2.9 = 10.3 Mev and the α_2-particles would appear with energies distributed around $\sim 2.90/2 = 1.45$ Mev. Applied to the spectrum of Fig. 14, the high-energy particles of $\sim$ 1.5 Mev would be α_2-particles while the α_1-particles would have to fill in the energy region 0.25 - 0.75 Mev. Since there are two α_2-particles for each α_1-particle, the distribution is clearly in the wrong direction, a reasonable number of α_2-particles corresponding to too few α_1-particles and vice-versa. Therefore, this model by itself cannot account for the observed spectrum. Further analysis shows that the spectrum of α_2-particles would be expected to rise quite rapidly at the high energy cut-off, much more so than the observed spectrum. Assuming then that the observed spectrum results primarily from the alpha-particle decay of a broad level in C^{12} proceeding through the ground state of Be^8, estimates show that less than 4 percent of the observed spectrum can be attributed to breakups through the 2.9-Mev state in Be^8. As mentioned previously the lack of fine structure in the spectrum rules out the possibility of the spectrum resulting from decays of the well-known states of C^{12} at 9.61 Mev and 10.8 Mev. The α_1-particles from these states would constitute separate groups each spread out by the target thickness and spectrometer resolution but still easily distinguishable with the

experimental arrangement described here. Assuming as before that the main contribution to the observed spectrum comes from the breakup of a broad level in C^{12}, it appears that no more than 10 and 3 percent of the spectrum can be attributed to breakups of the 9.61 and 10.8-Mev states respectively. The latest estimates (60) of the spin and parity of the 9.61-Mev state give 1^- or possibly 3^-. The β-decay from $B^{12}(1^+)$ would then be first forbidden (1^-) or second forbidden (3^-), and correspondingly the number of transitions should be down at least a factor of 100 from allowed transitions (61). This is consistent with the present observation. The spectrum does not vanish entirely above the cut-off; these particles could probably result from excitation of even higher states of C^{12}.

It has been assumed throughout the discussion thus far that the β-decay proceeds through an excited state of C^{12}. In the case of a broad level as envisaged here the distinction between passing through an intermediate stage and proceeding through the more direct breakups (54, 49, 62)

$$B^{12} \rightarrow Be^{8} + He^{4} + \beta^{-} + \nu_{-}$$

$$B^{12} \rightarrow 3He^{4} + \beta^{-} + \nu_{-}$$

is perhaps not clear. However, some insight into the problem may be gained by a consideration of the times necessary for the processes involved. A 3.3-Mev electron ($\beta = 0.99$, $\lambda = 6 \times 10^{-12}$ cm)

will travel 2×10^{-11} cm in the time necessary for a 1.5-Mev alpha-particle to cross the nuclear radius. It would appear that the electron is well outside the nuclear boundary before the residual nucleus has time to separate appreciably, and thus the nucleons comprise a C^{12} nucleus at least as far as the dynamics of the β-decay is concerned. Some experimental evidence is to be found in this regard. The observed alpha-particle spectrum from the decay of Li^{8} has found theoretical agreement (49) by assuming that the breakup proceeds mainly through the first excited state of Be^{8} ($\Gamma \approx 1.0$ Mev). It is concluded that it is not unreasonable under the present circumstances to assume the participation of a broad level in C^{12} as an intermediate stage in the decay of B^{12}.

A still different consideration is the direct breakup of the intermediate stage, C^{12}, into three alpha-particles. On the assumption, as made in the case of the low-energy alpha-particles, that the alpha-particles share the available energy equally, the three-particle breakup of C^{12} is inconsistent with the observed spectrum. However, some of the breakups could proceed in this manner, the resulting alpha-particles appearing in the spectrum at $\sim$ 0.9 Mev. These particles would tend to fill in the dip occuring in Fig. 14 curve A, allowing better fits to be obtained with smaller values of θ_{α}^{2}. It appears that < 15 percent of the breakups occur in this manner.

It was found necessary to discard the B^{11} target in the middle stages of the high-energy spectrum investigation when a

large and varying number of counts suddenly appeared, completely distorting the high-energy spectrum. A thorough check showed the particles to be in fact alpha-particles presumably originating from a Li^7 contamination which could have been deposited on the target during the measurement of its thickness. The target thickness was measured using the Kellogg Laboratory $10\frac{1}{2}$" double-focusing spectrometer; the target chamber of which has contained Li^7 on numerous occasions. The deuteron bombardment of Li^7 yields Li^8 through the reaction $Li^7(d,p)Li^8$. Li^8 beta-decays with a half-life of $\sim$ 0.84 sec (63) to Be^8 which subsequently breaks up into two alpha-particles, the energy spectrum of which has been shown (49, 64) to peak at approximately 1.5 Mev. The distorted spectrum observed in the present experiment peaked almost exactly at 1.5 Mev and furthermore was of the same distinctive shape as the spectrum of alpha-particles from Li^8. It was of course, perfectly possible for some of the Li^8 alpha-particles or any other delayed particles to appear in the spectrum unretarded by the mechanical shutter or electronic gate. Delayed particles other than alpha-particles could be distinguished by their momenta and pulse height characteristics but the only distinguishing characteristics between alpha-particles are the differences in the half-lives of their originators and in their energy spectra. It should be mentioned that the low-energy work had been completed before the target thickness was measured even though the

low-energy spectrum was unaffected by the Li^7 contamination and half-life measurements had proved that the low-energy alpha-particles originated with B^{12}.

Because of the previous trouble with the Li contamination, half-life measurements, as described before, were obtained for the high-energy spectrum ($\sim$ 1.5 Mev) with the freshly evaporated natural boron target. The ratio, R, of counts for the time, t_1, between bombardment and observation of 2.9 milliseconds as compared to the time, t_1', between bombardment and observation of 18.3 milliseconds was found to be $R = 1.61 \pm 0.12$. Assuming the only sources of alpha-particles to be B^{12} and Li^8, the ratio, R, is

$$R = \frac{N_B(e^{-\lambda_B t_1} - e^{-\lambda_B t_2}) + 2N_L(e^{-\lambda_L t_1} - e^{-\lambda_L t_2})}{N_B(e^{-\lambda_B t_1'} - e^{-\lambda_B t_2'}) + 2N_L(e^{-\lambda_L t_1'} - e^{-\lambda_L t_2'})}$$

where N_B and N_L are the respective numbers of B^{12} and Li^8 nuclei in the target at the end of each bombardment (assuming equilibrium) that emit alpha-particles of the observed energy (the factor of two arises since Li^8 emits two alpha-particles of equal energy), λ_B and λ_L are the respective decay constants of B^{12} and Li^8, t_1 and t_1' are defined above as 2.9 and 18.3 milliseconds respectively, and t_2 and t_2' are given by $t_1 - t_2 = t_1' - t_2' = 6.1$ milliseconds, the amount of time the spectrometer is exposed to the target. Taking the half-periods of B^{12} and Li^8 to be 20.6 ± 0.9

milliseconds and 0.841 ± .004 seconds respectively, a simple reduction gives

$$\frac{2N_L}{N_B} = 2.4 \pm 5.4$$

The ratio of alpha-particle counts from Li^8 to the number from B^{12} under normal operating conditions (2.9 milliseconds between bombardment and observation) is easily shown to be

$$\frac{C_L}{C_B} = \frac{2N_L}{N_B} \frac{e^{-\lambda_L t_1}(1 - e^{-\lambda_L (t_2 - t_1)})}{e^{-\lambda_B t_1}(1 - e^{-\lambda_B (t_2 - t_1)})} = 0.07 \pm 0.16$$

This implies that the fraction of alpha-particle counts that come from Li^8 is consistent with zero and almost certainly less than 25 percent. Assuming cross-sections of 0.15 ± 0.04 and 0.29 ± 0.04 barns for Li^8 and B^{12} production (64) respectively at the deuteron energy used in this experiment (1.65 Mev) and branching ratios of 0.13 percent and 90 percent for B^{12} and Li^8 respectively, the ratio of the number of atoms of Li^7 to the number of atoms of B^{11} on the target is found to be about $9 \pm 20 \times 10^{-5}$. Assuming no Li^7 contamination whatever, the value obtained for the half-life of B^{12} is 22 ± 3 milliseconds, in good agreement with the values previously reported in the literature (63) but differing somewhat from the most recent (34). It is concluded that < 7 percent of the 1.5-Mev alpha-particles

arise from Li^8 and hence their contribution to the total high-energy spectrum is practically negligible.

C. BETA-SPECTRUM AND BRANCHING RATIOS OF B^{12}

As mentioned previously the fraction of B^{12} nuclei decaying to the 4.4-Mev state of C^{12} has been found to be 1.5 ± 0.3 percent by measuring the ratio of 4.43-Mev gamma-rays to the total number of β-rays. In the case of the two alpha-emitting states described here, the branching ratios are found by measuring the number of alpha-particles emitted from each state and comparing it to the total number of β-rays. This assumes, of course, that these states break up only by alpha-particle emission; examination of the relative decay widths of the states, as will be discussed later, shows this assumption to be quite accurate.

The β-rays from the thin B^{11} target were counted with a large (4" long x 5" dia) plastic scintillator* backed by a Dumont 6364 photomultiplier tube. In this case the phototube was electronically gated and synchronized with the rotating beam shutter. The pulse heights were displayed, as before, on the 10-channel discriminator. To keep extraneous scattering to a minimum the analyzed beam was allowed to pass into a thin-walled

---

*The scintillator was obtained from the Pilot Chemical Company, Waltham, Mass. It is composed of diphenyl stilbene with a density of 1.03 gm/cm^3 and hydrogen to carbon ratio H/C = 1.10.

isolated target chamber shown in Fig. 18. The scintillator was mounted at 90^{o} to the incident beam and subtended a solid angle determined by a $1\frac{1}{4}$" hole in a $\frac{1}{4}$" Pb plate. Different solid angles were obtained by varying the distance between the target and the crystal. The crystal was calibrated by observing the Compton peaks from various γ-rays; Table II shows the γ-rays, their energies, and their Compton peaks. The Compton peak is given by the maximum energy transfer (65) to the electron and is

$$T_o = \frac{h\nu}{1 + \frac{1}{2}\alpha}$$

where

$$\alpha = \frac{h\nu}{m_o c^2}$$

TABLE II

Source	$h\nu$(Mev)	α	T_o(Mev)
Cs^{137}	0.662	1.29	0.477
Mn^{54}	0.835	1.63	0.639
Co^{60}	1.25 (Avg.)	2.45	1.04
Na^{22}	1.28	2.50	1.06
ThC"	2.62	5.12	2.38
$B^{11}(p,\gamma)B^{12}$	12.1	23.8	11.9
$B^{11}(p,\gamma)B^{12}$	16.6	32.5	16.3

Fig. 19 shows the pulse height spectra for several of the γ-rays used for calibration purposes. The calibration curve is shown in Fig. 20, the peak of the experimental spectrum being associated with the Compton-peak energy.

The observed β-ray spectrum, minus background and corrected for energy loss in the target chamber wall ($\frac{1}{16}$" lucite) and crystal housing (17 mil Al), is shown in Fig. 21 plotted as the number of counts per unit momentum interval versus Bρ. At low momenta the spectrum deviates somewhat from the known spectrum (57). As will be discussed later this was presumably due to back-scatter from the Ta target-backing. The background was obtained by taking runs under the following conditions:

(1.) A $2\frac{1}{2}$" long graphite block was placed between the target and the counter. This stopped all electrons from entering the crystal and gave the background due to stray neutrons and γ-rays. Graphite was used to keep bremmstrahlung as low as possible.

(2.) A $1\frac{1}{4}$" diameter, $\frac{1}{4}$" thick Pb disc was placed just in front of the $1\frac{1}{4}$" hole in the lead plate. This gave all the background of (1) plus electrons striking the Pb plate and scattering through the aperture to the crystal.

(3.) A $\frac{3}{8}$" diameter x $\frac{1}{4}$" thick Pb disc was placed against the target chamber between the target

chamber and the crystal. This gave background (1) and electrons scattered into the crystal from the target chamber and surrounding objects.

The background subtracted from the observed counts was obtained by subtracting (1) from the sum of (2) and (3). Above $B\rho = 35$ kilogauss-cm the total background was negligible; at $B\rho = 25$ it constituted about 7 percent of the observed number of counts.

The experimental points reduced to a Kurie plot are shown in Fig. 22. The observed "end point" of 27.2 $m_o c^2$ is in good agreement with 27.3 $m_o c^2$ obtained by Hornyak and Lauritsen (57) and speaks well for the energy calibration. The dotted line in Fig. 21 represents the spectrum corresponding to a straight line Kurie plot; the true Kurie plot being straight down to $\sim$ 12 $m_o c^2$. As mentioned earlier the observed deviation is thought to be attributable to backscatter from the Ta target-backing.

The number of β-rays observed per incident deuteron is

$$N_\beta = \sigma F n_\beta f_\beta \sec \phi_\beta \, (\Omega / 4\pi)_\beta$$

where σ is the cross-section for the formation B^{12}, n_β is the number of B^{11} nuclei/cm^2 in the target, ϕ_β is the angle of incidence of the deuterons to the target normal, F is the observed fraction of the total β-spectrum, f_β is the fraction of B^{12} nuclei that decay during the counting period, and $(\Omega / 4\pi)_\beta$

is the solid angle subtended by the counter. Comparison of Fig. 21 with the beta-ray spectrum of Hornyak and Lauritsen (57) gives $F = 0.436 \pm 0.048$ for a bias setting of $Bp = 24.3 \pm 1.3$. An elementary calculation for the experimentally determined time sequence of the electronic phototube chopper gives $f_\beta = 0.517 \pm 0.004$.

The observed number of alpha-particles per incident deuteron arising from the broad level is given by the integral over the α_1-particles (as predicted theoretically) and is

$$N(\alpha_1) = \int \frac{dN(\alpha_1)}{dp(\alpha_1)}\, dp(\alpha_1) = X_{\beta\alpha}(10.1)\ \sigma\ n'_\alpha\ \sec \phi_\alpha\ f_\alpha\ (\Omega/4\pi)_\alpha\ P$$

where $X_{\beta\alpha}(10.1)$ is the branching fraction, relative to all β-decay processes from B^{12}, for those β-transitions to the broad level which ultimately result in alpha-particle emission, $(\Omega/4\pi)_\alpha$ is the solid angle accepted by the spectrometer, P is the fraction of all B^{12} nuclei that remain in the target, and f_α, σ, n'_α and ϕ_α are as defined previously only now for the alpha-particle detection. The natural boron target used in this experiment gives n'_α as distinct from $n_\alpha = n_\beta$ for the B^{11} target. For the time sequence mentioned earlier $f_\alpha = 0.354 \pm 0.003$. The spectrometer solid angle was measured by elastically scattering protons from copper and carbon and comparing the yield with that calculated from the assumed Rutherford and the experimentally determined (66)

cross-sections respectively. The value thus obtained, $\Omega = 0.0063 \pm 0.0007$ steradians, differs by a factor of two from an earlier measurement (67) by the same method. The solid angle is known not to have varied during the experiments reported here since the peak counts in the frequent Al(p,p)Al calibrations remained constant.

Using the experimentally determined ratio $N(\alpha_1)/N_\beta$, one obtains $X_{\beta\alpha}(10.1) = 0.13 \pm 0.004$ percent, the major contribution to the uncertainty arising in the prediction of the low side of the α_1-particle spectrum. It should be noted that if one only counts the total number of observed alpha-particles down to $\sim$ 250 kev, $X_{\beta\alpha}(10.1)$ will be lowered by only about 40 percent.

In the case of the alpha-particles from the 7.653-Mev level the problem is most precisely handled in a different manner since the lower part of the spectrum is somewhat in doubt. The number of α_1-particles per incident deuteron which should be observed on the plateau of the thick target curve is

$$\frac{dN(\alpha_1)}{dp(\alpha_1)} = \frac{X_{\beta\alpha}(7.65)\rho f_\alpha (\Omega/4\pi)_\alpha}{\eta(\alpha)}$$

where $\eta(\alpha)$ is the momentum loss of the alpha-particles per cm in the target, f_α and $(\Omega/4\pi)_\alpha$ have been defined previously, $X_{\beta\alpha}(7.65)$ is the branching fraction for the 7.653-Mev level and ρ is the constant number of B^{12} nuclei per cm of depth in the target.

Under the assumptions made earlier with respect to the distribution within the target:

$$\rho = \frac{n_\alpha \sigma \sec \phi_\alpha \ \eta(B^{12})}{2p(B^{12})CM}$$

where n_α, σ, and ϕ_α are defined as before, $p(B^{12})cm$ is the momentum of the B^{12} nuclei in the center-of-mass system of the $B^{11}(d,p)B^{12}$ reaction and $\eta(B^{12})$ is the momentum loss per cm for B^{12} nuclei in tantalum. The experimental value of $dN(\alpha_1)/dp(\alpha_1)$ may be obtained from the normalization used in fitting the curve of Fig. 8. Using this result in the expressions above, one obtains $X_{\beta\alpha}(7.65) = 1.3 \pm 0.4$ percent. The major contribution to the uncertainty arises from the ratio $\eta(B^{12})/\eta(\alpha)$ which was taken to be 2.7 ± 0.5 from analysis of the relative stopping of boron nuclei and alpha-particles in air and emulsions (68).

As noted previously, $X_{\beta\alpha}(7.65)$ is the branching fraction for the β-α decays through the 7.653-Mev excited state of C^{12}, relative to all β-decay processes from B^{12}. The C^{12*}(7.65 Mev) state may also decay by gamma-ray emission directly to the ground state (0^+) or by a 3.22-Mev and 4.43-Mev gamma-ray cascade through the $J = 2^+$ first excited state of C^{12}. According to Beghian et al. (17), the cascade decay is observed in $Be^9(\alpha,n)C^{12}$, while the direct transition to the ground state is at least 100 times less probable. Independent limits for these modes may be derived from recent studies of the B^{12} decay by R. W. Kavanagh (36, 69)

who finds from βγ-coincidence measurements, $\gamma(7.65)/\beta(\text{total}) < 10^{-4}$, $\gamma(4.43)/\beta(\text{total}) = 0.013 \pm 0.004$ and, from γγ-coincidence studies, $\gamma(3.22)/\gamma(4.43) < 10^{-2}$. These results are consistent with those of Tanner (35), Bent et al. (25), Rasmussen et al. (28), and Hornyak (33). Thus the observed 4.43-Mev gamma-rays result almost entirely from direct β-transitions to the first excited state of C^{12} and the 3.22-Mev and 7.65-Mev gamma-rays occur in at most 10^{-4} of the β-decays. For the de-excitation of the 7.653-Mev state in C^{12} we thus have $\gamma(3.22)/\alpha \leq 10^{-2}$ and $\gamma(7.65)/\alpha \leq 10^{-2}$. Thus to a good approximation, $X_{\beta\alpha}(7.65)$ is just the branching ratio of all β-decays to the 7.653-Mev state. Using $W_\beta(\text{max}) = E_\beta(\text{max}) + m_o c^2 = 13.376 + 0.511 - 7.653 = 6.234$ Mev and $t_{1/2} = 0.0206/0.013 = 1.58$ sec for the effective half-life, one obtains log ft = 4.2 for this transition, placing it clearly in the class of allowed transitions. In the case of the broad level the branching ratio is clearly given by $X_{\beta\alpha}(10.1)$, the gamma-ray width being completely negligible compared to the large alpha-particle width. Using $W_\beta(\text{max}) = 13.376 + 0.511 - 10.1 = 3.787$ Mev and $t_{1/2} = \frac{0.0206}{0.0013} = 15.8$ sec for the effective half-life, log ft = 4.0 is obtained thus also representing an allowed transition. The corresponding values for the transitions to the ground state and to $C^{12*}(4.43)$ are log ft = 4.1 and 5.1 respectively. The transition to the ground state is definitely allowed and that to the 4.43-Mev state would seem to be allowed but unfavored or perhaps first

forbidden, but certainly not second forbidden. The allowed transition to the 0^+ ground state of C^{12} requires that B^{12} have spin and parity 1^+ since a 0^+ to 0^+ transition would violate the isotopic spin selection rule. The allowed nature of the transitions to the 7.653-Mev state and the broad level then indicates 0^+ or 2^+ for their spins and parities, the 1^+ possibility being ruled out by the observation of α-decay.

The branching ratios determined here together with the ratios to the 4.43-Mev state and the ground state are shown in Fig. 1. Upper limits for the ratios to the 9.61-Mev, 10.8-Mev, and higher states can be estimated from the present alpha-particle work and the above mentioned limit of Kavanagh, $\gamma(7.65)/\beta(\text{total}) < 10^{-4}$. (The counting equipment was biased to count γ-rays of energy greater than 4.43 Mev). Hence, the branching ratio to the 9.61-Mev state is $< 10^{-4}$ since the state is known (28) to break up primarily by alpha-emission. As noted before this is consistent with a 1^- or 3^- spin and parity assignment for the 9.61-Mev state, the assignments corresponding to first and second-forbidden β-transitions respectively. The upper limit for the branching ratio to the 10.8-Mev state and higher states is $< 10^{-4}$ using the γ-ray upper limit although if alpha-emission is allowed the ratios are probably considerably less; some evidence for these alpha-particles has appeared (38). Using the branching ratios of Fig. 1 the B^{12} β-spectrum has been

computed from the Fermi theory and the results compared with the experimental spectrum of Hornyak and Lauritsen (37). The spectra are in good agreement except at momentum < 10 kilogauss-cm where the theoretical spectrum does not account for about 2 percent of the experimental spectrum. Since a branching ratio of this order in this energy region would correspond to a super-allowed β-transition, it is concluded that the discrepancy is not in the branching ratios but is probably instrumental.

The fact that the γ-ray transitions from the 7.653-Mev state are at most 1 percent of the alpha-particle transitions makes possible a fairly definite choice between the 0^+ and 2^+ assignments for this state. Table III lists the partial widths expected for the alpha and gamma-transitions in the two cases. In these calculations we have taken $R(Be^8 + He^4) = 5.3 \times 10^{-13}$ cm. The maximum widths are given for alpha-particles in terms of θ_α^2, the dimensionless reduced width in units of $3\hbar^2/2MR^2$, and for gamma-rays in terms of the single-particle values, (sp)(70). The upper limit for θ_α^2 according to Wigner is unity, and a reasonable estimate for the present case is $\theta_\alpha^2 \sim 0.1$. For M1 gamma-transitions in light nuclei, Wilkinson (72) finds an average of 15 percent of the single-particle value. The E2 transitions can actually be enhanced over the single-particle estimates in the collective nuclear model. However, for the $0^+ \rightarrow 2^+$, 3.22-Mev transition, R. A. Ferrell (73) calculates $\Gamma_\gamma = 0.0014$ ev with an

TABLE III

Expected partial widths for α and γ-ray transitions for two possible assignments of 7.65-Mev state of C^{12}.

$J(C^{12*}, 7.65)$	Γ_α		$\Gamma_\gamma(3.22)$		$\Gamma_\gamma(7.65)$
	max (ev)	est.[a] (ev)	max(sp)[b] (ev)	est. (ev)	max(sp) (ev)
	($\ell_\alpha = 0$)		($0^+ \rightarrow 2^+$, E2)		($0 \rightarrow 0$, forbidden)
0^+					
	5	0.5	0.005	0.0014	$\Gamma_{+e} \sim 5 \times 10^{-5}$ ev[c]
	($\ell_\alpha = 2$)		($2^+ \rightarrow 2^+$, M1)		($2^+ \rightarrow 0^+$, E2)
2^+					
	0.1	0.01	0.6	0.1	0.08

a. est. designates the best estimate for the widths.

b. (sp) designates single-particle limits for radiation widths: (70).

c. Γ_{+e} calculated from $C^{12}(e,e')$; (71).

error of the order of a factor of two.

Table I shows that for the 0^+ assignment for $C^{12*}(7.65)$, it is reasonable that α-decay should exceed either γ-decay by a factor of at least 100, whereas for the 2^+ assignment, one would expect the α-decay and the two γ-ray transitions to be comparable in magnitude. Although $\gamma/\alpha \sim 0.01$ cannot be entirely ruled out for this assignment, it appears that the evidence rather strongly favors the 0^+ assignment. The fact that 7.65-Mev radiation has not been observed in other reactions resulting in the production of $C^{12*}(7.65)$ is strong confirming evidence.

The experiments discussed here have not established definitely that the 7.653-Mev state in C^{12} decays by gamma-radiation. This decay has been reported by other workers, however. The inelastic scattering of electrons by C^{12} leading to this state shows that in any case nuclear electron-positron pair emission will transform $C^{12*}(7.65)$ into C^{12}. As noted above, evidence for these pairs is somewhat conflicting. It should be observed, however, that the values of the ratio $\Gamma_{\pm e}/\Gamma_\alpha$ for the 7.65-Mev state as derived from the experimentally observed upper limits for pair emission of Kruse et al. (26) and Goldring et al. (27) are consistent to within a factor of 5 either way with the ratio computed from Table III.

The choice between the 0^+ and 2^+ assignments for the broad level is also not without reservation. It would appear from the

discussion that reduced widths somewhat larger than ordinarily encountered are necessary to obtain a reasonable fit assuming a 2^+ assignment. On the other hand, small contributions from competing modes of decay (for example, the direct breakup of the $C^{12*}(10.1)$ into three alpha-particles) could conceivably modify the shape of the spectrum thus allowing fits to be obtained with smaller and more reasonable values of the reduced width. It is concluded that while $J = 0^+$ appears to be the most reasonable assignment, $J = 2^+$ cannot be definitely excluded.

D. Q-VALUE OF Be^8

In connection with the determination of the energy of the alpha-particles from $C^{12*}(7.65) \rightarrow Be^8 + He^4$ and with the effort to obtain as directly as possible the overall Q-value for the transition $C^{12*}(7.65) \rightarrow 3He^4$, a new observation was made of the alpha-particle spectrum of $Be^8 \longrightarrow 2He^4$ as produced in $Be^9(p,d)Be^8$. With the large aperture (.0063 steradians) and the low resolution ($p/\Delta p = 56$) of the present spectrometer it was possible to work with thinner targets and to obtain higher counting rates than were possible in an earlier study made in this laboratory (5). The spectrum obtained with protons of laboratory energies 606 and 985 kev are shown in Figs. 23 and 24 respectively. The probable errors indicated are statistical only. The targets were layers of Be, 1-3 kev thick to 1 Mev protons, evaporated

on 0.2 mg/cm^2 Al foil. It was found necessary to cover the opposite side of the foil during evaporation to obtain a Be layer on one side of the foil only. The foil was thin enough to confine the elastically scattered protons to a narrow range of energies, thus permitting the alpha-particles to be observed without serious interference. A background of protons was nevertheless present and has been subtracted in plotting Figs. 23 and 24.

The fluxmeter of the proton beam analyzer was calibrated with the 993.3 $\pm$ 1.0 kev $Al^{27}(p,\gamma)Si^{28}$ resonance (74) and the spectrometer fluxmeter was calibrated with protons elastically scattered from Al and Be. Typical calibration curves are shown in Fig. 25. Using 990.8 $\pm$ 0.2 kev for the $Al^{27}(p,\gamma)Si^{28}$ resonance, as recently measured by Bumiller and Staub (75) would only lower the final Q-value by about 0.4 kev and not affect the probable error. During the course of preliminary experiments the calibration constants were found to vary somewhat from day to day, especially the spectrometer constant. Therefore both calibrations were checked before final runs and at least the spectrometer calibration checked after the runs.

It can be readily shown (76) that the calibration constant, K_S, for a magnetic spectrometer (as obtained from the elastic scattering of particles of known energy from a thick target)

may be expressed as:

$$K_s = \frac{M\alpha I^2 E_{10}}{Z^2}\left[1 - \frac{\varepsilon_2 + \varepsilon_1\alpha}{\varepsilon_1\alpha}\frac{\Delta E_1}{E_{10}} + \left(\frac{1-\alpha}{\alpha}\right)\frac{ZeV_T}{E_{10}} + \frac{\alpha E_{10}}{2Mc^2}\right]$$

where M, Ze, and E_{10} are respectively the rest mass, charge and bombarding energy of the elastically scattered particles, ΔE_1 is the energy loss of the incident particles in passing through any surface contamination layer that may be present on the target, ε_1 and ε_2 are the stopping cross-sections for the particles at the incoming and outgoing energies respectively in the contamination layer, V_T is approximately the potential of the target with respect to ground, I is the potentiometer reading corresponding to the midpoint of the rise of the scattered profile, and c is the velocity of light. In the case of particle 1 elastically scattered from particle 2 through an angle θ, α is given by:

$$\alpha^{1/2} = \frac{M_1\cos\theta}{M_1+M_2} \pm \left[\frac{M_2 - M_1}{M_1 + M_2} + \left(\frac{M_1\cos\theta}{M_1+M_2}\right)^2\right]^{1/2}$$

Similarly the calibration constant (K_A) for the magnetic analyzer (as obtained from a thick target bombarded by protons of energy near a narrow gamma-ray resonance) may be expressed as:

$$K_A = \frac{MI^2 E_1}{Z^2}\left[1 + \frac{\Delta E_1}{E} + \frac{ZeV_T}{E_1} + \frac{E_1}{Mc^2}\right]$$

where M, Ze, V_T, ΔE_1 and c are defined as before, E_1 is the proton energy corresponding to the gamma-ray resonance, and I is the potentiometer reading corresponding to the midpoint of the rise of the gamma-ray yield. The energy E' of a particle of mass M' and charge Z' passing through the spectrometer for a potentiometer setting I' is then given by

$$E' = \frac{(Z')^2 K_S}{M'(I')^2}\left[1 - \frac{E'}{2Mc^2} + \cdots\right] \approx \frac{(Z')^2 K_S}{M'(I')^2}$$

A similar equation holds for the magnetic analyzer. The calibration constants obtained on the days of final runs are listed in Table IV, where the values are computed for energies in kev, the mass in atomic mass units and I-values in the range shown in Fig. 25.

The spectrometer angle was measured with the use of a vertical slit 0.006" in width mounted on an 11/16" radius. Protons were used to bombard an Al foil, and the slit was rotated around the target chamber axis, first across the incoming beam to provide a zero setting, and then across the aperture of the magnet. Protons analyzed by the spectrometer were counted and recorded as a function of the slit angle. The experimental points are shown in Fig. 26. This data corrected for the Rutherford scattering angular dependence ($\sin^4 \frac{\theta}{2}$, which tends to remove the asymmetry) gives a mean spectrometer laboratory angle $\theta_L = 83.4 \pm 0.2^\circ$.

TABLE IV

The Calibration constants obtained on the days of final runs.

Run	$K_A \times 10^{-6}$	$K_S \times 10^{-5}$
1	55931	1704
2	55967	1699
3	55732	1696
4	55790	1694
Avg.	55855	1698

The constants are computed for energies in kev, the mass in atomic mass units, and I-values in the range shown in Fig. 25. In calculating Q-values the individual calibration constants were used rather than the average values.

The experimentally observed alpha-particle spectrum will be influenced by various factors and analysis similar to that previously described for the low-energy alpha-particles from B^{12} is necessary to obtain the desired Q-value for the Be^{8} breakup. The analysis has been discussed in detail (77, 78) in the literature for similar although not identical cases.

For an infinitely thin target the spectrum, plotted as number of counts per unit momentum interval, is a step function falling more or less linearly with decreasing momentum to zero at zero momentum. The high momentum cutoff corresponds to the case where the Be^{8} is omitted in the primary reaction in the direction of the spectrometer, followed by the emission of one of the alpha-particles from the Be^{8} in the same direction. This gives the greatest possible momentum to the alpha-particle.

For a target of thickness small compared to the maximum alpha-particle energy but greater than the spectrometer window (for the case at hand the target thickness for emerging alpha-particles was 28 kev and the spectrometer window was $\sim$12 kev) the high momentum end of the spectrum will rise linearly, to a good approximation, over a distance equal to the target thickness. The spectrometer window will round off the spectrum at the high momentum end and cause the low momentum end to fall off more rapidly since the window width is proportional to the momentum. The linear rise and rounded corners are readily recognized in

Figs. 23 and 24. A more detailed analysis is necessary to account for the broader maximum of the spectrum taken at the higher bombarding energy. Extrapolation of the high momentum rise, as shown, gives the maximum momentum and energy of the alpha-particles. Isotropy in both the initial $Be^9(p,d)Be^8$ and secondary $Be^8 \rightarrow 2He^4$ reactions is usually assumed in deriving the spectrum. The first assumption is quite good at low energies (< 600 kev) as evidenced in the measurements of the angular distribution of the deuterons (79). At higher energies, however, the anisotropy becomes pronounced. This will change the spectrum shape somewhat but for sufficiently thin targets it will produce a negligible effect in deducing the maximum alpha-particle energy. The second assumption is quite reasonable since the ground state of Be^8, having zero angular momentum, should emit the alpha-particles in an S-state and thus isotropically. As mentioned in the C^{12*} work, neglecting the width of the ground state of Be^8 (< 4 ev) introduces a negligible error in the spectrum.

The Q-value for the Be^8 breakup can be deduced from the maximum energy of the alpha-particles and is for the present case:

$$Q^{1/2} = 2^{1/2}\left\{-\left[\frac{M_\alpha}{M_8}\left(\frac{M_d}{M_d + M_8}\right)\left(Q_o + \frac{E_p M_9}{M_p + M_9}\right)\right]^{1/2} + \left[E_\alpha + \frac{M_\alpha M_p E_p}{(M_p + M_9)^2} - \frac{2\cos\theta_L}{M_p + M_9}(M_\alpha M_p E_p E_\alpha)^{1/2}\right]^{1/2}\right\}$$

where E and M refer to the energies and nuclear masses of the ions indicated by the subscript in Table V,

TABLE V

Nuclear Masses used in the Calculations

Nucleus	Symbol	Nuclear Mass (Mass Units on the Physical Scale)
H^1	M_p	1.0076
H^2	M_d	2.0142
He^4	M_α	4.0028
Be^8	M_8	8.0057
Be^9	M_9	9.0128

Q_o is the Q-value for the primary reaction $Be^9(p,d)Be^8$, and θ_L is the laboratory angle of the spectrometer with respect to the incident beam. A summary of the results and error assignments are shown in Table VI. The errors have been divided into the systematic errors (for example, the uncertainty in the angle measurement) which are common to all the runs and the random or statistical errors (the uncertainty in the determination of the extrapolated cut-off for each run and the random uncertainty in the energy calibrations). The evaluation of the systematic errors in the table is carried out for the high energy (985 kev) data, since this error is slightly greater than the corresponding

TABLE VI

Summary of Results and Probable Error Assignments

$$Be^9 + p \rightarrow Be^8 + d + Q_o$$

$$Be^8 \rightarrow 2\alpha + Q_2$$

A. Random Errors

Run	$E_p \pm \Delta E_p$ (kev)	$E_\alpha \pm \Delta E_\alpha$ (kev)	Q	Rel. Wgt.
1	984.9 ± 1.2	344.4 ± 0.9	93.68 ± 0.64	15
2	985.5 ± 1.2	345.0 ± 1.2	94.05 ± 0.88	10
3	981.7 ± 0.9	343.8 ± 1.5	93.51 ± 1.04	3
4	982.7 ± 0.9	343.5 ± 2.2	93.25 ± 1.56	1
		Weighted Mean	93.77 ± 0.44	
1	606.0 ± 0.8	298.1 ± 0.7	94.28 ± 0.54	15
2	606.4 ± 0.8	296.9 ± 1.5	93.32 ± 1.17	3
		Weighted Mean	94.12 ± 0.49	
		Overall	93.90 ± 0.33	

B. Systematic Errors

Source of Error	Quantity Affected	$\frac{\partial Q_2}{\partial X_i}$	ΔX_i	$\delta Q_2 = \frac{\partial Q_2}{\partial X_i}\Delta X_i$ (kev)	
Contamination Layers					
2.06 ± 0.90 kev	E_α	+ 0.696	± 0.90	± 0.63	
0.29 ± 0.15 kev	E_p	- 0.084	± 0.15	∓ 0.01	± 0.62
θ_L = 83.4 ± 0.2 deg.	θ_L	+ 2.94	± 0.2		± 0.59
Q_o = 559 ± 1 kev	Q_o	-.11	± 1.0		± 0.11
$Al^{27}(p,\gamma)Si^{28}$	E_α	+ 0.696	± 0.34	± 0.24	
993.3 ± 1.0 kev	E_p	- 0.084	± 0.99	∓ 0.08	± 0.16
			High Energy	$[\Sigma(\delta Q_2^2)]^{\frac{1}{2}}$ =	± 0.88
				Q_2 = 93.90	± 0.94

Correction for Small Effects ΔQ_2 = -0.2

Final Value Q_2 = 93.7 ± 0.9

error for the low-energy data. The probable error in Q for independent errors in its variables, X_i, has been calculated using the law of the propagation of errors (80):

$$\Delta Q = \left[\sum_i^n \left(\frac{\partial Q}{\partial X_i} \Delta X_i \right)^2 \right]^{1/2}$$

In assigning an error to a weighted average the greater of the external and internal error (81) is chosen. It is evident from Table VI that the total error is almost entirely of systematic origin, the large number of runs having reduced the contribution of the statistical errors to a practically negligible amount. The largest systematic errors arose from the uncertainty in the measurement of the angle of observation and in the uncertainty in the thickness of the contamination layers. The angle measurement has been discussed above and it would appear from Fig. 26 that an error of $\pm$ 0.2° is a reasonably conservative estimate.

The contamination layers for freshly evaporated targets were measured by observing elastically scattering protons from the contaminations as well as from the Al target-backing. After considerable bombardment, with the effect of increasing the amount of contamination on the target, the spectrum was taken again. From the observed shift of the protons scattered from the Al and the increase in area under the carbon peak, the contamination layer for a "clean" target was estimated. By this

method the energy loss for the emerging alpha-particles was found to be approximately 2 kev. A rather large error of $\pm$ 0.9 kev was assigned to account for different layers on different targets. The contamination studies were carried out using the $10\frac{1}{2}$" double-focusing spectrometer rather than the strong-focusing spectrometer. The observed buildup of contamination layers while using the strong-focusing spectrometer was found to be negligible.

Calculations indicate that neglecting relativistic effects, the target potential, and the thermal motion of the target atoms in the calculations leads to an error of $\Delta Q_2 = -0.2$ kev in the final Q_2-value. With this correction the final value is $Q_2(Be^8 - 2He^4) = 93.7 \pm 0.9$ kev which may be compared with previously reported values of 103 $\pm$ 10 kev (4), 89 $\pm$ 5 kev (5) and 94.5 $\pm$ 1.4 kev (78).

E. $B^{11}(d,p)B^{12}$ ABSOLUTE CROSS-SECTION

The B^{12} beta-spectrum was also investigated using the equipment previously described and a "thick" (14 mg/cm^2) natural boron target backed with 1/4 mil Al. The boron was thick enough to stop the incident deuterons and could therefore be used to provide an absolute normalization for the cross-section work of R. W. Kavanagh (36). At the same time the target was thin enough to the β-rays to give an indication of the amount of backscatter observed in the previous work with the "thin" Ta-backed target; the Ta backing was about 1 gm/cm^2. The spectrum and Kurie plot so obtained are shown in Figs. 27 and 28. Comparison of these figures with Fig. 21 and 22

shows that the thick target spectrum follows the known spectrum to much lower momenta than does the thin target spectrum. Since the experimental arrangements were identical in the two cases, the difference in the observed spectra is attributed to backscatter from the Ta-backing of the B^{11} target.

Determination of the absolute cross-section for B^{12} formation from the thin target data requires among other things a knowledge of the number of B^{11} nuclei per cm^2, n_β, in the target. This quantity was measured by comparing the momentum shift of elastically scattered protons from pure Ta and the Ta-backed target; the observed profiles are shown in Fig. 29. Analysis of the profiles in the Appendix gives $n_\beta = 39 \pm 2$ micrograms/cm^2. The absolute cross-section is then obtained from the equation given previously; values for several different deuteron energies are tabulated in Table VII.

Absolute cross-sections are obtained for the thick target experiments by determining K, the absolute normalizing constant from the following formula:

$$N_\beta(E_d) = F f_\beta (\Omega/4\pi)_\beta \int_0^{E_d} \frac{K\sigma(E)}{\varepsilon_d} \, dE$$

where $N_\beta(E_d)$ is the number of β-rays per incident deuteron, F, f_β and $(\Omega/4\pi)_\beta$ are as defined before, E_d is the incident deuteron energy, ε_d is the stopping cross-section for deuterons in boron, and $\sigma(E)$ are the thin target cross-sections of Kavanagh. The proton

stopping cross-sections in boron, ε_p, were obtained by interpolation for Z = 5 on curves of $\varepsilon_p(Z)$ for protons versus Z for constant energies. The curves were obtained from the data of Fuchs and Whaling (81). The deuteron stopping cross-sections were then obtained from ε_p in the usual manner. Values of K for several incident deuteron energies, E_d, were obtained by numerical integration; the results are tabulated in Table VII. The mean value of the absolute normalizing constant is K = 0.67 ± 0.09; the data of Kavanagh with this normalization is shown in Fig. 30.

TABLE VII

Absolute Cross-sections for $B^{11}(d,p)B^{12}$.

Deuteron Energy E_d(Mev)	σ (B^{11} target) Barns	σ (Natural Boron) Barns
0.918	0.09 ± 0.01	
1.11	0.15 ± 0.02	0.14 ± 0.02
1.37	0.22 ± 0.03	0.21 ± 0.03
1.57	0.28 ± 0.04	0.26 ± 0.04
1.65	0.29 ± 0.04	0.27 ± 0.04

Errors of ± 15 percent are assigned to the cross-sections. The major contribution arises from the uncertainty in F which was taken to be F = 0.436 ± 0.048.

ASTROPHYSICAL CONCLUSION

It has been shown that the second excited state of C^{12} decays into three alpha-particles through an intermediate stage involving He^4 and the ground state of Be^8. The general reversibility of nuclear reactions thus allows the conclusion that C^{12} can be produced through the 7.65-Mev state in the Salpeter processes:

$$2He^4 \rightleftharpoons Be^8;\ Be^8(\alpha,\gamma \text{ or } e^{\pm})C^{12}$$

The experiments reported here show that $Q(C^{12} - 3\ He^4) = 372 \pm 4$ kev; the reaction rate of the conversion of helium into carbon is then

$$p = 2.37 \times 10^{-4}\ (\rho x_\alpha)^2\ \frac{\Gamma_\gamma}{T_8^3}\ \exp\left(-\frac{43.2}{T_8}\right) \qquad \text{sec}^{-1}$$

where $\Gamma_\gamma \sim 0.0014$ ev. If the gamma radiation is highly forbidden, then Γ_γ must be replaced by $\Gamma_{\pm e} \sim 5 \times 10^{-5}$ ev.

As mentioned previously, the C^{12} nuclei formed in the above manner are expected to be destroyed mainly in the reaction $C^{12}(\alpha,\gamma)O^{16}$. On this assumption Hoyle (7) has shown that the ratio, K, of the reaction rate of

$$3He^4 \rightarrow C^{12} + \gamma \ (\text{ or } e^{\pm})$$

to the reaction rate of

$$C^{12} + He^4 \rightarrow O^{16} + \gamma$$

can be related to observed cosmic abundances of C^{12} and O^{16}. A reasonable value of this ratio, according to Hoyle, is $K \approx 1/9$.

Calculation of the reaction rate for $C^{12}(\alpha,\gamma)O^{16}$ in the manner described in detail by Salpeter (1) and Hoyle (7) yields

$$p(C^{12} \rightarrow O^{16}) = \frac{1.43 \times 10^{10} \, (\rho x_\alpha) \exp(-69.2/T_8^{\frac{1}{3}})}{T_8^2 \, (1 + 0.16 \, T_8^{-2/3})^2} \quad \text{sec}^{-1}$$

where the dimensionless reduced width for alpha-particle decay has been taken to be $\theta_\alpha^2 = 0.1$. The entire reaction rate, in this case, comes from the non-resonant contribution of the fourth excited state (1^-) in O^{16}, the contributions from other states being negligible. The reaction rate for the formation of C^{12}, assuming no contribution from the 7.653-Mev state, is found by considering the non-resonant contribution from the 4.43-Mev state. The ratio between the resonant (7.65-Mev) and non-resonant reaction rates is

$$\frac{p}{p_{nr}}(3He^4 \rightarrow C^{12}) = \frac{1.41 \times 10^{-3} \exp(-50.8 \, T_8^{-\frac{1}{3}} + 32.2 \, T_8^{-1})}{(T_8)^{5/6}}$$

where again we have taken $\theta_\alpha^2 = 0.1$. The mean life for the various reaction rates as a function of the temperature is shown in Fig. 31. Salpeter estimates that the reaction rates calculated in this manner are accurate to better than a factor of twenty either way; the quantities indicated on the curves give rise to the major

uncertainties. It is apparent then that K is much too large for the non-resonant formation of C^{12} which would imply a very low abundance of observed C^{12}. On the other hand, the resonant reaction involving the 7.65-Mev level permits a value of $K = 1/9$ at $T \sim 1.2 \times 10^8$ °K; at higher temperatures helium burning primarily produces C^{12}, at lower temperatures O^{16}. It thus appears that the 7.653-Mev level plays a dominant role in the synthesis of elements from helium as predicted by Hoyle.

As noted above, however, there are still considerable uncertainties in the computed reaction rates. The γ-ray width, Γ_γ, for the $Be^8 + He^4 \rightarrow C^{12}$ reaction can probably best be obtained by measuring $\Gamma_\gamma/\Gamma_\alpha$ and $\Gamma_{\pm e}/\Gamma_\alpha$ and using the experimentally measured matrix element (71) to give $\Gamma_{\pm e}$. Alternatively a lifetime measurement of $C^{12*}(7.65)$ would give $\tau \approx 1/\Gamma_\alpha$ and hence Γ_γ from a measurement of $\Gamma_\gamma/\Gamma_\alpha$. More information on the O^{16} producing reaction may perhaps be obtained by studying $C^{12}(\alpha,\gamma)O^{16}$ directly. Table VIII lists the calculated cross-sections as a function of energy, assuming $\theta_\alpha^2 = 0.1$. The expected thick target yield is thus of the order of 10^{-12} γ-rays per alpha-particle. A 10 μamp beam of alpha-particles would produce $\sim$ 30 γ-rays/sec which is not very prolific, to say the least.

TABLE VIII

Cross-sections for $C^{12}(\alpha,\gamma)O^{16}$ assuming $\theta_\alpha^2 = 0.1$

E_α(Mev)	σ(barns)
1.0	3.5×10^{-12}
1.5	5.2×10^{-11}
2.0	1.4×10^{-10}
2.5	4.2×10^{-10}
3.0	3.9×10^{-10}
3.5	2.8×10^{-10}
4.0	2.1×10^{-10}

APPENDIX

CALCULATION OF THE THICKNESS OF THE B^{11} TARGET

The target is composed of B^{11} nuclei imbedded in a Ta backing. Protons elastically scattered from the target and from pure Ta yield the profiles shown in Fig. 29. The energy loss per unit path length in the target is

$$\frac{dE}{dx} = 2\left(\frac{\rho_T(x)}{\rho_T}\,\varepsilon_T' + \frac{\rho_B(x)}{\rho_B}\,\varepsilon_B'\right) \qquad (1)$$

where x is the distance from the target edge along the proton path, ρ_T and ρ_B are the normal densities of tantalum and boron respectively, $\rho_T(x)$ and $\rho_B(x)$ are the respective densities of the tantalum and the B^{11} in the target as a function of x, and ε_T' and ε_B' designate the proton energy loss per unit path length in normal Ta and normal boron respectively. The factor of two accounts for the energy loss encountered by the protons in both entering and leaving the target.

The number of protons scattered from Ta per unit path length is

$$dN = \frac{\rho_T(x)}{\rho_T}\,C\,dx = \frac{\rho_T(x)}{\rho_T}\,\frac{C\,dE}{2\left(\frac{\rho_T(x)}{\rho_T}\,\varepsilon_T' + \frac{\rho_B(x)}{\rho_B}\,\varepsilon_B'\right)} \qquad (2)$$

where C is a constant of proportionality to be evaluated later.

The energy of the particles expressed in terms of the inverse momentum, I, is

$$E = \frac{K_S}{I^2}, \quad dE = \frac{-2K_S dI}{I^3} \tag{3}$$

where K_S is the spectrometer calibration constant.

Letting N_I represent the number of counts observed at the spectrometer setting, I, we have:

$$N_I = \frac{dN}{dI}\,\frac{I}{R} = \frac{dN}{dE}\,\frac{dE}{dI}\,\frac{I}{R} = -\frac{dN}{dE}\,\frac{2K_S}{I^2 R} \tag{4}$$

where $R = \frac{I}{\Delta I}$ is the resolution of the spectrometer.

Therefore from equations 2 and 4

$$N_I = \frac{-CK_S}{(\varepsilon_T' + \frac{\rho_T}{\rho_T(x)}\,\frac{\rho_B(x)}{\rho_B}\,\varepsilon_B')I^2 R} \tag{5}$$

The constant C is evaluated by observing that when $\rho_B(x) = 0$, $N_I = N_{I\ max}$. Solving for C and substituting back into equation 5 gives

$$N_I = \frac{N_{I\ max}}{(1 + \frac{\rho_T}{\rho_B}\,\frac{\rho_B(x)}{\rho_T(x)}\,\frac{\varepsilon_B'}{\varepsilon_T'})} \tag{6}$$

Equation 6 may be solved for $\rho_B(x)$ giving

$$\rho_B(x) = \rho_T(x) \frac{\rho_B}{\rho_T} \frac{\varepsilon'_T}{\varepsilon'_B} \left(\frac{N_{I\ max}}{N_I} - 1 \right) \tag{7}$$

In a similar manner one obtains

$$dx = \frac{\rho_T}{\rho_T(x)} \frac{K_S}{\varepsilon'_T} \frac{N_I}{N_{I\ max}} \frac{dI}{I^3} \tag{8}$$

The area density of B^{11} is then given by:

$$s = \int_o^{x_1} \rho_B(x)dx = \frac{K_S \rho_B}{\varepsilon'_B} \int_{I_o}^{I_1} \left(1 - \frac{N_I}{N_{I\ max}}\right) \frac{dI}{I^3} \tag{9}$$

which can be evaluated numerically. For small displacements, the value of I is approximately constant over the integration, and

$$s \approx \frac{K_S \rho_B}{\varepsilon'_B I^3} \left\{ \frac{\int_{I_o}^{I_1} N_{I\ max}\, dI - \int_{I_o}^{I_1} N_I\, dI}{N_{I\ max}} \right\} \tag{10}$$

The quantity in braces is simply the displaced area divided by the maximum number of counts which is approximately the average displacement, δI,

$$\therefore \quad s \approx \frac{K_S \rho_B \delta I}{\varepsilon'_B I^3} \approx \frac{\rho_B \delta E}{\varepsilon'_B} \tag{11}$$

where δE is the average energy displacement. The quantity ε'_B is related to the stopping cross-section ε_B by

$$\varepsilon_B = \frac{\varepsilon'_B}{N_B} = \frac{\varepsilon'_B A}{\rho_B N_o} \tag{12}$$

where N_B is the number of B^{11} atoms/cc, N_o is Avogadro's number and A the atomic mass of B^{11}. This substitution gives

$$s \approx \frac{A\delta E}{N_o \varepsilon_B} \tag{13}$$

Evaluating the integral of equation 9 numerically for the observed profile, making the small angle correction and using $K_S = 3.866 \times 10^8$, $\varepsilon_B = 3.83 \times 10^{-21}$ ev-cm^2, $N_o = 6.025 \times 10^{23}$ atoms/mole, and A = 11.01 gm/mole we obtain $s_n = 36 \pm 2 \mu gm/cm^2$. The B^{11} thickness over the target was surveyed with the β-ray counter; at the position used for the work described previously;

$$s_n = 39 \pm 2 \ \mu gm/cm^2.$$

REFERENCES

1. E. E. Salpeter, Ap. J., 115, 326 (1952); Annual Review of Nuclear Science 2, 41 (1953); Phys. Rev. (to be published).
2. E. J. Öpik, Proc. Roy. Irish Acad. A54, 49 (1951); Mem. Soc. Roy. Sci. Liege, 14, 131 (1953).
3. F. Hoyle and M. Schwarzchild, Ap. J. Suppl. 2, 1 (1955).
4. A. Hemmendinger, Phys. Rev. 73, 806 (1948); Phys. Rev. 75, 1267 (1949).
5. A. V. Tollestrup, W. A. Fowler and C. C. Lauritsen, Phys. Rev. 76, 428 (1949).
6. Early measurements by O. Laaff, Ann. d. Physik 32, 760 (1938) and K. Fink, Ann. d. Physik 34, 717 (1939) were analyzed by J. A. Wheeler, Phys. Rev. 59, 27 (1941) to yield an energy of instability of 125 kev with an uncertainty of 25 kev.
7. F. Hoyle, Ap. J. Suppl. 1, 121 (1954).
8. M. G. Holloway and B. L. Moore, Phys. Rev. 58, 847 (1940).
9. K. M. Guggenheimer, H. Heitler, and C. F. Powell, Proc. Roy. Soc. (London) A190, 196 (1947).
10. R. Malm and W. W. Buechner, Phys. Rev. 81, 519 (1951).
11. C. F. Powell, Proc. Roy. Soc. (London) A181, 344 (1942).
12. T. W. Bonner and W. M. Brubaker, Phys. Rev. 50, 308 (1936).
13. W. M. Gibson, Proc. Phys. Soc. (London) A62, 586 (1949).
14. V. R. Johnson, Phys. Rev. 86, 302 (1952).
15. W. H. Guier, H. W. Bertini and J. H. Roberts, Phys. Rev. 85, 426 (1952); B. G. Whitmore and W. B. Baker, Phys. Rev. 78, 799 (1950).

16. G. Harries and W. T. Davies, Proc. Phys. Soc. (London) A65, 564 (1952); G. Harries, Proc. Phys. Soc. (London) A67, 153 (1954).

17. L. E. Beghian, H.H. Halban, T. Hussain, and L. G. Sanders, Phys. Rev. 90, 1129 (1953).

18. R. Britten, Phys. Rev. 88, 283 (1952).

19. F. Hoyle, D. N. F. Dunbar, W. A. Wenzel, and W. Whaling, Phys. Rev. 92, 1095 (1953); D. N. F. Dunbar, R. E. Pixley, W. Wenzel, and W. Whaling, Phys. Rev. 92, 649 (1953).

20. R. T. Pauli, Arkiv. f. Fysik 9, 571 (1955).

21. K. Ahnlund, Arkiv. f. Fysik 10, 369 (1956).

22. A. H. Wapstra, Jr. and R. Huizenga, Physica 21, 367 (1955).

23. R. G. Uebergang, Australian J. Phys. 7, 279 (1954); K. G. Steffen, O. Hinrichs and H. Neuert, Zeits. f. Physik 145, 156 (1956).

24. G. C. Phillips, D. B. Cowie, and N. P. Heydenburg, Phys. Rev. 83, 1049 (1951).

25. R. D. Bent, T. W. Bonner, J. H. McCrary, and W. A. Ranken, Phys. Rev. 100, 771 (1955).

26. T. H. Kruse, R. D. Bent, and C. E. Eklund, Bull. Am. Phys. Soc. 2, 29 (1957) and R. D. Bent, private communication.

27. G. Goldring, Y. Wolfson, and R. Wiener, private communication (to be published).

28. V. K. Rasmussen, D. W. Miller, and M. B. Sampson, Phys. Rev. 100, 181 (1955).

29. H. J. Watters, Phys. Rev. 103, 1763 (1956).

30. J. Seed, Phil. Mag. 46, 100 (1955).

31. K. G. Steffen, O. Hinrichs, and H. Neuert, Zeits f. Physik. 145, 156 (1956).

32. J. H. Fregeau and R. Hofstadter, Phys. Rev. 99, 1503 (1955).

33. W. F. Hornyak, Bull. Amer. Phys. Soc. 1, 197 (1956).

34. Weighted mean of published values including E. Norbeck, Jr., Bull. Amer. Phys. Soc. 1, 329 (1956).

35. N. W. Tanner, Phil. Mag. 1, 47 (1956).

36. R. W. Kavanagh, Thesis, California Institute of Technology (1956)

37. W. F. Hornyak and T. Lauritsen, Phys. Rev. 77, 160 (1950).

38. L. W. Alvarez, Phys. Rev. 80, 519 (1950).

39. H. J. Martin and A. A. Kraus, Revs. Sci. Instr. (in press).

40. H. J. Martin, Thesis, California Institute of Technology (1956).

41. P. M. Stier, C. F. Barnett, and G. E. Evans, Phys. Rev. 96, 973 (1954); G. A. Dissanaike, Phil. Mag. 43, 1051 (1953).

42. The targets were obtained from the A.E.R.E., Harwell, England.

43. N. P. Heydenburg and G. M. Temmer, Phys. Rev. 104, 123 (1956).

44. J. L. Russell, G. C. Phillips, and C. W. Reich, Phys. Rev. 104, 135 (1956).

45. J. D. Jackson and D. I. Wanklyn, Phys. Rev. 86, 381A (1953).

46. F. D. Goward and J. J. Wilkins, Proc. Phys. Soc. (London) A63, 1171 (1950).

47. R. A. Douglas, J. W. Broer, Ren Chiba, D. F. Herring, and E. A. Silverstein, Phys. Rev. 104, 1059 (1956).

48. D. L. Livesey and C. L. Smith, Proc. Phys. Soc. (London) A66, 689 (1953).

49. T. W. Bonner, J. E. Evans, C. W. Malich, and J. R. Risser, Phys. Rev. 73, 885 (1948).

50. J. A. Wheeler, Phys. Rev. 59, 27 (1941).

51. H. A. Bethe, Rev. Mod. Phys. 9, 218 (1937).

52. P. B. Treacy, Phil. Mag. 44, 325 (1953).

53. R. F. Christy, private communication.

54. K. M. Watson, Phys. Rev. 88, 1163 (1952); V. K. Rasmussen, D. W. Miller, M. B. Sampson, and U. C. Gupta, Phys. Rev. 100, 851 (1955).

55. R. G. Thomas, Phys. Rev. 81, 148 (1951).

56. D. S. Bayley and H. R. Crane, Phys. Rev. 52, 604 (1937).

57. W. F. Hornyak and T. Lauritsen, Phys. Rev. 77, 160 (1950).

58. W. T. Sharp, H. E. Gove, and E. B. Paul, A.E.C.L. Report TPI-70, Chalk River, Canada (1955).

59. W. A. Fowler, R. J. Tuttle, and F. S. Mozer, private communication.

60. R. A. Ferrell and W. M. Visscher, Phys. Rev. 104, 475 (1956); A. Graue, Phil. Mag. 45, 1205 (1954); E. E. Maslin, J. M. Calvert, and A. A. Jaffee, Proc. Phys. Soc. 69A, 754 (1956).

61. M. Goeppert-Mayer, M. Goldhaber, and A. W. Sunyar, "Nuclear Shell Systematics", Beta and Gamma-Ray Spectroscopy, K. Siegbahn, ed., North Holland Pub. Co., Amsterdam (1955).

62. L. H. Rumbaugh, R. B. Roberts, and L. R. Hafstad, Phys. Rev. 54, 657 (1938), Phys. Rev. 51, 1106 (1937).

63. F. Ajzenberg and T. Lauritsen, Rev. Mod. Phys. 27, 77 (1955).

64. F. C. Gilbert, Phys. Rev. 93, 499 (1954); S. Baskin, Phys. Rev. 95, 1012 (1954) and this thesis.

65. R. D. Evans, The Atomic Nucleus, Page 676, McGraw-Hill Book Co., New York (1955).

66. H. L. Jackson, A. I. Galonsky, F. J. Eppling, R. W. Hill, E. Goldberg, and J. R. Cameron, Phys. Rev. 89, 365 (1953).

67. H. J. Martin, private communication.

68. A. B. Lillie, Phys. Rev. 87, 716 (1952); D. L. Livesey, Can. J. Phys. 34, 203 (1956); P.M.S. Blackett and D. S. Lees, Proc. Roy. Soc. (London) A134, 658 (1932).

69. R. W. Kavanagh, private communication.

70. S. A. Moszkowski, "Theory of Multipole Radiation", Beta and Gamma-Ray Spectroscopy, K. Siegbahn, ed., North Holland Pub. Co., Amsterdam (1955).

71. J. H. Fregeau, Phys. Rev. 104, 225 (1956); J. R. Oppenheimer and J. S. Schwinger, Phys. Rev. 56, 1066 (1939).

72. D. H. Wilkinson, AECL Report PD-260, Chalk River, Canada (1955).

73. R. A. Ferrell, private communication.

74. R. G. Herb, S. C. Snowden, and O. Sala, Phys. Rev. 75, 246 (1949).

75. F. Bumiller and H. H. Staub, Hel. Phys. Acta 28, 355 (1955).

76. F. S. Mozer, Ph.D. Thesis, California Institute of Technology (1956).

77. R. R. Carlson, Phys. Rev. 84, 749 (1951).

78. K. W. Jones, D. J. Donahue, M. T. McEllistrem, R. A. Douglas, and H. T. Richards, Phys. Rev. 91, 879 (1953).

79. J. A. Neuendorffer, D. R. Inglis and S. S. Hanna, Phys. Rev. 82, 75 (1951).

80. A. B. Brown, C. W. Snyder, W. A. Fowler and C. C. Lauritsen, Phys. Rev. 82, 159 (1951).

81. D. M. Van Patter and Ward Whaling, Revs. Mod. Phys. 26, 402 (1954).

82. R. Fuchs and W. Whaling, unpublished.

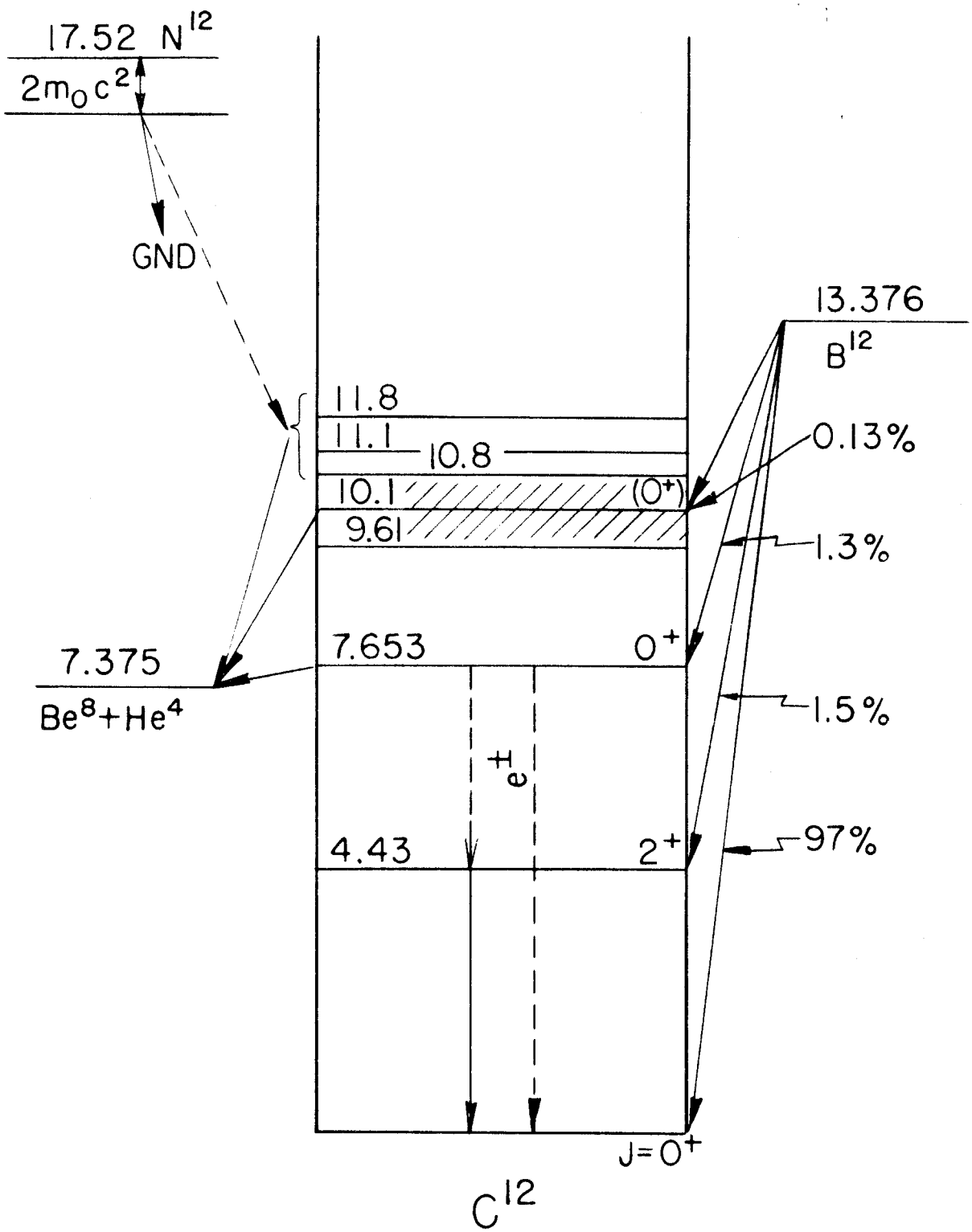
17.52 N12
2m0c2
GND
13.376
B12
0.13%
11.8
11.1
10.8
10.1
(0+)
9.61
1.3%
7.375
Be8+He4
7.653
0+
1.5%
+
e
4.43
2+
97%
J=0+
C12

FIGURE 1

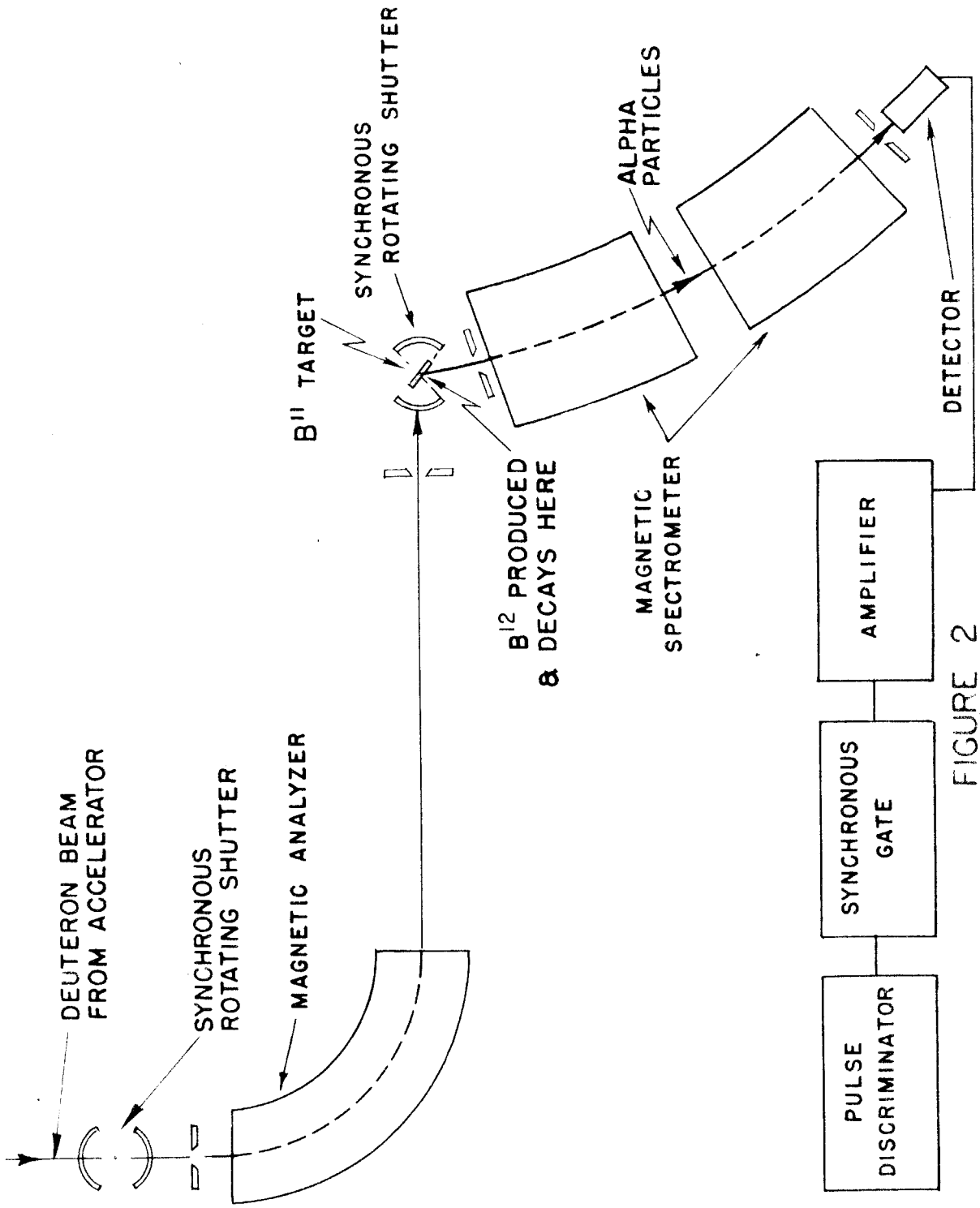
DEUTERON BEAM FROM ACCELERATOR
SYNCHRONOUS ROTATING SHUTTER
MAGNETIC ANALYZER
B11 TARGET
SYNCHRONOUS ROTATING SHUTTER
B12 PRODUCED & DECAYS HERE
MAGNETIC SPECTROMETER
ALPHA PARTICLES
DETECTOR
AMPLIFIER
SYNCHRONOUS GATE
PULSE DISCRIMINATOR

FIGURE 2

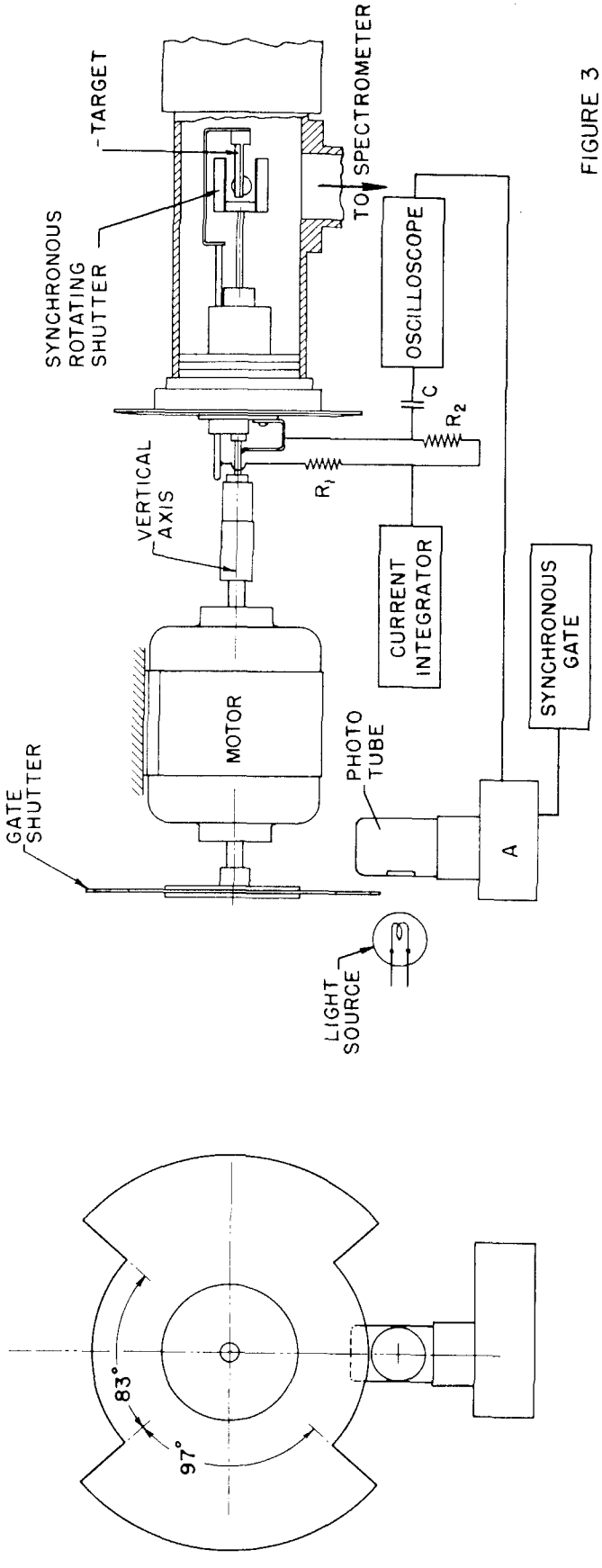
TARGET
SYNCHRONOUS ROTATING SHUTTER
TO SPECTROMETER
OSCILLOSCOPE
C
R2
R1
VERTICAL AXIS
CURRENT INTEGRATOR
SYNCHRONOUS GATE
MOTOR
PHOTO TUBE
A
GATE SHUTTER
LIGHT SOURCE
83°
97°

FIGURE 3

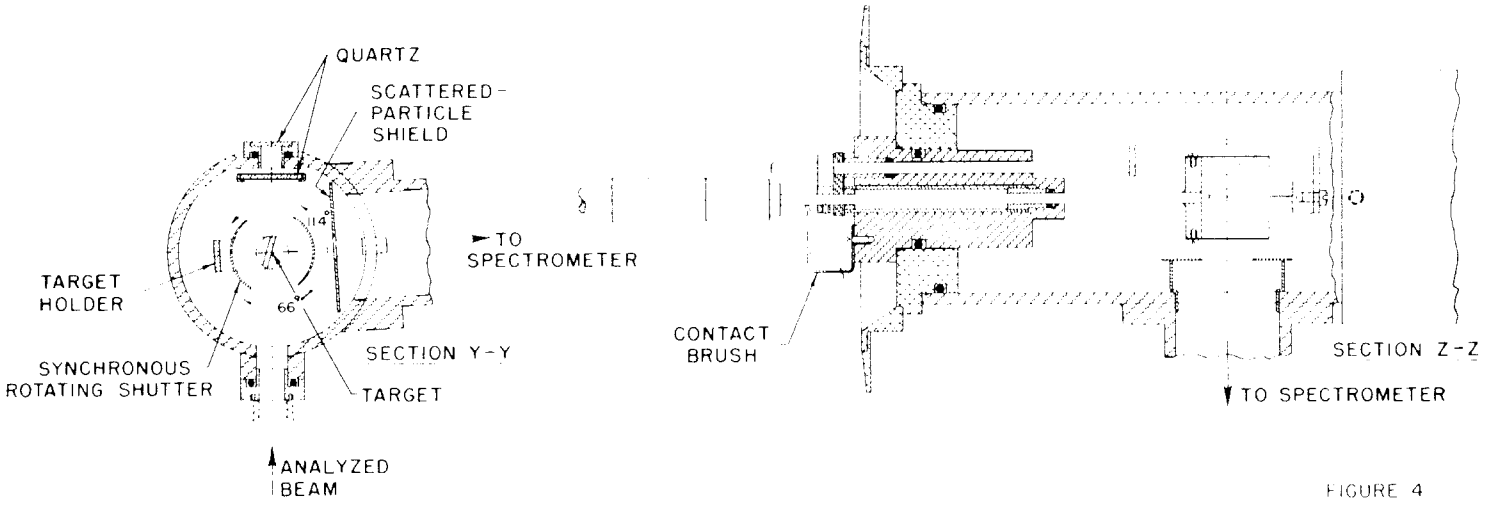
QUARTZ
SCATTERED-PARTICLE SHIELD
TO SPECTROMETER
TARGET HOLDER
66°
SECTION Y-Y
SYNCHRONOUS ROTATING SHUTTER
TARGET
ANALYZED BEAM
CONTACT BRUSH
SECTION Z-Z
TO SPECTROMETER

FIGURE 4

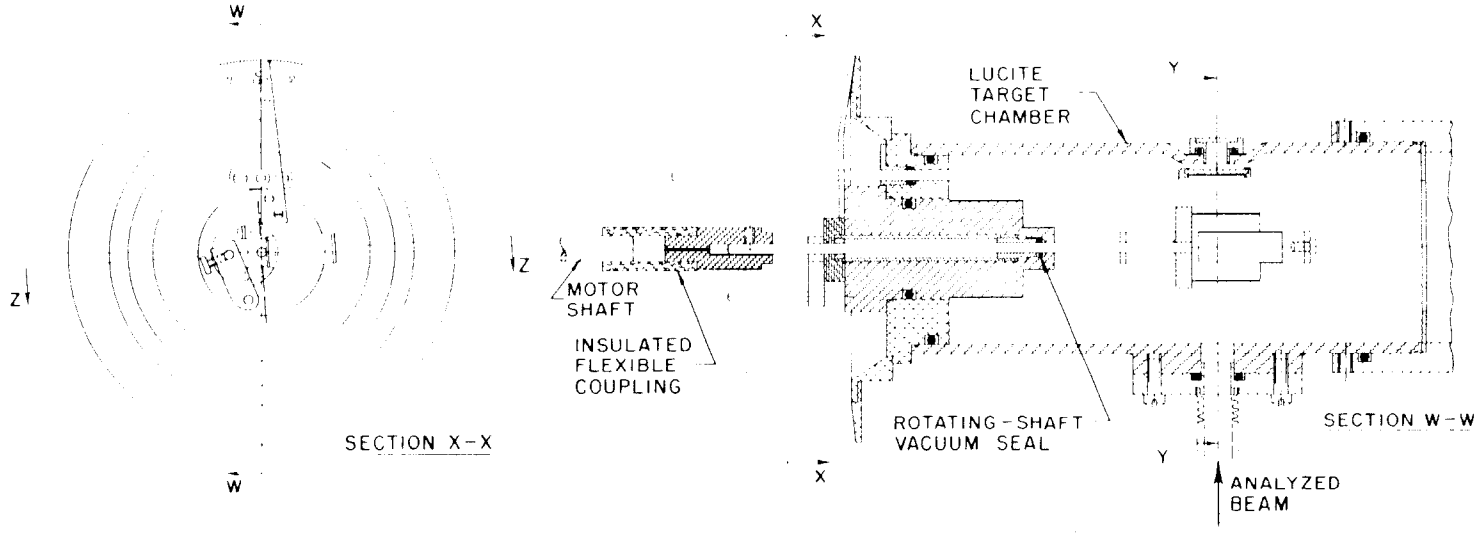
W
Z
SECTION X-X
W
Z
MOTOR SHAFT
INSULATED FLEXIBLE COUPLING
X
Y
LUCITE TARGET CHAMBER
ROTATING-SHAFT VACUUM SEAL
SECTION W-W
Y
X
ANALYZED BEAM

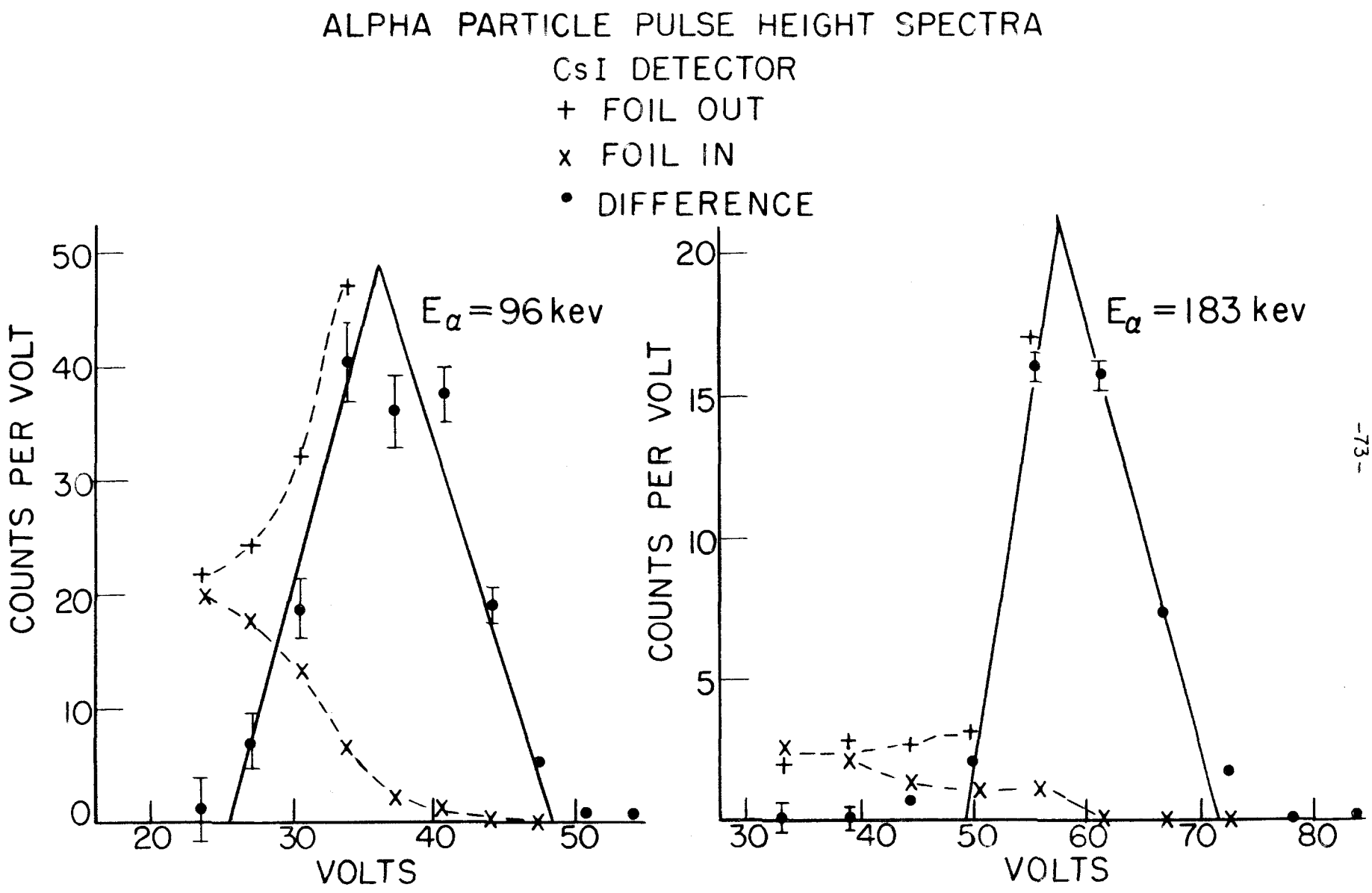
ALPHA PARTICLE PULSE HEIGHT SPECTRA
CsI DETECTOR
+ FOIL OUT
x FOIL IN
• DIFFERENCE
COUNTS PER VOLT
VOLTS
E_α = 96 kev
E_α = 183 kev
0
10
20
30
40
50
5
15
60
70
80

FIGURE 5

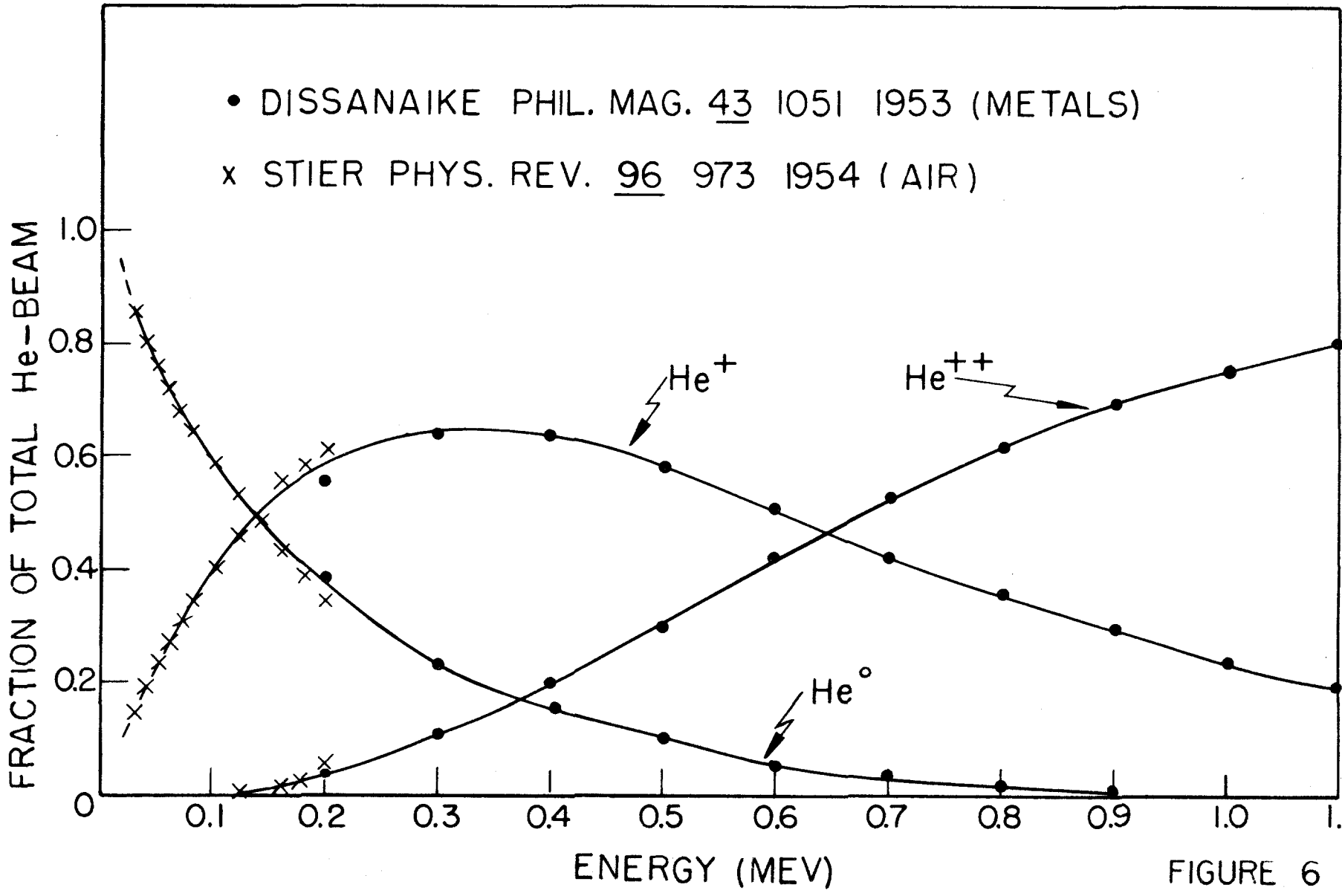
• DISSANAIKE PHIL. MAG. 43 1051 1953 (METALS)
x STIER PHYS. REV. 96 973 1954 (AIR)
FRACTION OF TOTAL He-BEAM
1.0
0.8
0.6
0.4
0.2
0
He+
He++
He°
0.1
0.2
0.3
0.4
0.5
0.6
0.7
0.8
0.9
1.0
1.1
ENERGY (MEV)

FIGURE 6

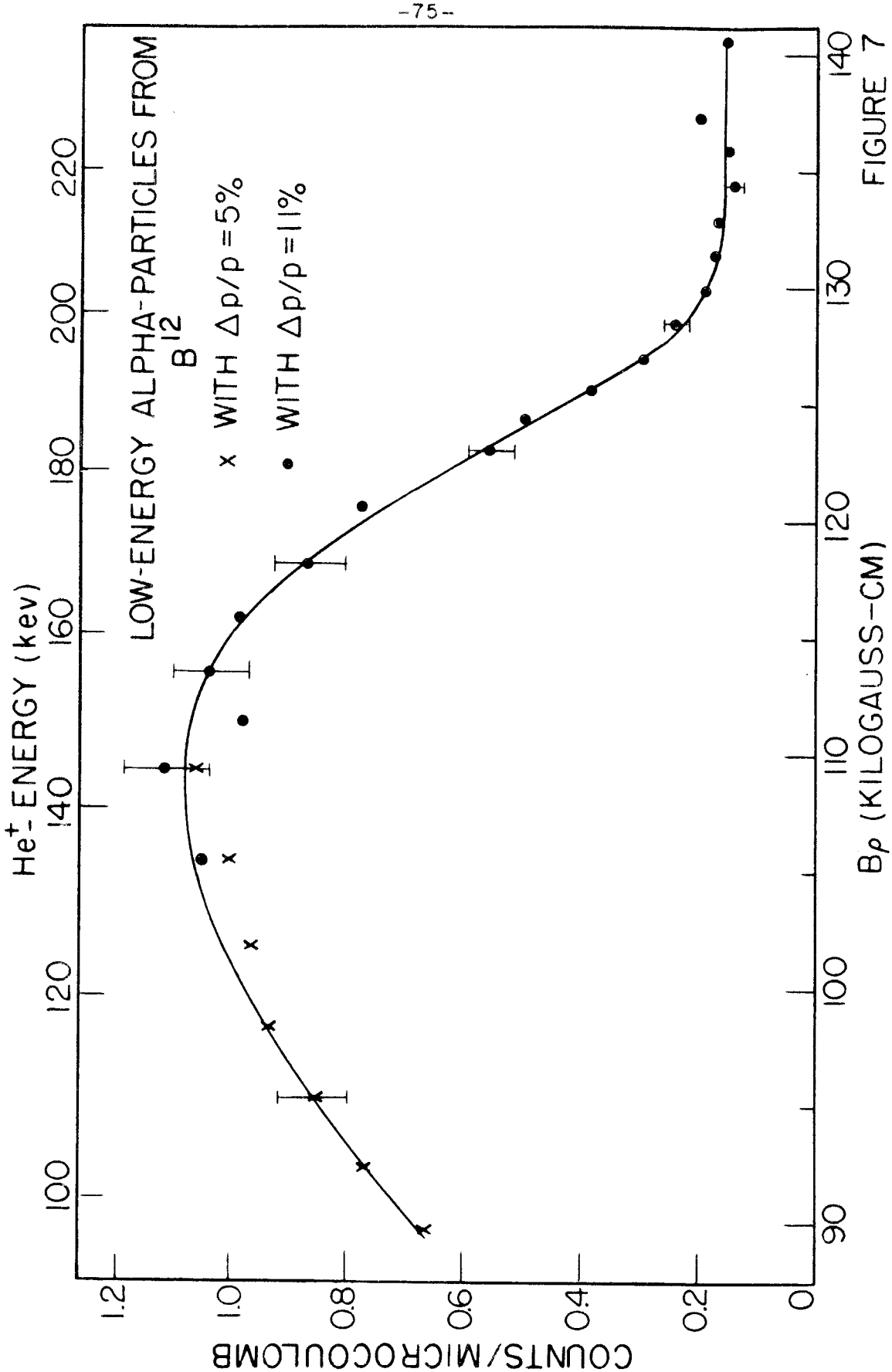
LOW-ENERGY ALPHA-PARTICLES FROM B12
x WITH Δp/p = 5%
• WITH Δp/p = 11%
He+ ENERGY (kev)
100
120
140
160
180
200
220
COUNTS/MICROCOULOMB
0
0.2
0.4
0.6
0.8
1.0
1.2
90
100
110
120
130
140
Bρ (KILOGAUSS-CM)

FIGURE 7

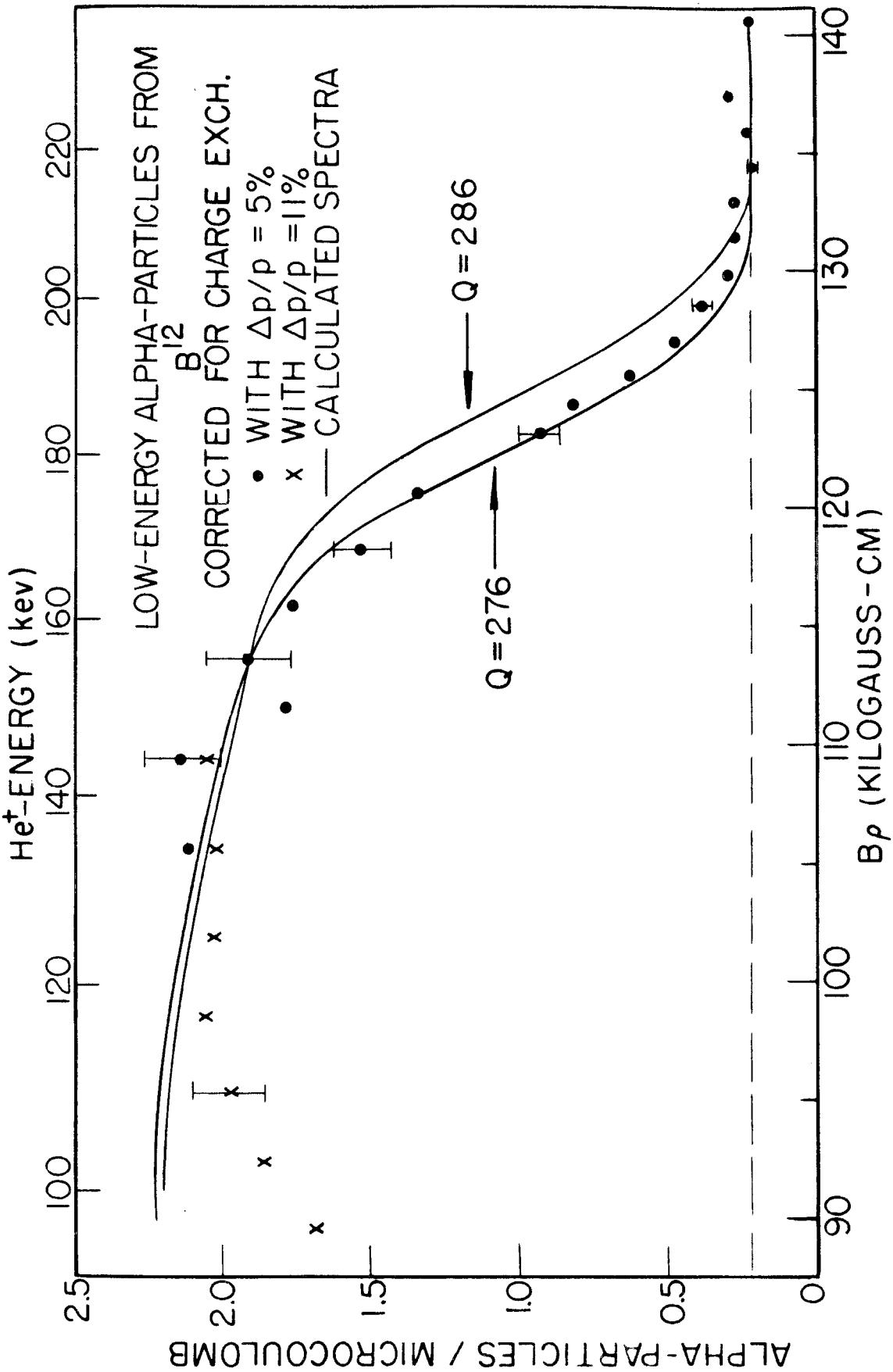
LOW-ENERGY ALPHA-PARTICLES FROM B12
CORRECTED FOR CHARGE EXCH.
• WITH Δp/p = 5%
x WITH Δp/p = 11%
— CALCULATED SPECTRA
Q=286
Q=276
He+-ENERGY (kev)
Bρ (KILOGAUSS-CM)
ALPHA-PARTICLES / MICROCOULOMB
100
120
140
160
180
200
220
90
100
110
120
130
140
0
0.5
1.0
1.5
2.0
2.5

FIGURE 8

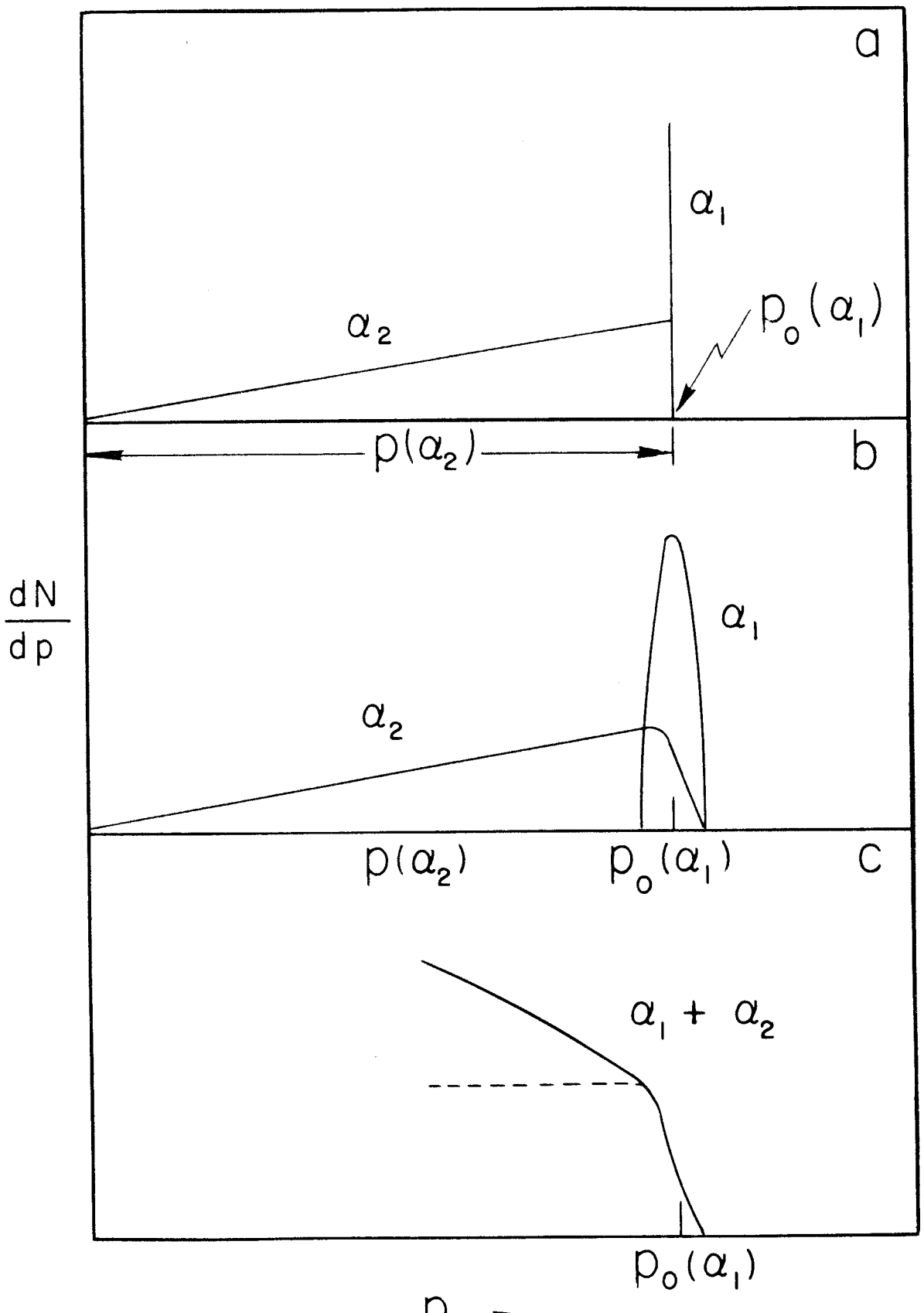
a
α_1
α_2
$p_o(\alpha_1)$
$p(\alpha_2)$
b
$\frac{dN}{dp}$
α_1
α_2
$p(\alpha_2)$
$p_o(\alpha_1)$
c
$\alpha_1 + \alpha_2$
$p_o(\alpha_1)$
p →

FIGURE 9

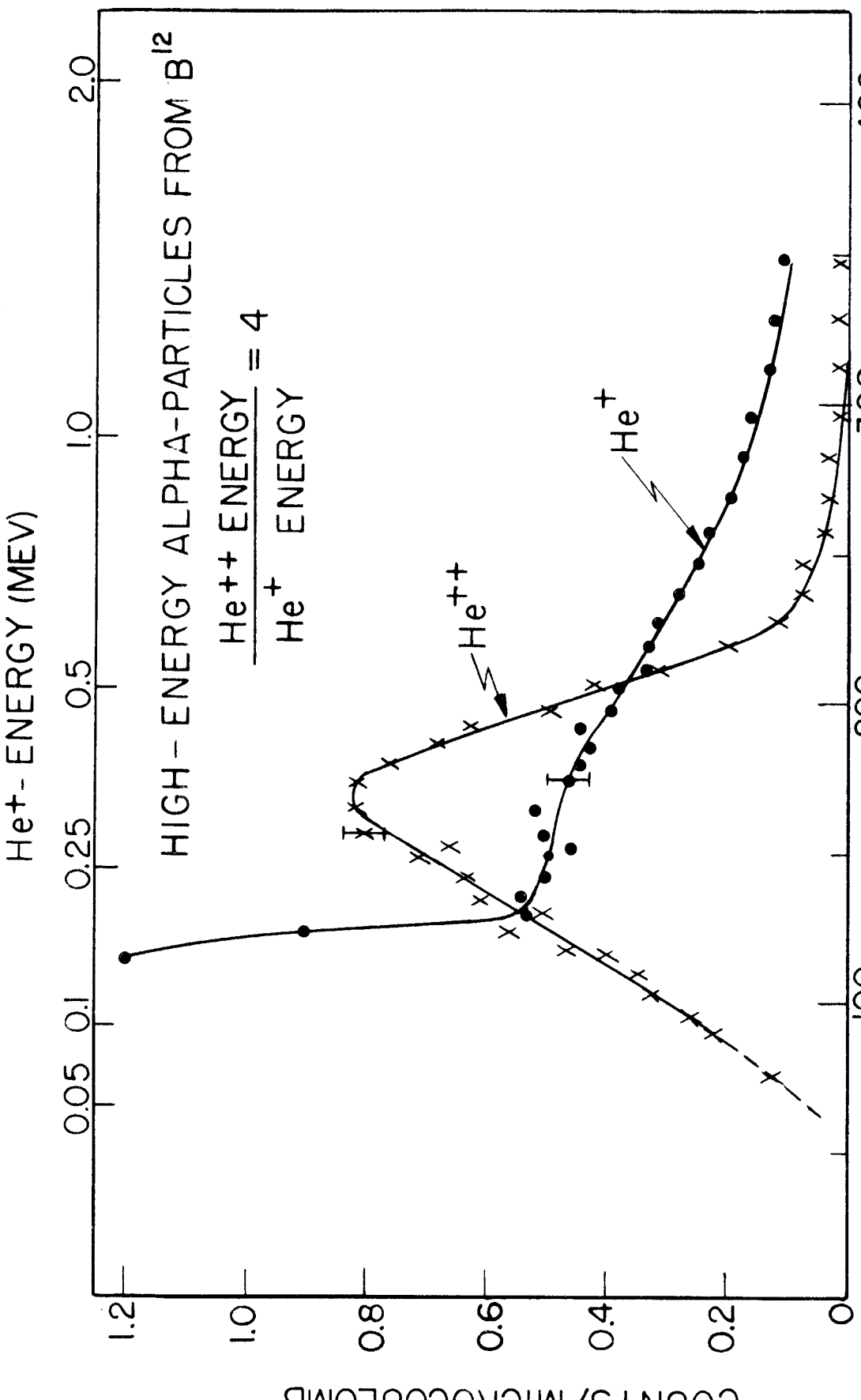
HIGH-ENERGY ALPHA-PARTICLES FROM B^{12}
$\frac{He^{++}\ ENERGY}{He^{+}\ ENERGY} = 4$
He^{++}
He^{+}
He^{+}- ENERGY (MEV)
0.05
0.1
0.25
0.5
1.0
2.0
COUNTS/MICROCOULOMB
0
0.2
0.4
0.6
0.8
1.0
1.2
100
200
300
400
$B\rho$ (KILOGAUSS-CM)
x1

FIGURE 10

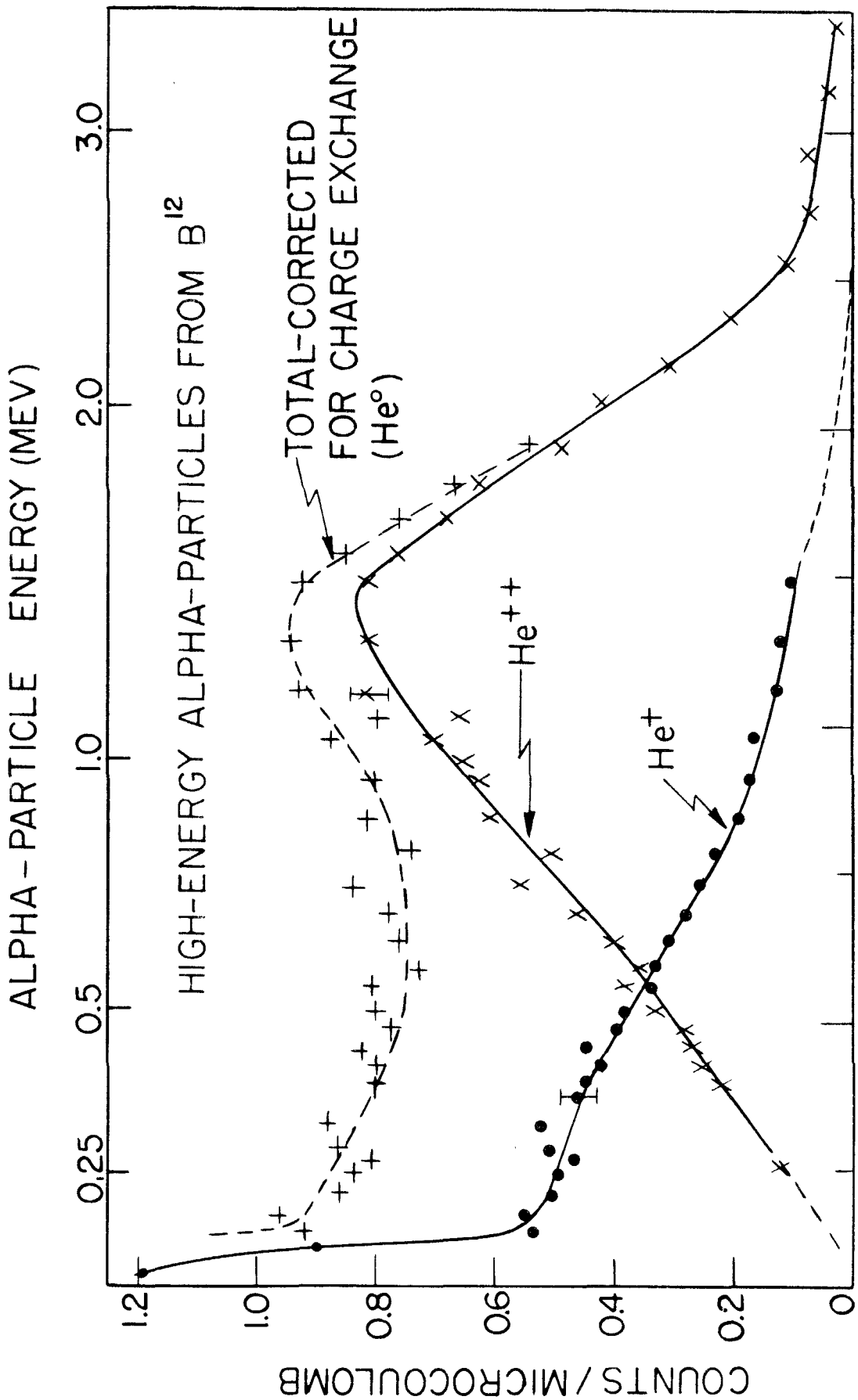
ALPHA-PARTICLE ENERGY (MEV)
0.25
0.5
1.0
2.0
3.0
HIGH-ENERGY ALPHA-PARTICLES FROM B^{12}
TOTAL-CORRECTED FOR CHARGE EXCHANGE (He^0)
He^{++}
He^{+}
COUNTS / MICROCOULOMB
1.2
1.0
0.8
0.6
0.4
0.2
0
200
300
400
500
$zB\rho$ (KILOGAUSS-CM)

FIGURE 11

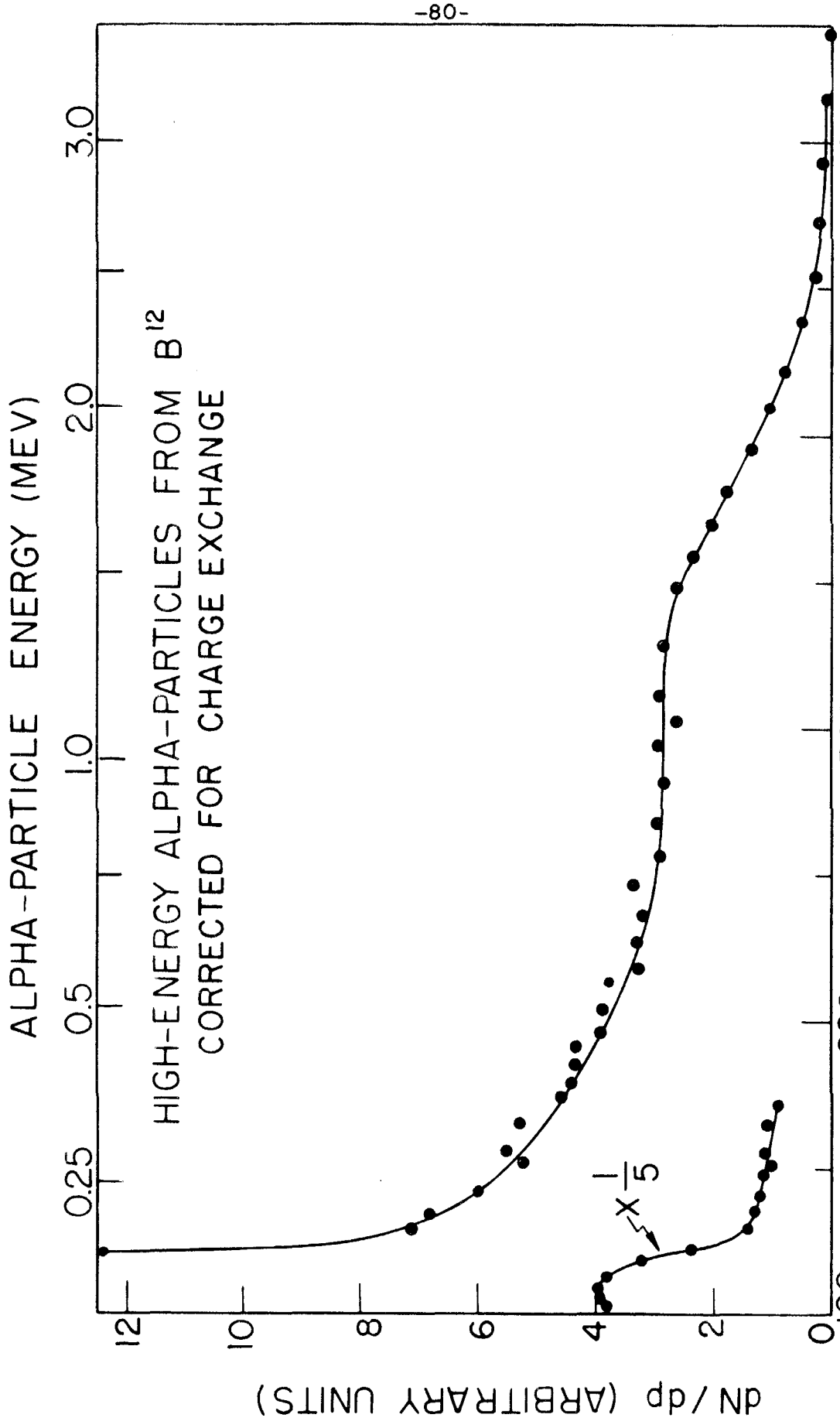
ALPHA-PARTICLE ENERGY (MEV)
0.25
0.5
1.0
2.0
3.0
HIGH-ENERGY ALPHA-PARTICLES FROM B12
CORRECTED FOR CHARGE EXCHANGE
X 1/5
dN/dp (ARBITRARY UNITS)
0
2
4
6
8
10
12
100
200
300
400
500
zBρ (KILOGAUSS-CM)

FIGURE 12

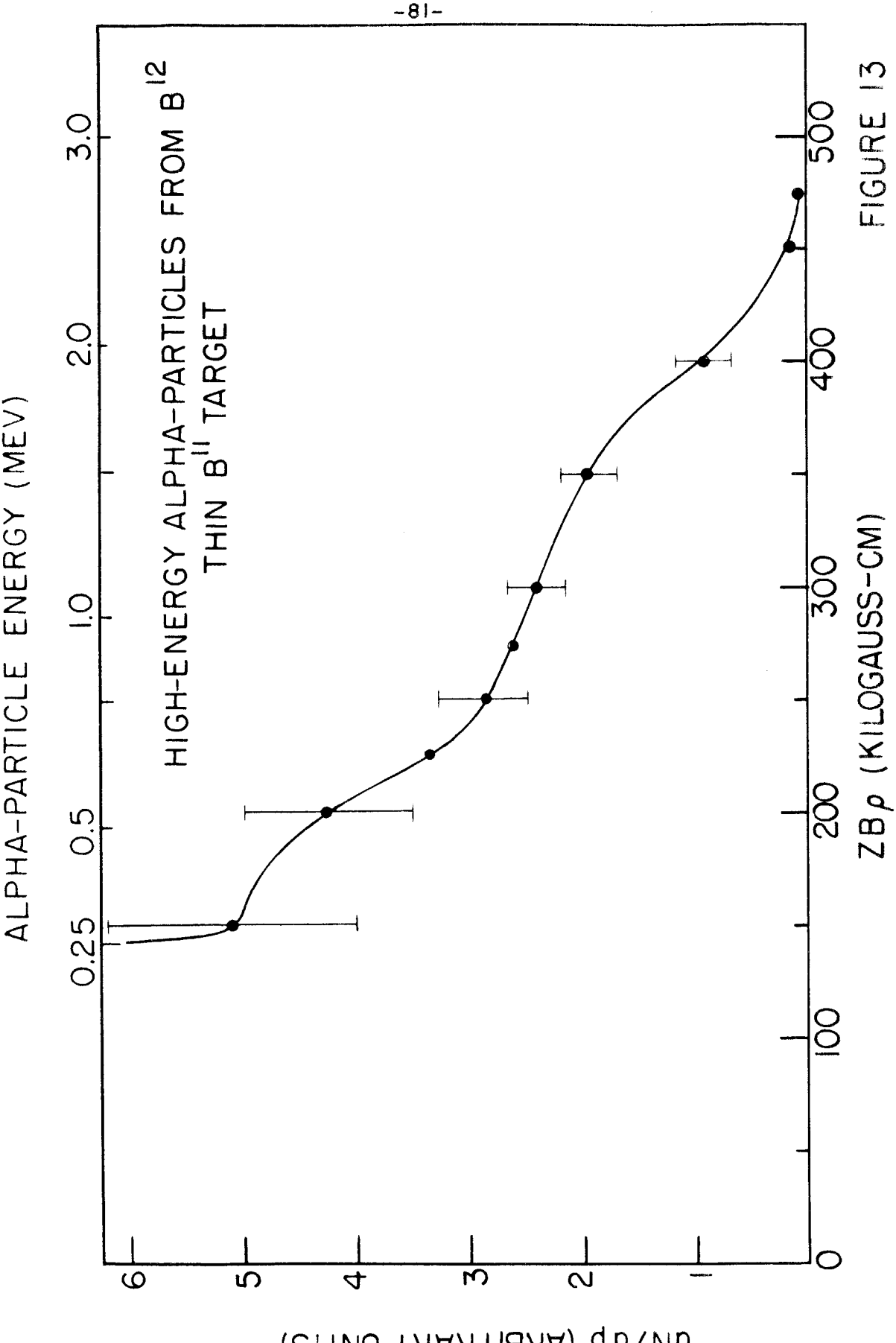
HIGH-ENERGY ALPHA-PARTICLES FROM B^{12}
THIN B^{11} TARGET
ALPHA-PARTICLE ENERGY (MEV)
0.25
0.5
1.0
2.0
3.0
dN/dp (ARBITRARY UNITS)
1
2
3
4
5
6
0
100
200
300
400
500
ZBp (KILOGAUSS-CM)

FIGURE 13

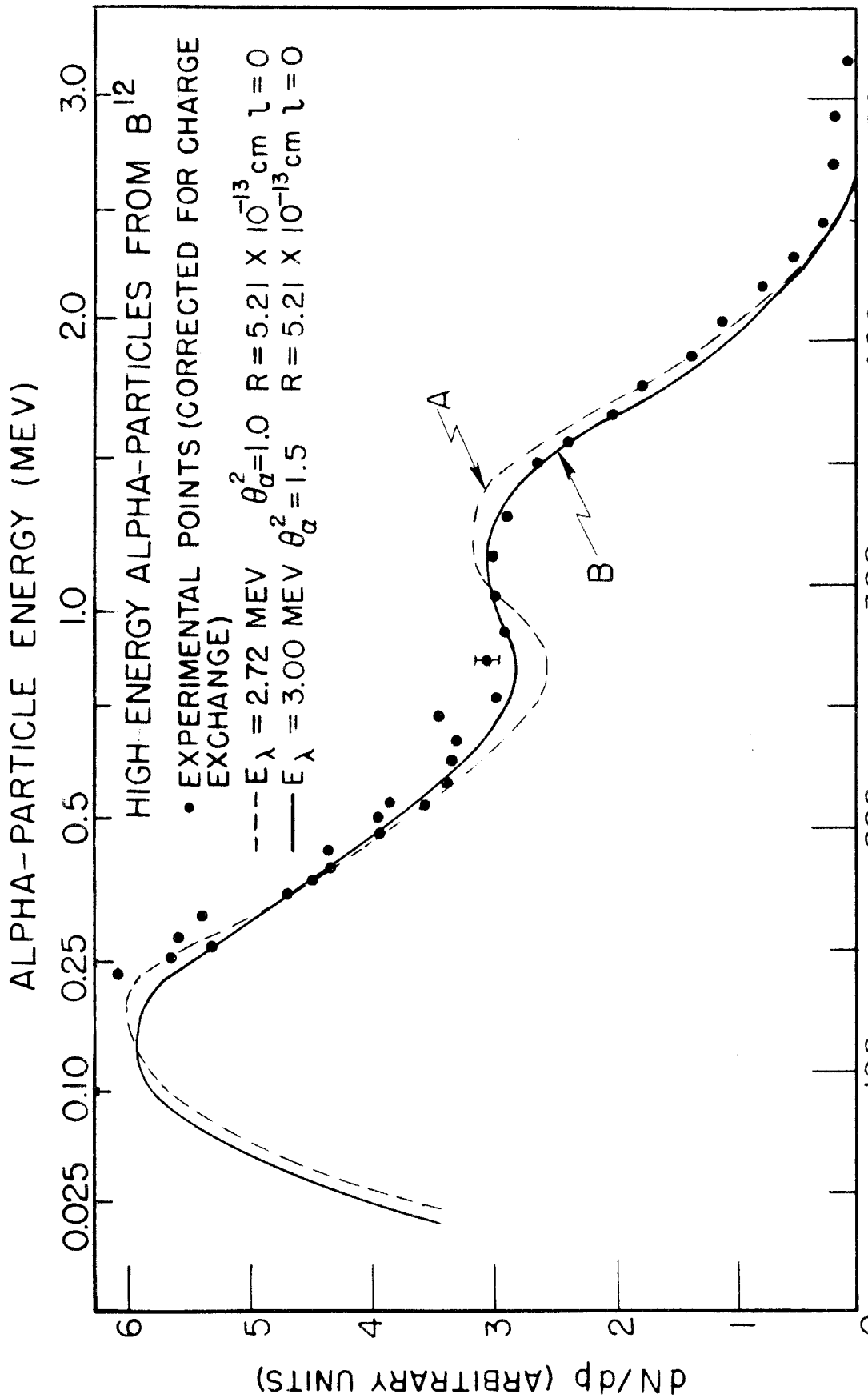
HIGH-ENERGY ALPHA-PARTICLES FROM B^{12}
• EXPERIMENTAL POINTS (CORRECTED FOR CHARGE EXCHANGE)
- - - E_λ = 2.72 MEV θ_α^2=1.0 R = 5.21 X 10^{-13} cm l = 0
—— E_λ = 3.00 MEV θ_α^2=1.5 R = 5.21 X 10^{-13} cm l = 0
A
B
ALPHA-PARTICLE ENERGY (MEV)
0.025
0.10
0.25
0.5
1.0
2.0
3.0
dN/dp (ARBITRARY UNITS)
0
1
2
3
4
5
6
zBρ (KILOGAUSS-CM)
100
200
300
400
500

FIGURE 14

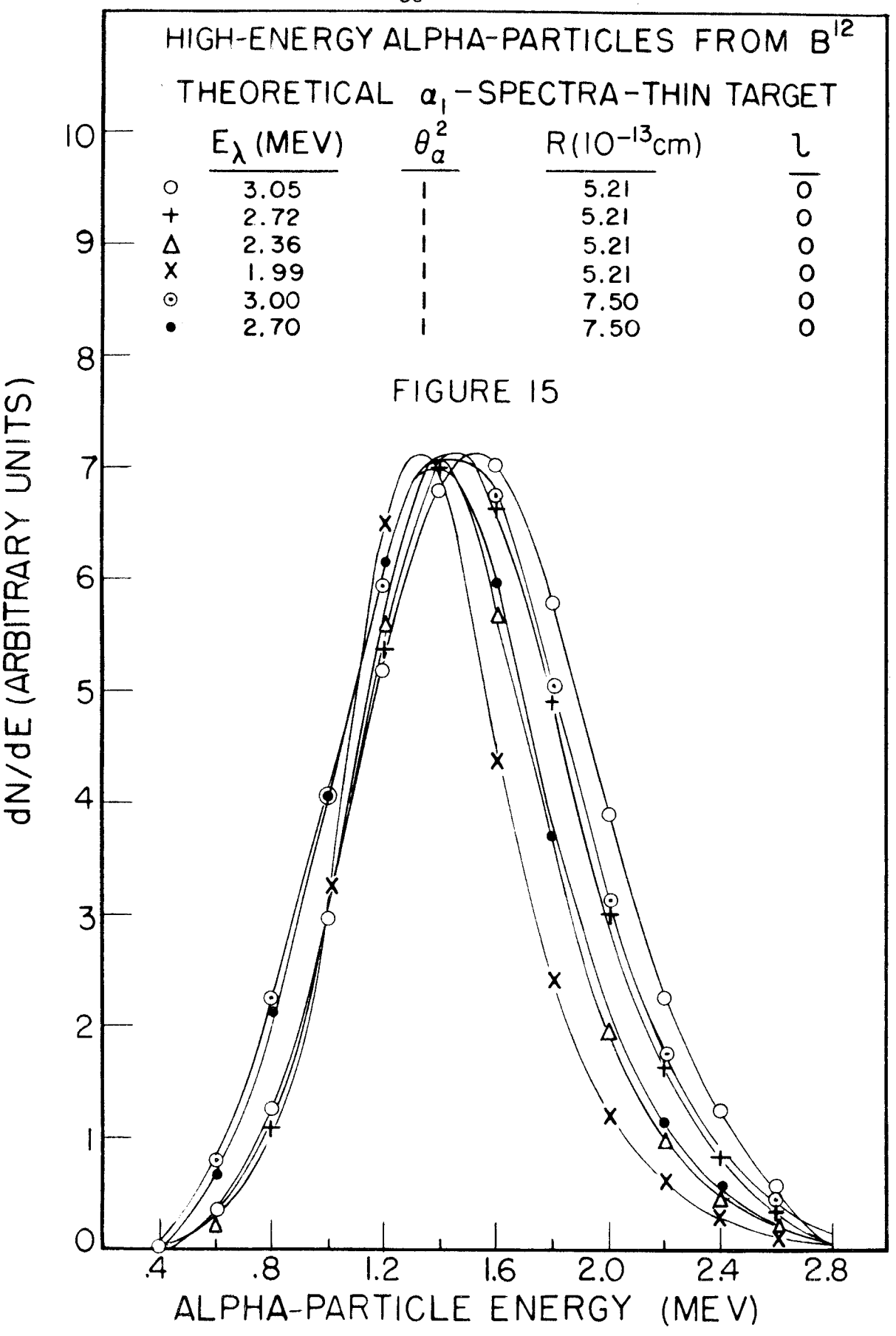
HIGH-ENERGY ALPHA-PARTICLES FROM B^{12}
THEORETICAL α_1 - SPECTRA - THIN TARGET
E_λ (MEV) θ_α^2 R(10^{-13}cm) l
○ 3.05 1 5.21 0
+ 2.72 1 5.21 0
Δ 2.36 1 5.21 0
X 1.99 1 5.21 0
⊙ 3.00 1 7.50 0
● 2.70 1 7.50 0
dN/dE (ARBITRARY UNITS)
0
1
2
3
4
5
6
7
8
9
10
.4
.8
1.2
1.6
2.0
2.4
2.8
ALPHA-PARTICLE ENERGY (MEV)

FIGURE 15

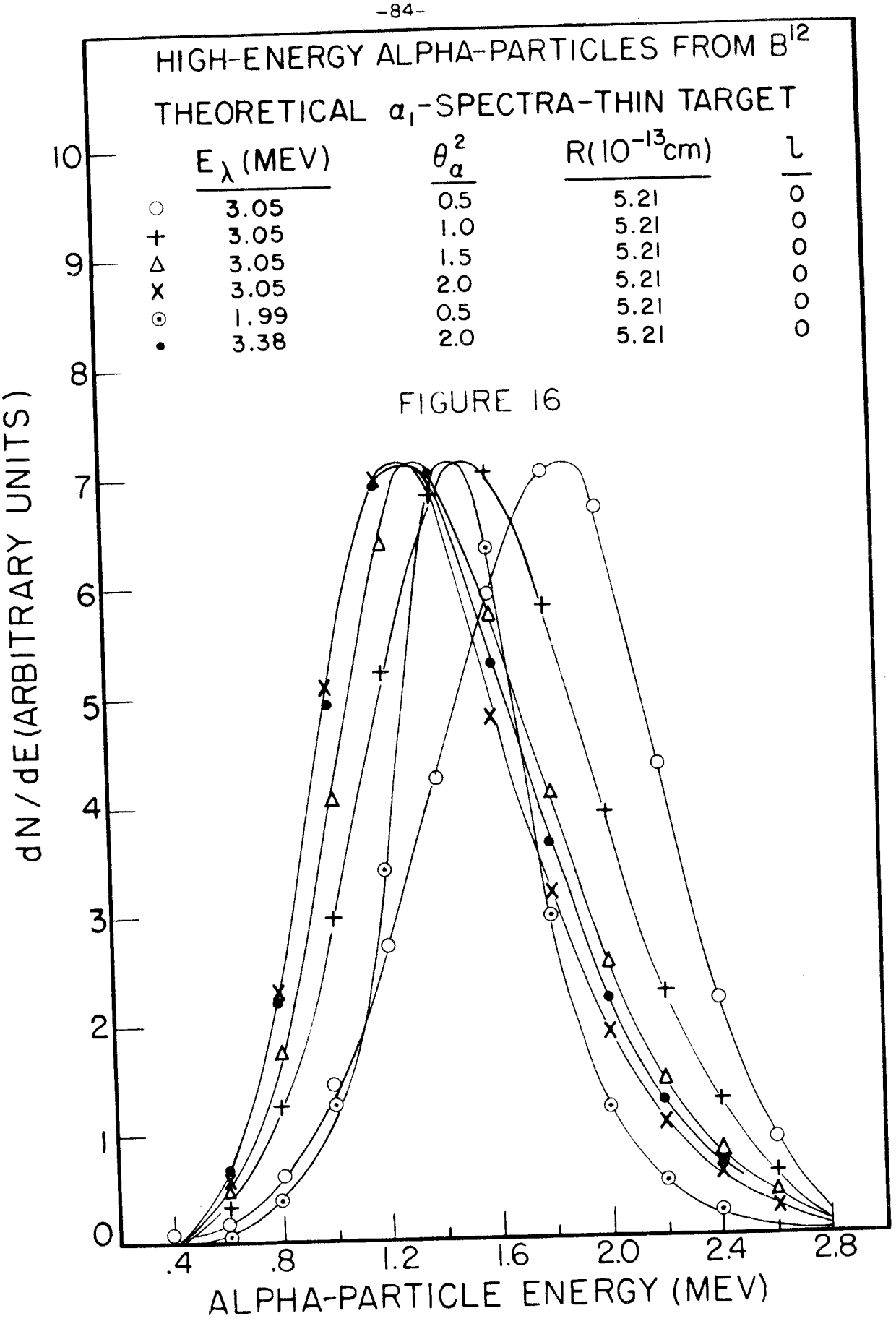
HIGH-ENERGY ALPHA-PARTICLES FROM B12
THEORETICAL α1-SPECTRA-THIN TARGET
Eλ (MEV) θα2 R(10-13cm) l
○ 3.05 0.5 5.21 0
+ 3.05 1.0 5.21 0
△ 3.05 1.5 5.21 0
X 3.05 2.0 5.21 0
⊙ 1.99 0.5 5.21 0
• 3.38 2.0 5.21 0
dN/dE (ARBITRARY UNITS)
0
1
2
3
4
5
6
7
8
9
10
.4
.8
1.2
1.6
2.0
2.4
2.8
ALPHA-PARTICLE ENERGY (MEV)

FIGURE 16

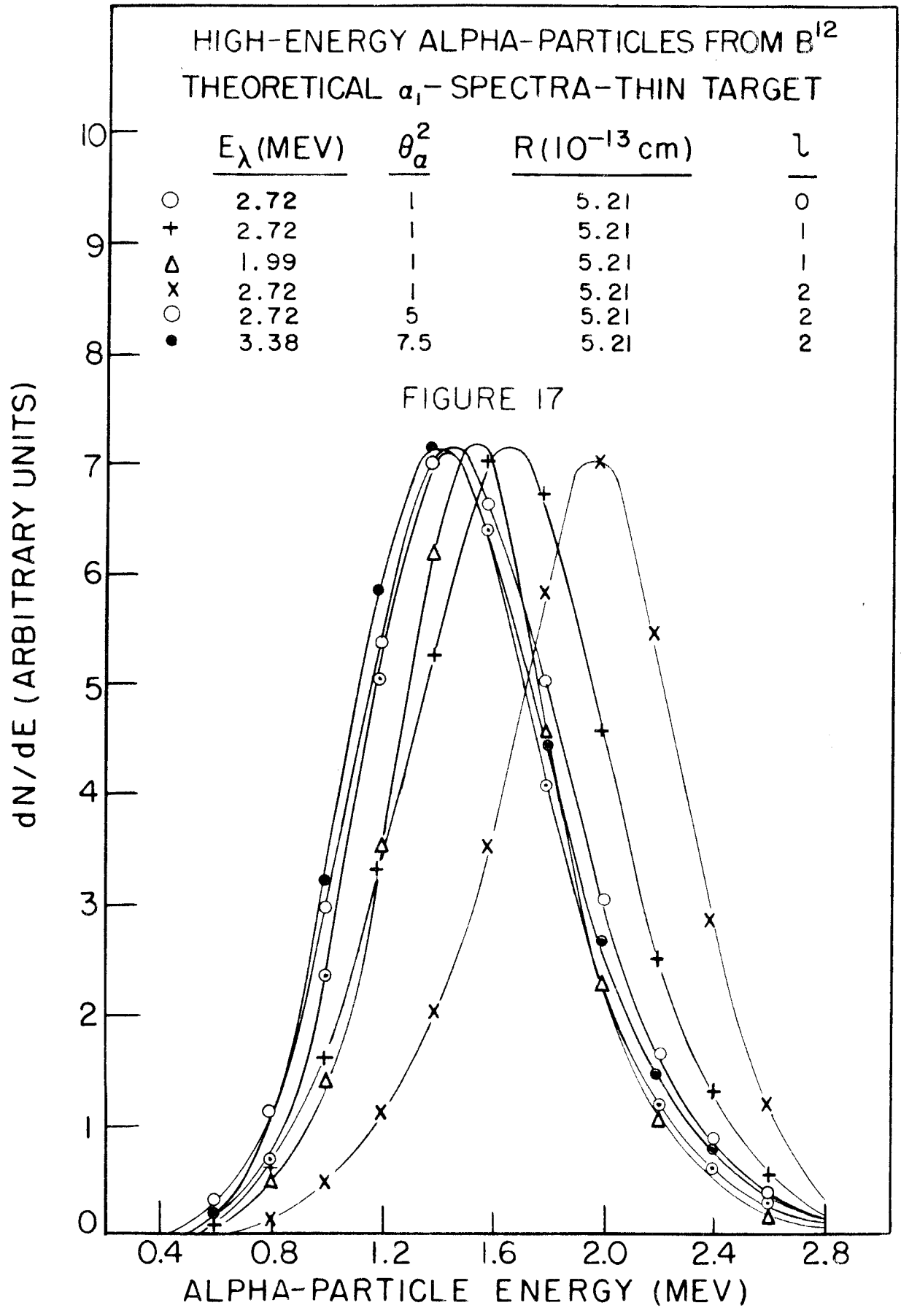
HIGH-ENERGY ALPHA-PARTICLES FROM B12
THEORETICAL α1 – SPECTRA – THIN TARGET
Eλ (MEV) θα2 R (10-13 cm) l
○ 2.72 1 5.21 0
+ 2.72 1 5.21 1
Δ 1.99 1 5.21 1
x 2.72 1 5.21 2
○ 2.72 5 5.21 2
● 3.38 7.5 5.21 2
FIGURE 17
dN/dE (ARBITRARY UNITS)
0
1
2
3
4
5
6
7
8
9
10
0.4
0.8
1.2
1.6
2.0
2.4
2.8
ALPHA-PARTICLE ENERGY (MEV)

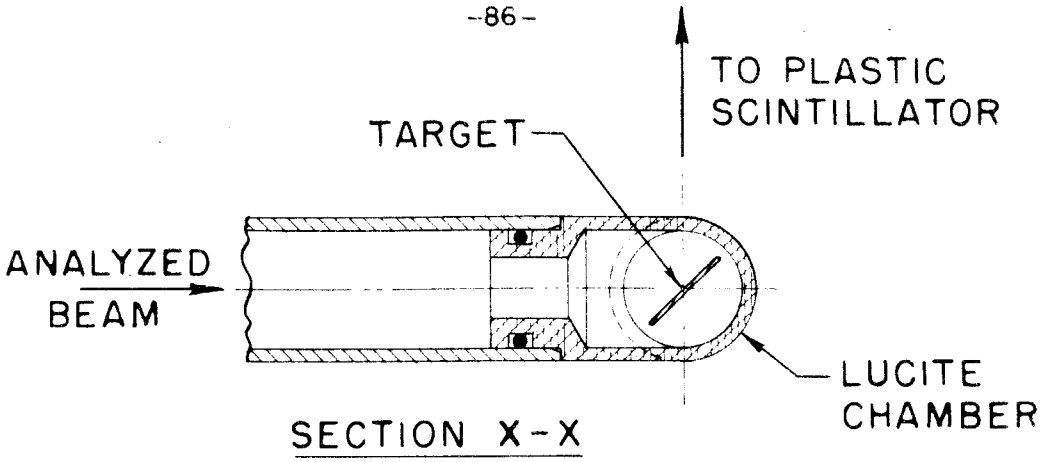
TO PLASTIC
SCINTILLATOR
TARGET
ANALYZED
BEAM
LUCITE
CHAMBER
SECTION X-X

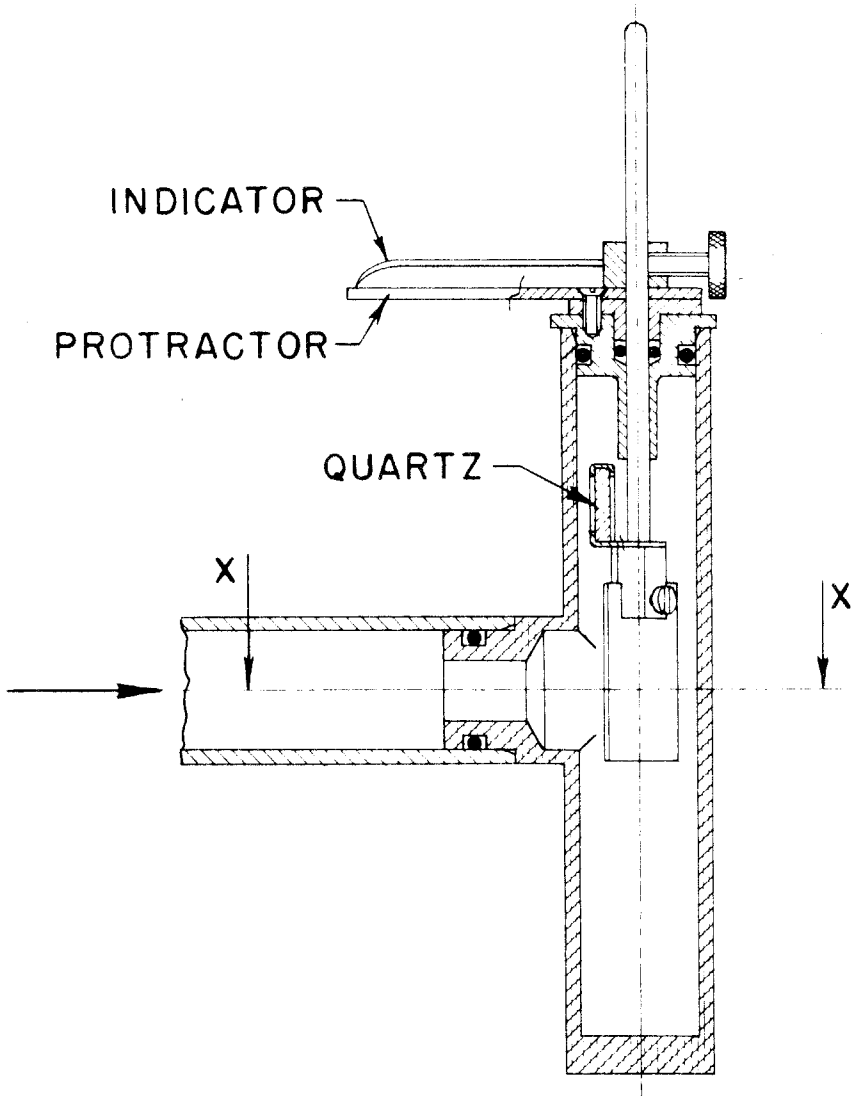
INDICATOR
PROTRACTOR
QUARTZ
X
X

FIGURE 18

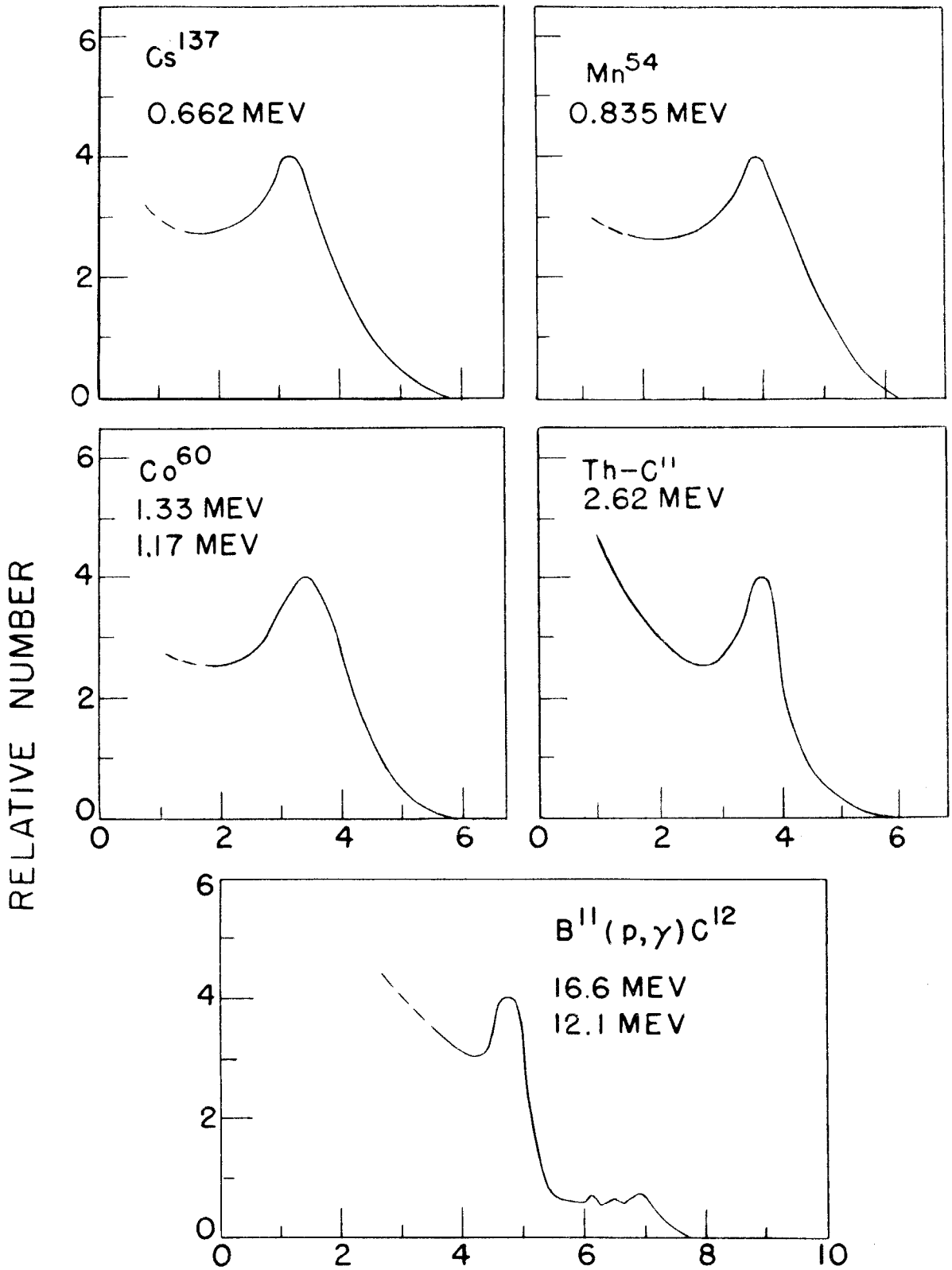
Cs137
0.662 MEV
Mn54
0.835 MEV
Co60
1.33 MEV
1.17 MEV
Th-C''
2.62 MEV
B11(p,γ)C12
16.6 MEV
12.1 MEV
RELATIVE NUMBER
PULSE HEIGHT (ARBITRARY UNITS)

FIGURE 19

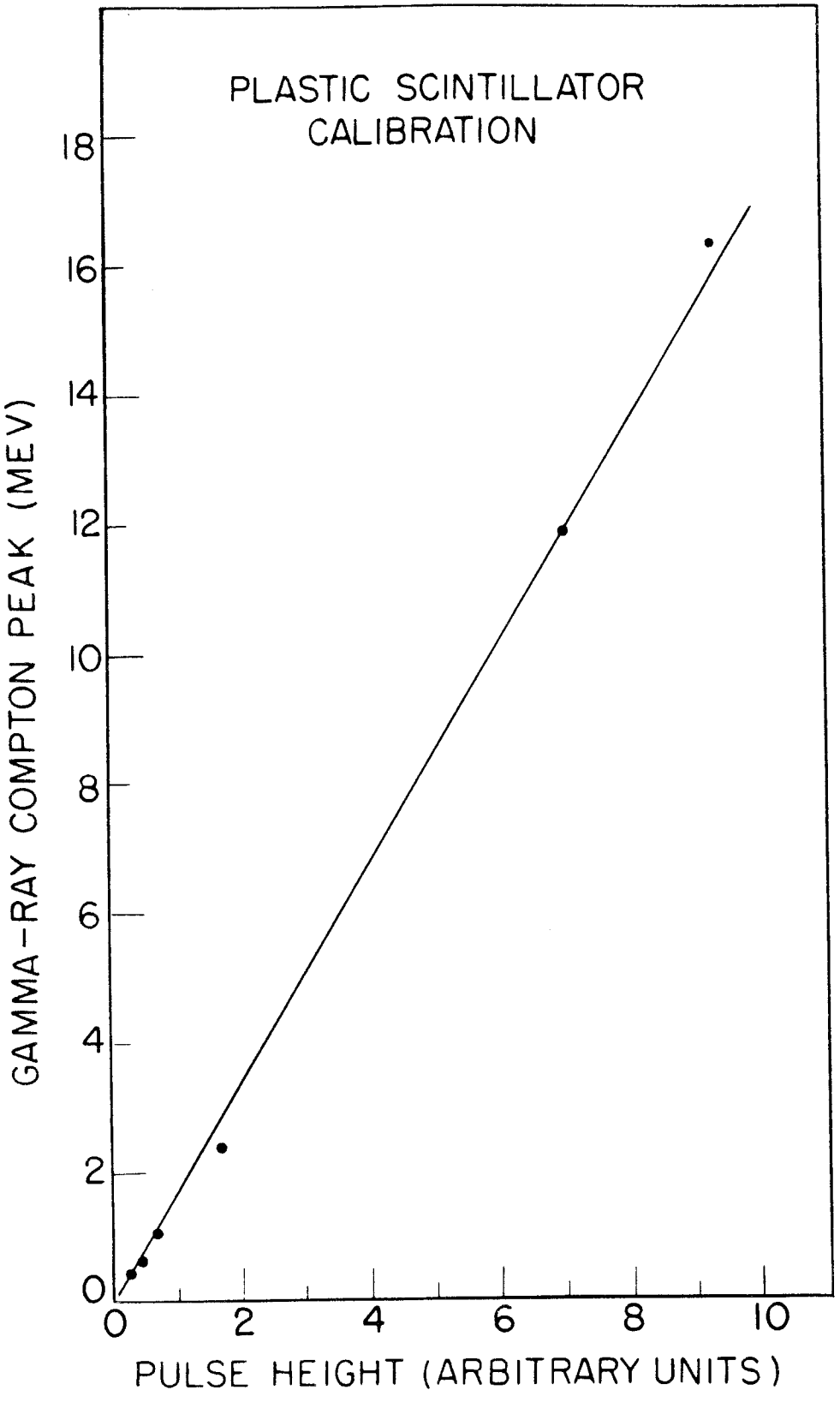
PLASTIC SCINTILLATOR
CALIBRATION
GAMMA-RAY COMPTON PEAK (MEV)
0
2
4
6
8
10
12
14
16
18
0
2
4
6
8
10
PULSE HEIGHT (ARBITRARY UNITS)

FIGURE 20

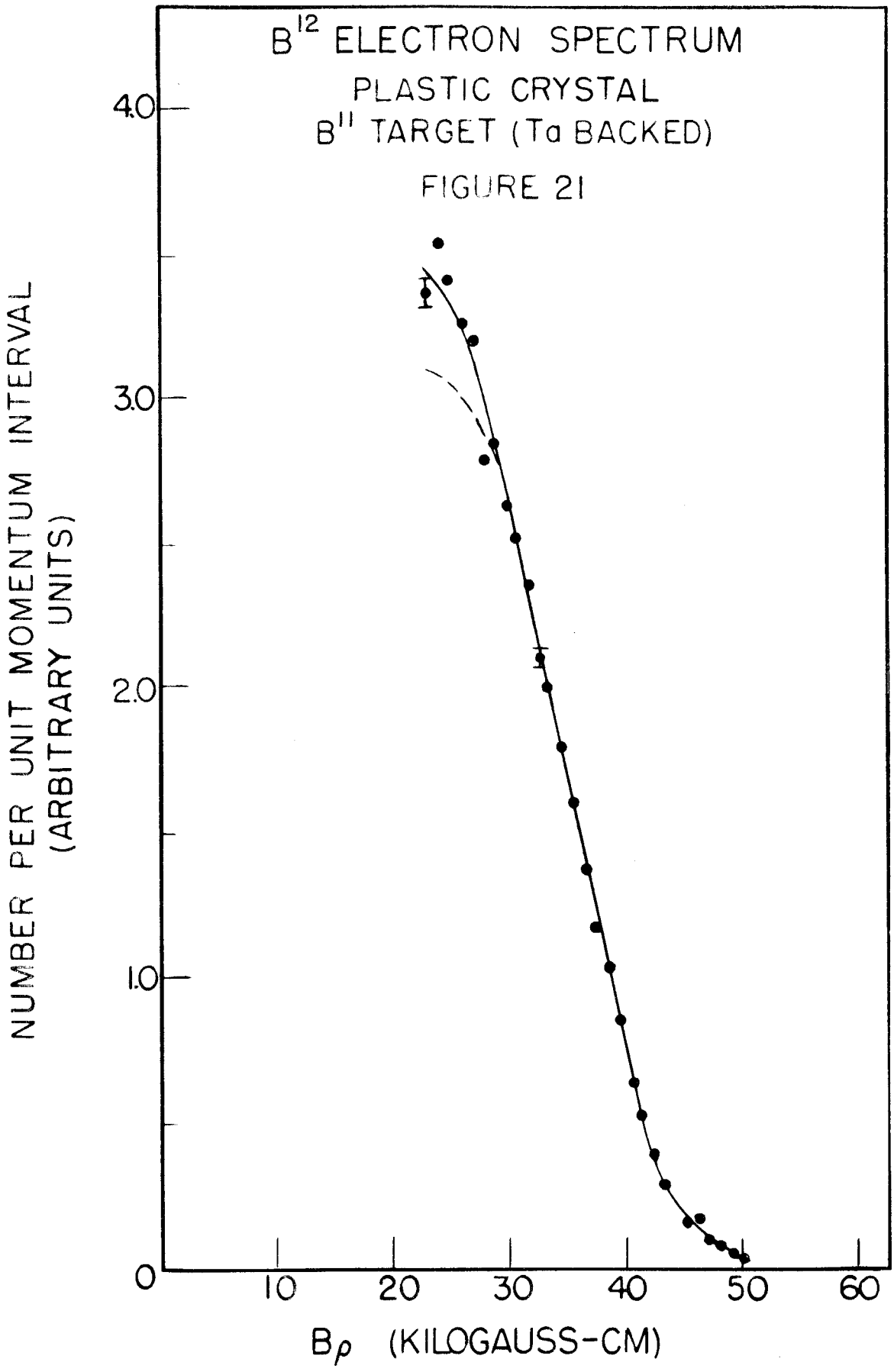
B12 ELECTRON SPECTRUM
PLASTIC CRYSTAL
B11 TARGET (Ta BACKED)
FIGURE 21
NUMBER PER UNIT MOMENTUM INTERVAL
(ARBITRARY UNITS)
4.0
3.0
2.0
1.0
0
10
20
30
40
50
60
Bρ (KILOGAUSS-CM)

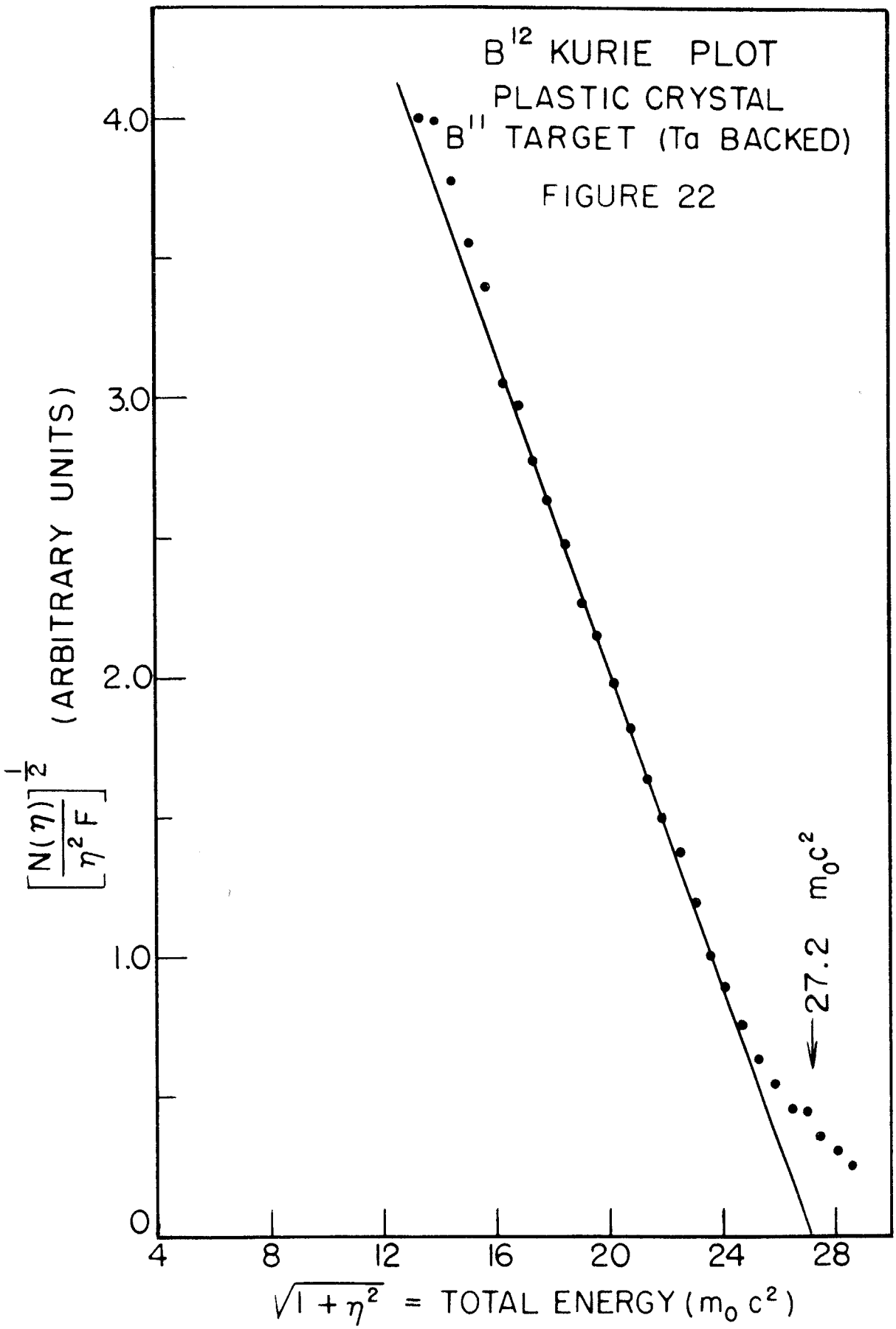
B12 KURIE PLOT
PLASTIC CRYSTAL
B11 TARGET (Ta BACKED)
FIGURE 22
4.0
3.0
2.0
1.0
0
4
8
12
16
20
24
28
27.2 m0c2
[N(η)/η2F]1/2 (ARBITRARY UNITS)
√1+η2 = TOTAL ENERGY (m0 c2)

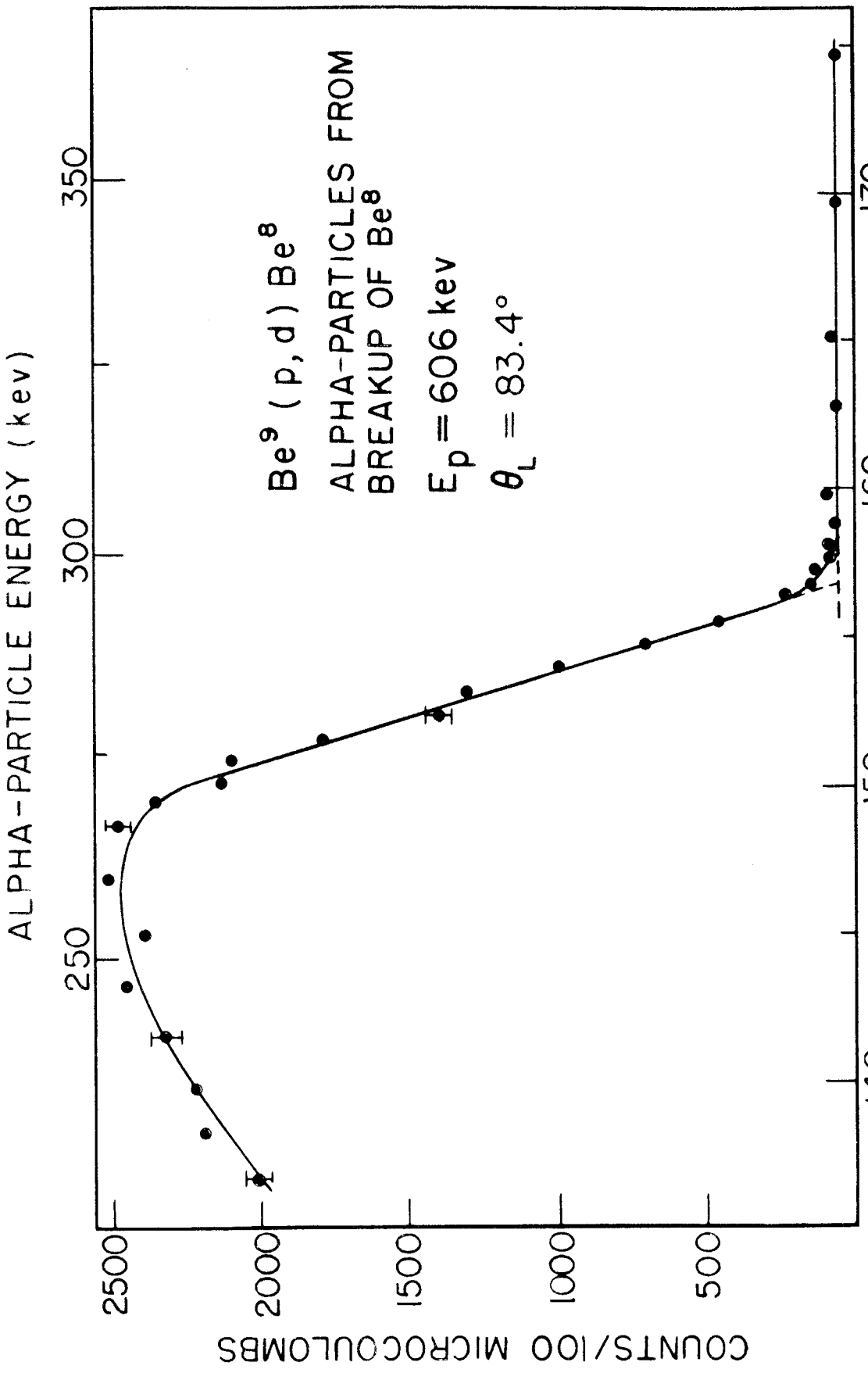
ALPHA-PARTICLE ENERGY (kev)
250
300
350
Be^9 (p, d) Be^8
ALPHA-PARTICLES FROM
BREAKUP OF Be^8
$E_p = 606$ kev
$\theta_L = 83.4°$
COUNTS/100 MICROCOULOMBS
2500
2000
1500
1000
500
140
150
160
170
$B\rho$ (KILOGAUSS-CM)

FIGURE 23

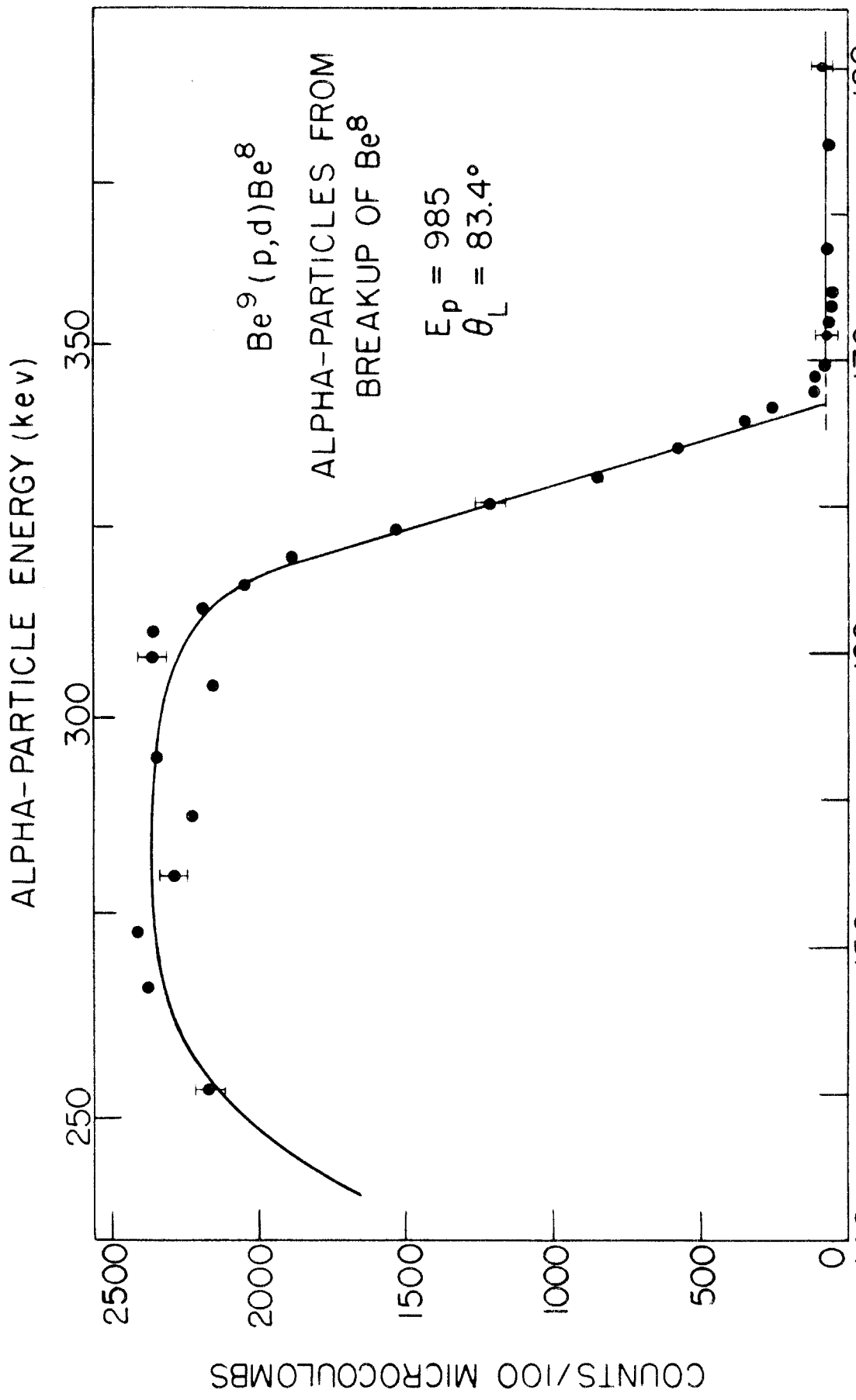
ALPHA-PARTICLE ENERGY (kev)
250
300
350
$Be^9(p,d)Be^8$
ALPHA-PARTICLES FROM
BREAKUP OF Be^8
E_p = 985
θ_L = 83.4°
2500
2000
1500
1000
500
0
COUNTS/100 MICROCOULOMBS
140
150
160
170
180
Bρ (KILOGAUSS-CM)

FIGURE 24

TYPICAL MAGNETIC SPECTROMETER AND ANALYZER CALIBRATIONS

FIGURE 25

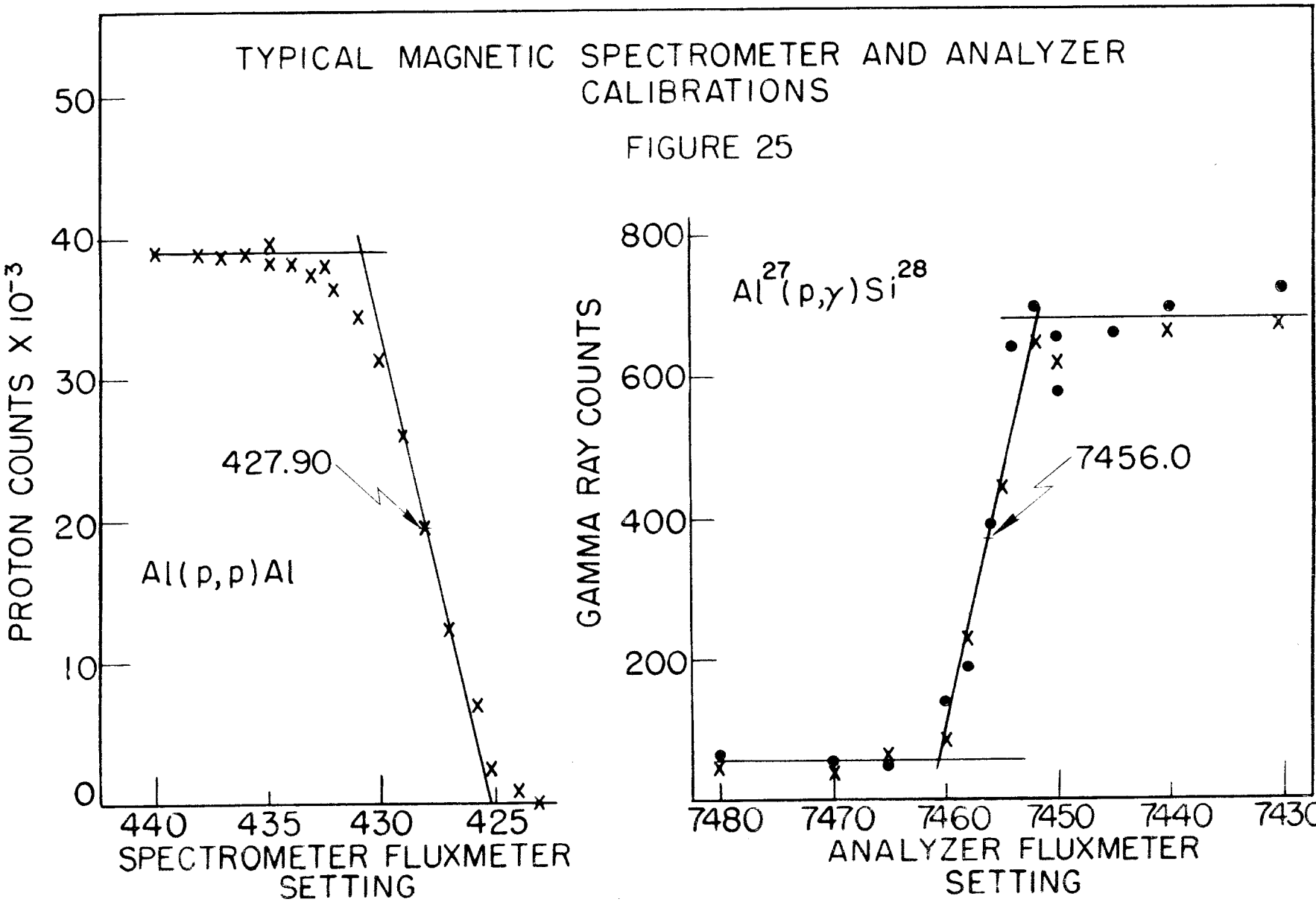

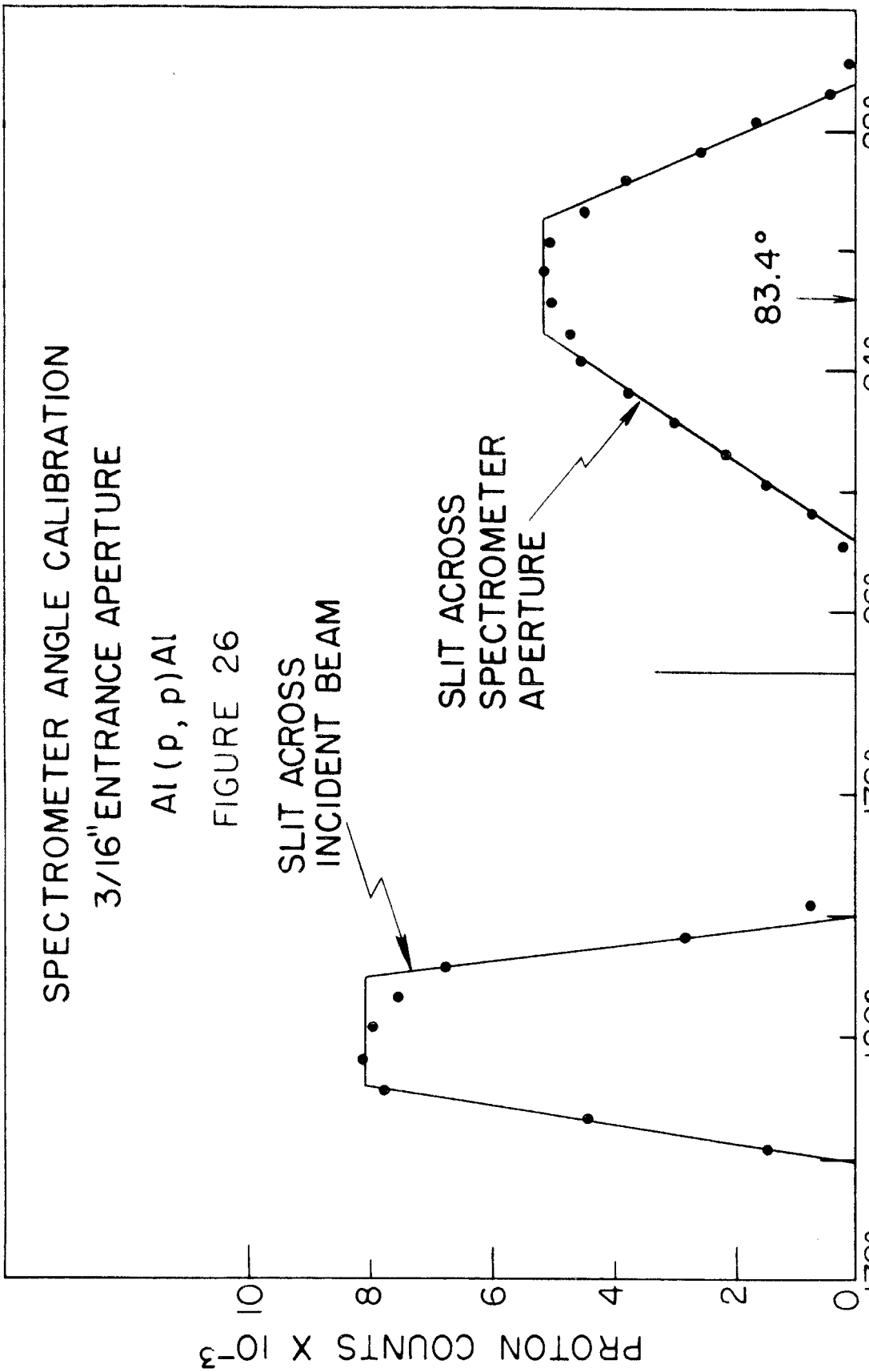
SPECTROMETER ANGLE CALIBRATION
3/16" ENTRANCE APERTURE
Al (p, p) Al
SLIT ACROSS INCIDENT BEAM
SLIT ACROSS SPECTROMETER APERTURE
83.4°
PROTON COUNTS X 10⁻³
0
2
4
6
8
10
-178°
180°
178°
86°
84°
82°
LABORATORY ANGLE OF VERTICAL SLIT

FIGURE 26

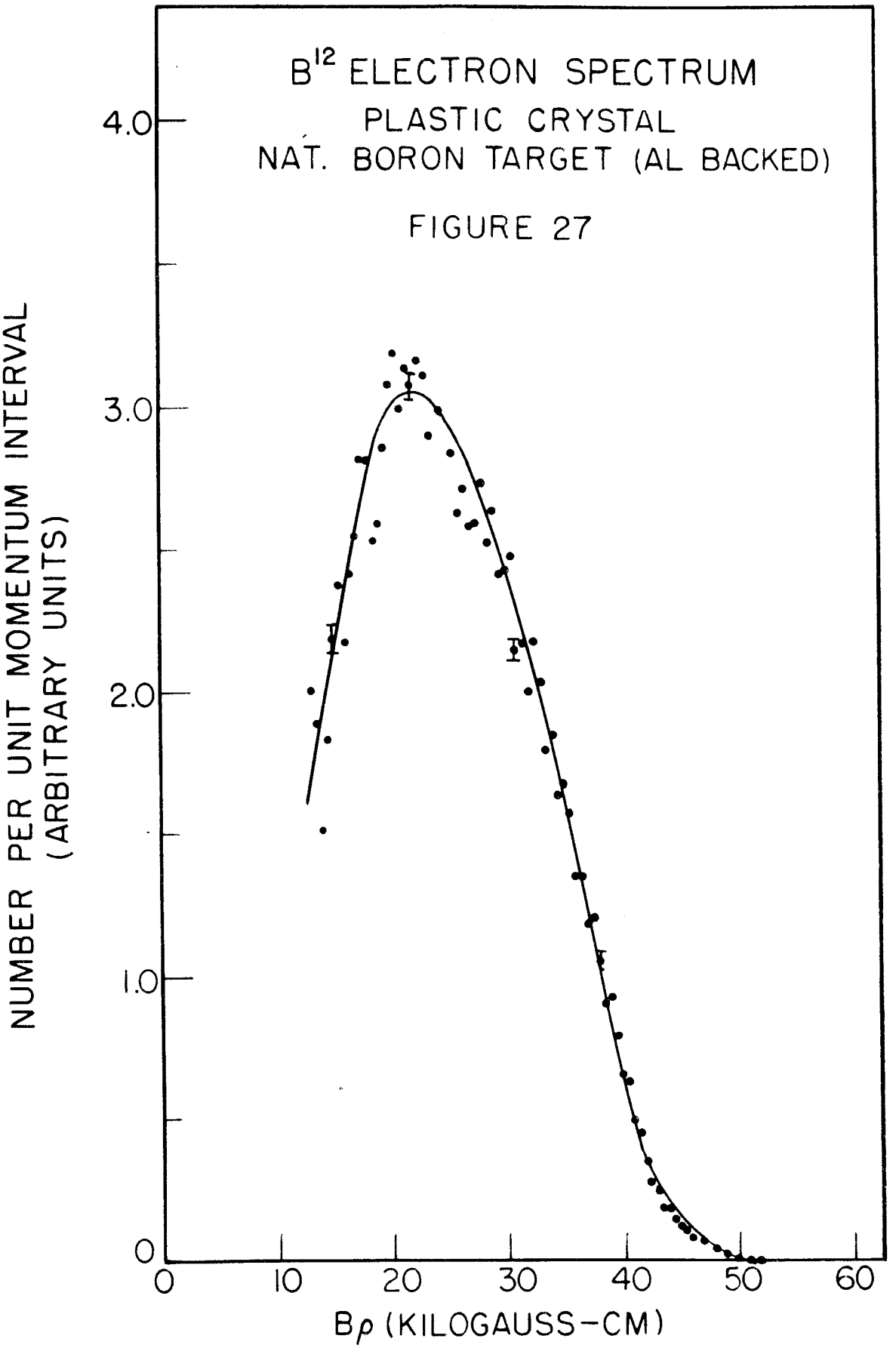
B12 ELECTRON SPECTRUM
PLASTIC CRYSTAL
NAT. BORON TARGET (AL BACKED)
FIGURE 27
NUMBER PER UNIT MOMENTUM INTERVAL
(ARBITRARY UNITS)
4.0
3.0
2.0
1.0
0
0
10
20
30
40
50
60
Bρ (KILOGAUSS-CM)

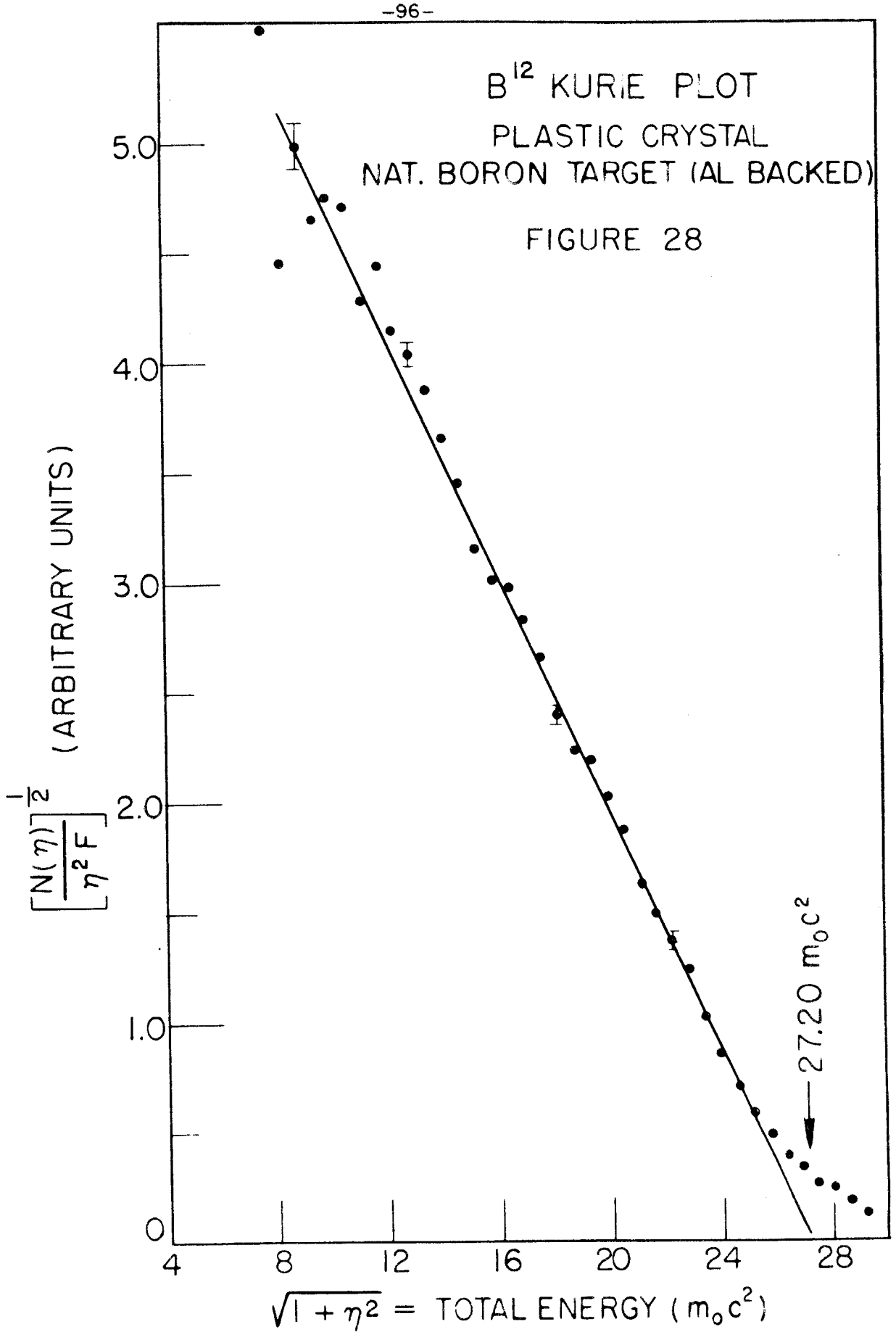
B12 KURIE PLOT
PLASTIC CRYSTAL
NAT. BORON TARGET (AL BACKED)
FIGURE 28
5.0
4.0
3.0
2.0
1.0
0
4
8
12
16
20
24
28
27.20 m0c2
[N(η)/η2F]1/2 (ARBITRARY UNITS)
√1 + η2 = TOTAL ENERGY (m0c2)

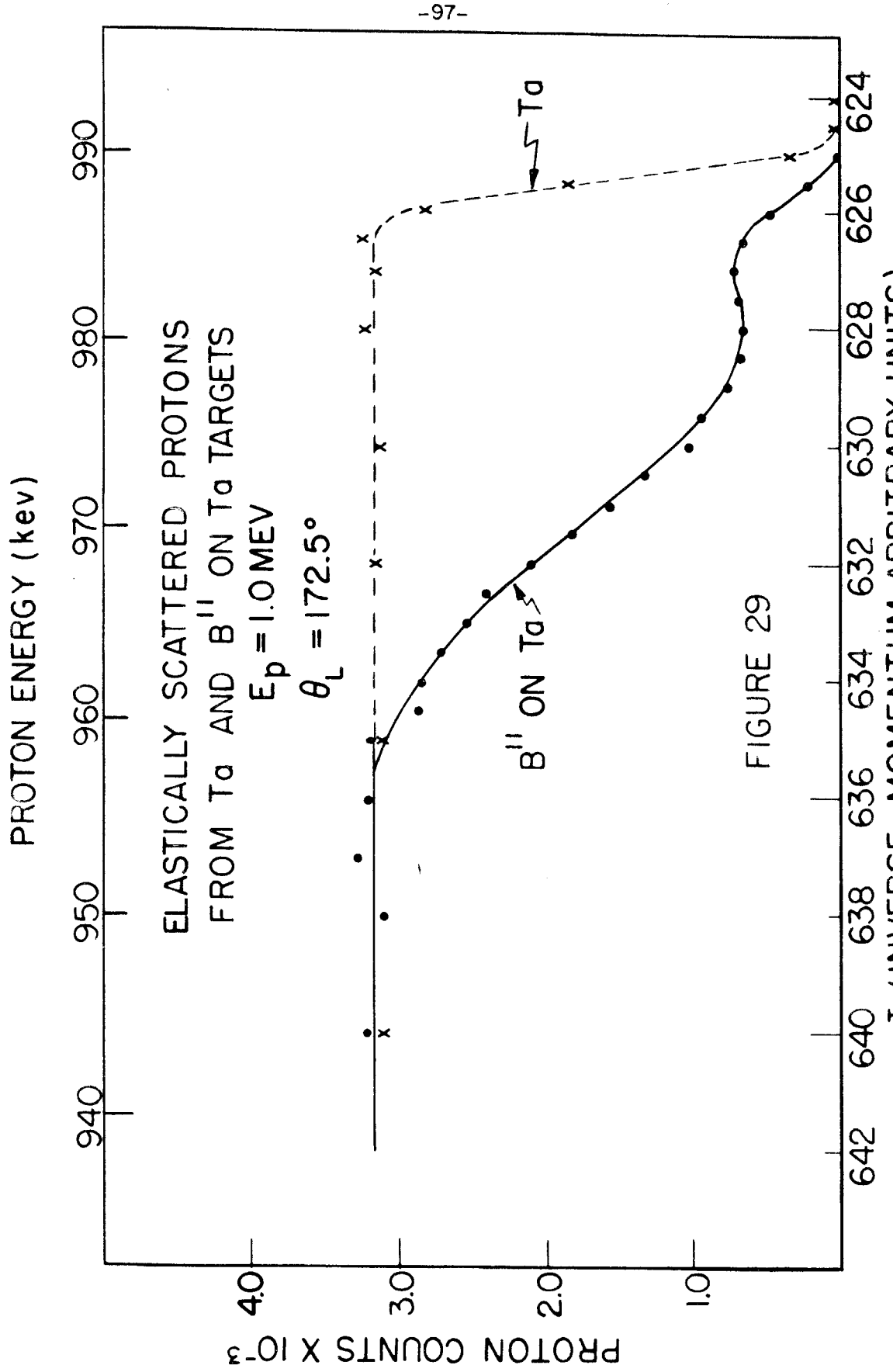
ELASTICALLY SCATTERED PROTONS
FROM Ta AND B11 ON Ta TARGETS
Ep = 1.0 MEV
θL = 172.5°
Ta
B11 ON Ta
PROTON ENERGY (kev)
940
950
960
970
980
990
I (INVERSE MOMENTUM ARBITRARY UNITS)
642
640
638
636
634
632
630
628
626
624
PROTON COUNTS X 10-3
4.0
3.0
2.0
1.0

FIGURE 29

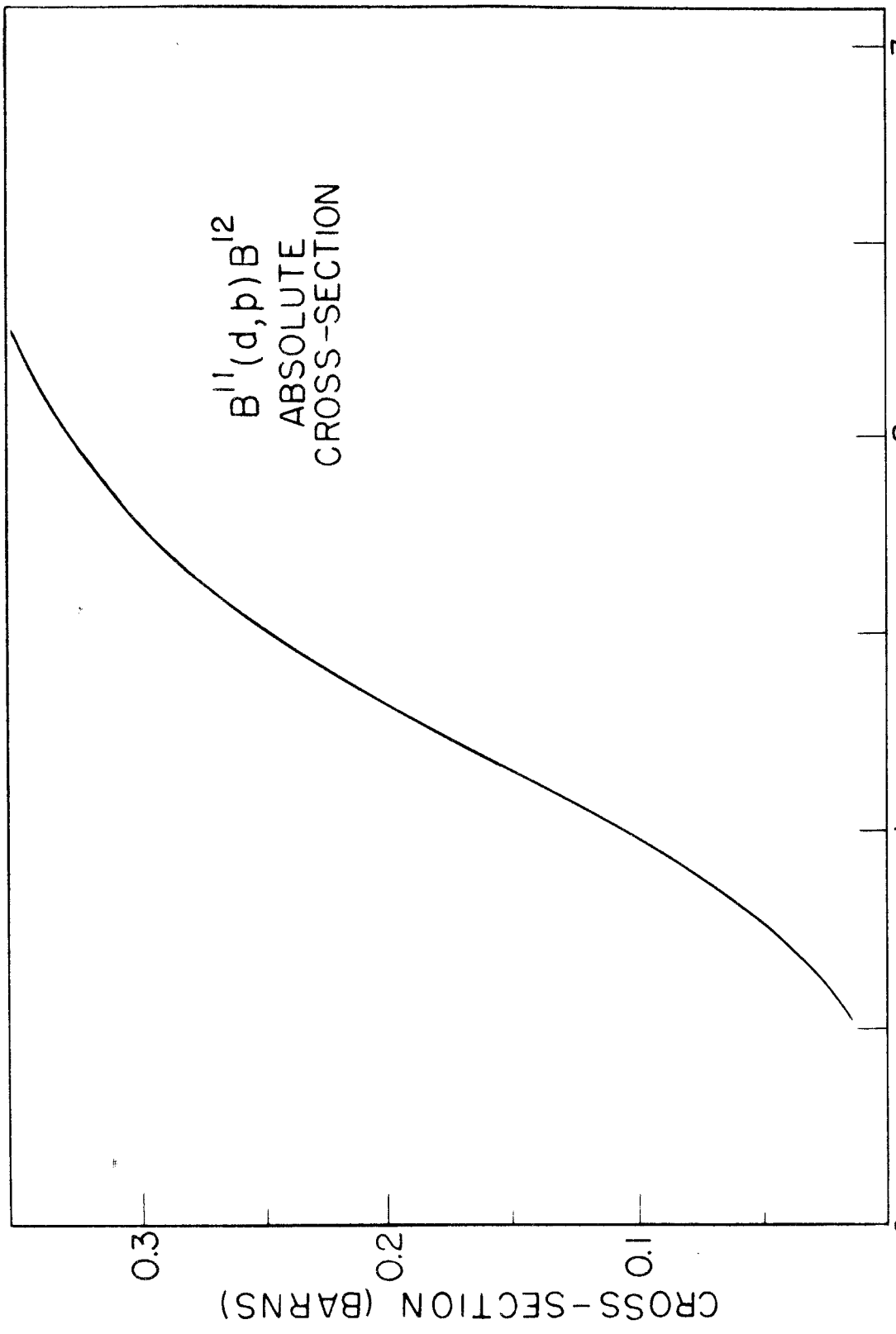
$B^{11}(d,p)B^{12}$
ABSOLUTE
CROSS-SECTION
CROSS-SECTION (BARNS)
0.3
0.2
0.1
0
1
2
3
DEUTERON ENERGY (MEV)

FIGURE 30

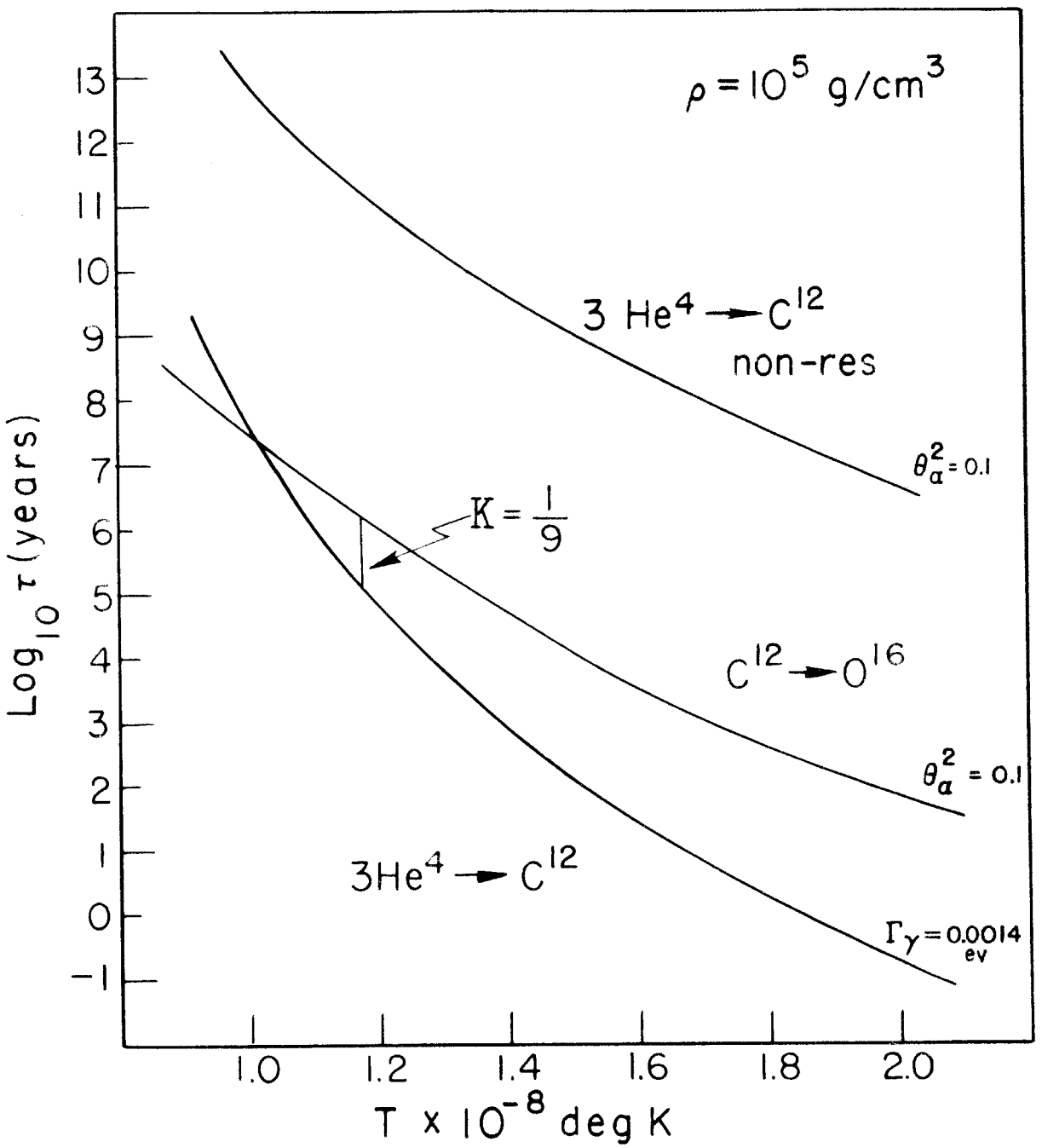
$\rho = 10^5$ g/cm^3
3 He^4 → C^{12}
non-res
$\theta_\alpha^2 = 0.1$
K = 1/9
C^{12} → O^{16}
$\theta_\alpha^2 = 0.1$
3He^4 → C^{12}
$\Gamma_\gamma = 0.0014$ ev
Log$_{10}$ τ (years)
T x 10^{-8} deg K
13
12
11
10
9
8
7
6
5
4
3
2
1
0
-1
1.0
1.2
1.4
1.6
1.8
2.0

FIGURE 31